

Numerical investigation of stress concentration in preloaded, galvanized threaded fasteners of large diameter



Kamal Manoj
Student number: 5928656

Committee: Prof. Dr. M. Veljkovic
Dr. A. Cabboi
Dr. H. Slot
Dr. I. Shakeri
Ir. J. Rodenburg

TU Delft (Chair)
TU Delft
TNO
TU Delft
TNO

 **TU Delft**

TNO innovation
for life

(Page intentionally left blank)

Numerical investigation of stress concentration in preloaded, galvanized threaded fasteners of large diameter

by

Kamal Manoj

5928656

*In partial fulfilment of the requirements for the degree of
Master of Science in Civil Engineering at the
Delft University of Technology*



In collaboration with TNO

An electronic version of this thesis is available at
<http://repository.tudelft.nl/>.

(Page intentionally left blank)

Author**Kamal Manoj**

MSc. Civil Engineering
Faculty of Civil Engineering and Geosciences
Delft University of Technology

GRADUATION COMMITTEE**Chair & Main Supervisor****Prof. dr. M. (Milan) Veljkovic**

Professor and Head of section
Steel and Composite Structures group
Department of Engineering Structures
Faculty of Civil Engineering and Geosciences
Technische Universiteit Delft

Committee member**Dr. A. (Alessandro) Cabboi**

Assistant Professor
Mechanics and Physics of Structures section
Department of Engineering Structures
Faculty of Civil Engineering and Geosciences
Technische Universiteit Delft

Additional Supervisor**Dr. I. (Iman) Shakeri**

Postdoctoral Researcher
Steel and Composite Structures group
Department of Engineering Structures
Faculty of Civil Engineering and Geosciences
Technische Universiteit Delft

Company Supervisors**Dr. ing. H.M. (Henk) Slot**

Senior Scientist
Reliable Structures group
Mobility and Built Environment unit
TNO

Ir. J.D. (Jorrit) Rodenburg

Scientist
Reliable Structures group
Mobility and Built Environment unit
TNO

(Page intentionally left blank)

Preface

This thesis is part of my Master of Science in Civil Engineering at the Delft University of Technology, specializing in Structural Engineering, marking the completion of my time as a structural engineering student. Describing the behavior of large-diameter preloaded, galvanized threaded fasteners utilized in offshore wind turbine connections, my study aims to contribute to the future of sustainable and renewable energy generation. My thesis work is part of the larger Bolt and Beautiful project in which TU Delft and TNO are part of, as was my 3 month initial stint at TNO studying the loss of preload in these bolts. The past 6 months where I have worked on the research and compilation of the report have been incredibly fulfilling.

This has been a dream in the making for the past 10 years, where a bright-eyed young man, mesmerized by the world of buildings and bridges, decided that he wanted to be a structural engineer. Not influenced by external factors or opinions, I am incredibly grateful to my younger self for sticking to the plan, wading through unexplored waters and taking challenges head on. I consider this period in my life to be incredibly fruitful, thanks to my family, teachers, professors, friends and well-wishers.

I would like to thank my teachers and professors for imparting the knowledge to proudly call myself a structural engineer. The effort that goes into elucidating complex knowledge to enthusiastic young engineers while contributing to the society with research and development will not be unseen. I would like to thank my colleagues throughout my career, who became my role-models to whom I would always look up to. Your camaraderie and support will always be remembered. My parents and my brother, without whom I would not be able to think of being here today. I owe all my success and blessings to them. My friends, for being with me through the ups and downs in my life. And lastly, to my thesis committee for their confidence in me and supporting me to makes my thesis possible.

I would specially like to thank: Henk and Jorrit from TNO, for trusting a naive engineer with an important topic such as this and guiding me towards the right direction at times of doubt and confusion; Iman, for always providing clarity, direction and the right help everytime we met; professor Milan, for his expertise and guidance in helping me shape the output here; and Alessandro, for his critical questions and being an important part of the committee.

Kamal Manoj
Delft, July 2025

Abstract

The accelerated development of renewable wind energy sources and their large-scale adoption involves an increasing global size of offshore wind turbines, leading to larger structures and connections. This requires the improvement of assessment methods used for these large connections as well as their optimization which ensures low cost and increased structural integrity of these critical components.

As a part of the Bolt and Beautiful project, this research focuses on threaded fasteners of large diameter (M36 and above) which are hot-dip galvanized for corrosion protection, and preloaded for use in ring flange connections. The objective of this thesis is to numerically investigate the local stress state at the critical engaged thread roots, in the presence of galvanized zinc layer and nominal preload. This broad objective is divided into measurable parts: 1) to understand the effect of galvanization, 2) to compare the local stress state in fasteners of increasing diameter, and 3) to quantify the cracking parameters in these fasteners using the fracture mechanics approach.

Based on the numerical research findings, the following conclusions were drawn. Firstly, the presence of inter-metallic layers formed due to hot-dip galvanization has different properties which causes the initiation of brittle cracks inside the galvanization layer even under nominal preloads. Initiation of these microcracks, which may not be visible on the exterior, is detrimental to the lifetime of fasteners under external loading, and a fracture mechanics approach is utilized to quantify them. Secondly, the comparison between increasing diameters of fasteners suggest that the local stress state greatly depend on the geometry of the threads and the fastener. This geometric size effect is signified by larger stress peaks, peak stresses closer to the root boundary, reduced redistribution of stresses as diameter and therefore sharpness of the notch-like thread root increases. These findings also call for modifications to geometric parameters which allow for a consistent stress behavior between different diameters. Thirdly, the fracture mechanics approach evaluated that micro-cracks in galvanized zinc layer has a greater effect on larger diameter threaded fasteners than smaller ones. This is quantified by a larger crack driving force, signified by the J-integral, which suggests a larger amount of energy released per unit crack extension.

The findings highlight that larger diameter preloaded fasteners are more prone to a reduced lifetime, and even more due to the effect of hot-dip galvanization, by numerically ascertaining the mechanism using a comparative analysis and fracture mechanics approach. This is consistent with the reduced endurance limits reported through experimental investigations [14] for hot-dip galvanized threaded fasteners with increasing diameter.

Contents

1	Introduction	1
2	Research Description	5
3	Literature review	8
3.1	Production of threaded fasteners	8
3.2	Preloading	10
3.3	Hot-dip galvanization	11
3.4	Finite element method	13
3.5	Fracture mechanics	15
3.6	Summary	17
4	Two-dimensional analysis	19
4.1	Geometry and model setup	19
4.2	Inter-metallic phases	21
4.3	Material models	22
4.3.1	Material model for steel substrate	22
4.3.2	Material model for inter-metallic layers	23
4.4	Contact definition and thread interaction	24
4.5	Meshing and sensitivity studies	26
4.6	Results	27
4.6.1	Linear elastic material conditions	28
4.6.2	Elastic-plastic material conditions	31
4.7	Discussion	33
5	Three-dimensional analysis	36
5.1	Model setup	37
5.2	Results	39
5.3	Discussion	41
6	Comparison of bolt models of larger diameters	44
6.1	Model setup	46
6.2	Results	48
6.3	Discussion	56
7	Comparison of bolt models with cracked galvanization layer	58
7.1	Model setup	58
7.2	Results	60
7.3	Discussion	62

8 Conclusion and Recommendations 63

8.1 Conclusions 63

8.2 Limitations 65

8.3 Recommendations 66

Appendix A 3D axisymmetric model 72

A.1 Results 73

A.2 Discussions 74

Appendix B Model parameters and inputs 77

List of Figures

1.1	Offshore wind farm Borssele, off the coast of Middelburg, Zeeland. Commissioned in 2020 by Orsted [45]	1
1.2	Typical bolted ring flange connection at various locations on the offshore wind turbine supporting structure [35]	2
1.3	Schematic of corrosion process of steel in saline solution [23]	3
1.4	Galvanized (normal temperature - NT and high temperature - HT) and ungalvanised (black) HV bolts [48]	3
2.1	Simplified engineering model for boundary layers	5
2.2	SEM image of an M36 coated stud. Mild etching done to show Zn-layer with phases δ and ζ . Noticeable cracks in δ phase.	6
2.3	Research methodology	7
3.1	Characteristics of thread rolling	9
3.2	Types of ring flange connection assemblies in segment representation - IHF Fastener Systems	9
3.3	Results from parametric study - Domblesky and Feng (2002)[12]	10
3.4	Bolt force vs. external force curve - Seidel and Schaumann (2001) [49]	11
3.5	Hot-dip galvanisation process - American Galvanizers Association	12
3.6	SEM images showing thickness of galvanized zinc layer (TNO)	12
3.7	Different integration approaches used in explicit and implicit solvers	14
3.8	A representation of closed contour for J-integral calculation [16]	16
3.9	A representation of contour for J-integral calculation at crack tip [16]	17
4.1	Snapshot from the two-dimensional model in ABAQUS showing the boundary conditions	20
4.2	Schematic of inter-metallic layer in increasing order of Zn content from the steel substrate [42]	21
4.3	SEM image showing scale of thickness of each inter-metallic layer	21
4.4	True stress vs true strain plot of steel substrate material model choices	22
4.5	SEM imagery of compression and bending microbeam testing by Okamoto et al.	24
4.6	Stress-strain curve of inter-metallic phases as per Okamoto et al.[42][43]	24
4.7	Shear stress vs total slip relation [1]	25
4.8	"Hard" pressure-overclosure relationship [1]	26
4.9	General mesh layout of first engaged thread	27
4.10	Mesh layout at thread root	27
4.11	Mesh sensitivity plot showing convergence in values beyond 60 elements along thread root radius	28
4.12	Paths used to present results at first engaged thread root	28
4.13	Principal stress plots from linear elastic ungalvanised M36 fastener model	29
4.14	Stress plots from linear elastic ungalvanised M36 fastener model	29

4.15	Comparison of linear elastic stress concentration between results obtained and theory	30
4.16	Stress plots from linear elastic galvanised M36 fastener model	30
4.17	Stress plots from linear elastic galvanised M36 fastener model	30
4.18	Principal stress plots from elastic-plastic ungalvanised M36 fastener model	31
4.19	Stress plots from elastic-plastic ungalvanised M36 fastener model	31
4.20	Comparison of stress plot between results and schematics available from theory . . .	32
4.21	Stress plots from elastic-plastic galvanized M36 fastener model	32
4.22	Stress plots from elastic-plastic galvanized M36 fastener model	33
4.23	Brittle nature of inter-metallic layers	33
4.24	Stress plots compared along the thread root section	34
4.25	Mises stress up to 2mm depth from the thread root boundary. Notice the zeta and delta layer values (first two plateaus) have attained ultimate tensile strength as seen in figure 4.6	35
5.1	Local stresses (L) and local strain (R) inside the paired thread of an M36 bolt from calculation with 2D axisymmetric and full 3D model under elastic-plastic material behavior [14]	36
5.2	Global setup of the three-dimensional M36 model. The different colored parts signifies different components as seen in the two-dimensional segment model	37
5.3	Meshed parts of the full 3D model	38
5.4	Principal stress and plastic strain distribution in the engaged thread roots of full 3D model	40
5.5	Comparison of stress plots between full 3D model with helical pitch and axisymmetric 2D model	41
5.6	Path along which local stress is evaluated in full 3D model	41
5.7	Engaged threads in both models corresponding to locations mentioned in the comparison plot in figure 5.5	41
5.8	Point of start of full engagement and regions with partial engagement in full 3D model	42
6.1	Stress distribution at notch and about thread root section for different nominal diameters [36]	44
6.2	Design thread profiles from [27]. Notice the fully rounded thread root for external (stud/bolt) thread. '1' represents the body of the bolt/stud and nut respectively	46
6.3	Thread geometry parameters and their dependence on pitch value	46
6.4	SEM images from TNO showing consistent thickness of galvanized zinc layer irrespective of size of threaded fastener	47
6.5	Comparison of principal stress distribution at critical thread root for fasteners of different diameters. a - M36, b - M48, c - M64, d - M72, e - M80. Visual comparison suggest identical stress distribution	48
6.6	Max principal stress plots on the absolute length scale at the critical thread root section	49
6.7	Max principal stress plots on the normalized length scale at the critical thread root section	49
6.8	Max principal stress plots up to 2mm from the critical thread root section edge	49
6.9	Mises stress plots on the absolute length scale at the critical thread root section	51
6.10	Mises stress plots on the normalized length scale at the critical thread root section . .	52
6.11	Mises stress plots up to 2mm from the critical thread root section edge	52
6.12	Axial stress plots on the absolute length scale at the critical thread root section	53
6.13	Axial stress plots on the normalized length scale at the critical thread root section . .	53
6.14	Axial stress plots up to 2mm from the critical thread root section edge	54
6.15	Radial stress distribution at critical thread root - M36	55
6.16	Radial stress plots on the absolute length scale at the critical thread root section	55

6.17	Radial stress plots on the normalized length scale at the critical thread root section . . .	55
6.18	Radial stress plots up to 2mm from the critical thread root section edge	56
7.1	Crack sub-model and mesh	59
7.2	Crack definition and parameters to be defined for contour integral analysis	59
7.3	Definition of contour integral analysis parameters in ABAQUS/CAE [1]	59
7.4	Undeformed and deformed crack region at the first engaged thread root - M72 fastener	60
7.5	von Mises stress comparison along predefined path from crack tip	61
7.6	Max principal stress comparison along predefined path from crack tip	61
7.7	Axial stress comparison along predefined path from crack tip	61
A.1	Meshed part of the 3D axisymmetric model	72
A.2	Three-dimensional axisymmetric submodel representing inter-metallic layers in assembly. Box 1 and 2 are further explained in the next figure	73
A.3	Magnified locations of interest. The layers are as follows (left to right): Nut steel substrate, δ phase on nut, ζ phase on nut, ζ phase on stud, δ phase on stud, stud steel substrate	73
A.4	Sketch of the δ phase from ABAQUS	74
A.5	Principal stress map at the engaged thread roots. The numbers signify the first and second engaged thread root.	74
A.6	Principal strain map at the engaged thread roots	75
A.7	Max principal stress distribution at first engaged thread root for 2D and 3D axisymmetric model - Ungalvanized	75
A.8	Max principal stress plots for 2D and 3D axisymmetric model - Ungalvanized	75
A.9	Max principal stress distribution at first critical thread root for 2D and 3D axisymmetric model - Galvanized	76
A.10	Max principal stress plot for 2D and 3D axisymmetric model - Galvanized	76
A.11	Strain plot for ungalvanized 2D and 3D axisymmetric model along the thread root radius	76
B.1	Step definition manager	78
B.2	Step definition details	78
B.3	Field output selection	79
B.4	Contact interaction definition	80
B.5	Contact property definition	80
B.6	Load input manager	81

List of Tables

3.1	HV fastener sizes and d/p ratio	10
3.2	Geometry parameters	17
3.3	Material parameters	17
3.4	Contact parameters	18
4.1	Elastic properties of steel substrate	23
4.2	Material properties of δ phase [42][43]	24
4.3	Material properties of ζ phase [42][43]	24
4.4	Mesh sensitivity results	27
5.1	Nominal preload levels corresponding to different curves in figure 5.1. $R_{p,0.2}$ corresponds to the nominal stress value at 0.2% plastic strain limit = 900 N/mm ²	37
6.1	Fastener specifications and pitch value	46
6.2	Pitch and corresponding maximum coating thickness in HDG fasteners	48
6.3	Fastener size and peak principal stress values.	50
6.4	Distance of peak from root boundary for various fastener sizes	50
6.5	Width of stressed region from thread root boundary on a normalized scale	51
7.1	J-integral values (J/mm ²)	62
B.1	Elastic properties of δ layer	77
B.2	Elastic properties of ζ layer	77
B.3	Elastic properties of steel substrate	77
B.4	Plastic properties of δ layer	77
B.5	Plastic properties of ζ layer	77
B.6	Plastic properties of steel substrate	78

List of abbreviations

HDG hot-dip galvanization

FEA finite element analysis

OECD Organisation for Economic Co-operation and Development

3D three-dimensional

2D two-dimensional

SCF stress concentration factor

M36 metric thread designation of 36mm nominal diameter

tet tetrahedral element

hex hexahedral element

NDT non-destructive testing

LEFM linear elastic fracture mechanics

EPFM elastic-plastic fracture mechanics

K stress intensity factor

Chapter 1

Introduction

Humankind has always been on the quest to seek materials to support their comfortable lives. Electricity has, to a large extent, been a cornerstone of progress in terms of sustaining our lives and proliferating development in various aspects. The shift towards renewable energy came as a result of an ever-increasing population and harmful output when processing traditional sources of energy. Aided by technological advancements and innovations, renewable energy sources are being widely adopted throughout the world, and it is not too long before we achieve fully sustainable energy production.



Figure 1.1: Offshore wind farm Borsselle, off the coast of Middelburg, Zeeland. Commissioned in 2020 by Orsted [45]

The importance of wind energy is quite high in the Eurozone. To promote a transition to sustainable energy sources, most European countries have signaled a proactive shift in considering tapping other natural sources for providing electricity. A welcoming measure to this was the electricity generated from wind energy exceeding coal power for the first time in Europe in 2023. The Netherlands' location on the North sea shore and favourable terrain makes wind energy, especially offshore wind energy, a great opportunity to tap into [38]. The Energy Transition Outlook 2024 by DNV [11], the world's leading classification society and technical advisory for energy value chain and management, suggests a lower forecast of offshore wind installed capacity compared to previous executive reports. This is owed to difficulties in costs, reliability and lack of government support encountered by projects in Organisation for Economic Co-operation and Development (OECD) countries. The report also suggests a revival from these negative forecast in the upcoming years.

The forecast suggested the need for an improved design methodology and increased reliability of upcoming wind turbines. Ring flange connections are a major component of the offshore wind turbine supporting structure, used to connect the monopile to the superstructure of the wind turbine supporting

structure. As with most engineering or structural components, these ring flange connections and their components are crucial to ensure the reliability and safe functioning of these wind towers, apart from the mechanical components of the turbine itself, and therefore these connections are a major focus when it comes to reliable offshore energy structures. Numerous challenges associated with bolted joints can arise during the assembly of these components and during the service lifetime. Some of the major concerns include the corrosion of these components and the gradual loosening of threaded fasteners used in these connections. Preloading of these fasteners is done to ensure the working stress ranges of these threaded fasteners are within the limits to ensure adequate lifetime even in the presence of fatiguing cyclic loads from the external environment. Ensuring accurate and lasting tensioning, along with their robust protection from the marine environment will ensure their longevity. Add to this larger, high capacity connections which minimizes the number of individual components (threaded fasteners) used in a ring flange connection, these measures can minimize the work cost involved and thereby provide impetus to the adoption of offshore wind energy systems. Therefore three major requirements can be pointed out here as necessary for future-proofing wind energy adoption: effective corrosion protection, adequate preloads and larger components. The intersection of all these needs are being answered in this research project, along with the larger Bolt and Beautiful project, supported and funded by the Dutch government. The larger project aims to provide calibrated models and procedures to effectively (re)design and maintain ring flanges of existing and future monopile foundations, with an optimal use of material and labor resources. The innovation will offer faster installation, less maintenance costs and safer connections, and allow bolted connections to be used for large turbine size [53].

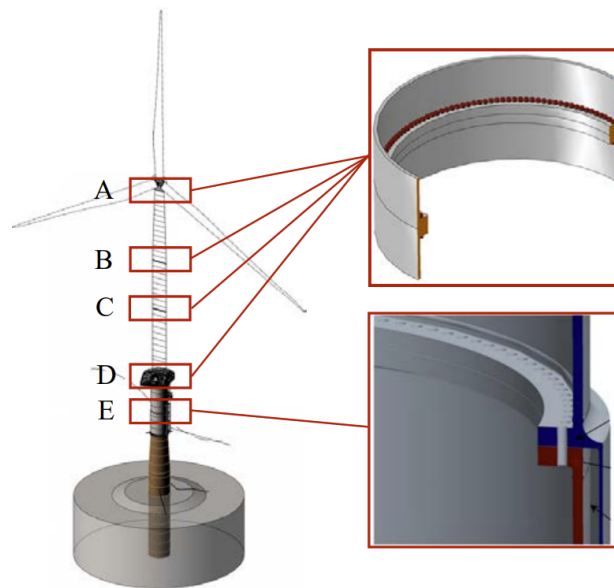


Figure 1.2: Typical bolted ring flange connection at various locations on the offshore wind turbine supporting structure [35]

Today, the largest bolt size used is mostly M72, with the idea of increasing this size to M80 or more in the future. A consortium of suppliers, research organizations, developers and operators have therefore come together to evaluate the need of the hour. As part of the larger project, the industry has indicated a strong need to improve the assessment methods for ring flange connections, considering design, manufacturing and maintenance aspects. They have learned that current design, installation and operation procedures are insufficient to apply to larger flanges and components. The optimization they look forward to is two-fold: to develop a deterministic bolt fatigue model and a structural safety assessment via a probabilistic approach.

The offshore environment is an unforgiving one due to its corrosive effect on metals. The combination of seawater, high humidity and extreme weather conditions accelerate the process of degradation of

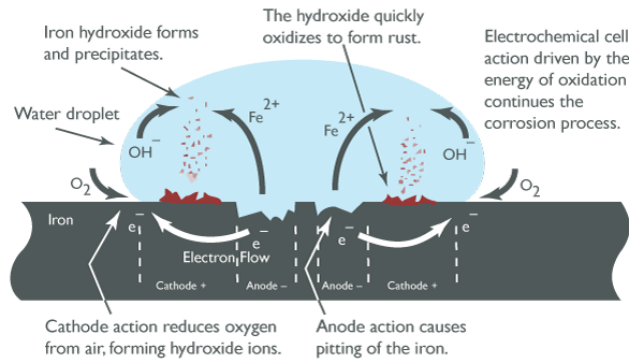


Figure 1.3: Schematic of corrosion process of steel in saline solution [23]

metals. This leads to failure of structures under stress as corrosion weakens them, manifested as surface damage, reduced thickness, or even the formation of brittle structures. The process of corrosion is driven by the electrochemical cell action, involving the movement of electrons and ions between two parts, one where oxidation occurs (anode) and the other where reduction occurs (cathode). Figure 1.3 schematically explains the corrosion process in steel. The anodic area is the "active" site where the steel itself is being attacked and dissolved during the corrosion process, whereas the cathodic area is region where steel oxidises and precipitates as rust.

Galvanization prevents this with the help of an external coating which acts as a physical barrier and a sacrificial anode, promoting the corrosion of zinc to protect the steel article. This is of high importance to fasteners used in bolted ring flange connections of offshore wind turbines, as they serve as the major load transfer component in the supporting tower. The reliability of these fasteners directly affects the safety and resilience of the offshore wind turbine, highlighting the requirement of test and standards to confirm the strength and lifetime of these fasteners. Studies have shown the drawback of galvanization on the fatigue lifetime of fasteners, but the comprehensive mechanism behind this and the extent to which it is applicable to different sizes of fasteners needs to be further studied. Our research contributes to the development of a deterministic model for bolt fatigue, as we shall see in the subsequent sections, by studying the effect of galvanization, known to reduce the fatigue lifetime of fasteners, on the local stress state of fasteners of increasing diameters. This will be done with the help of numerical models considering the effect of a galvanization boundary layer.

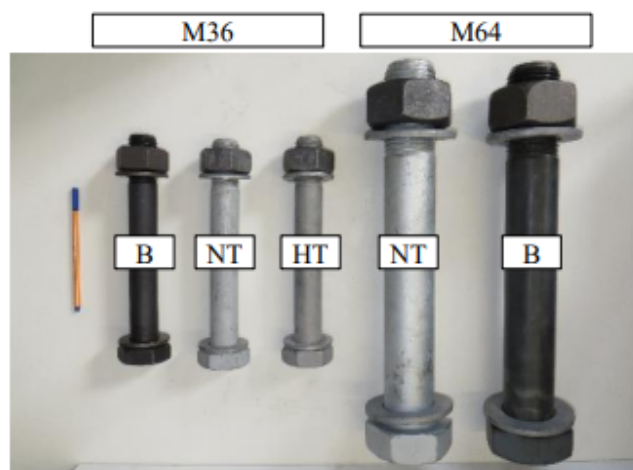


Figure 1.4: Galvanized (normal temperature - NT and high temperature - HT) and ungalvanised (black) HV bolts [48]

This is followed by the effect of preloading, which is the pre-tensioning of threaded fasteners in ring flange connections. This is done during tightening to create a clamping force preventing gap formation, fatigue failure and loosening due to vibration - actions affecting the safety of these important connections. Various methods of preload application is considered by the industry today, and studies

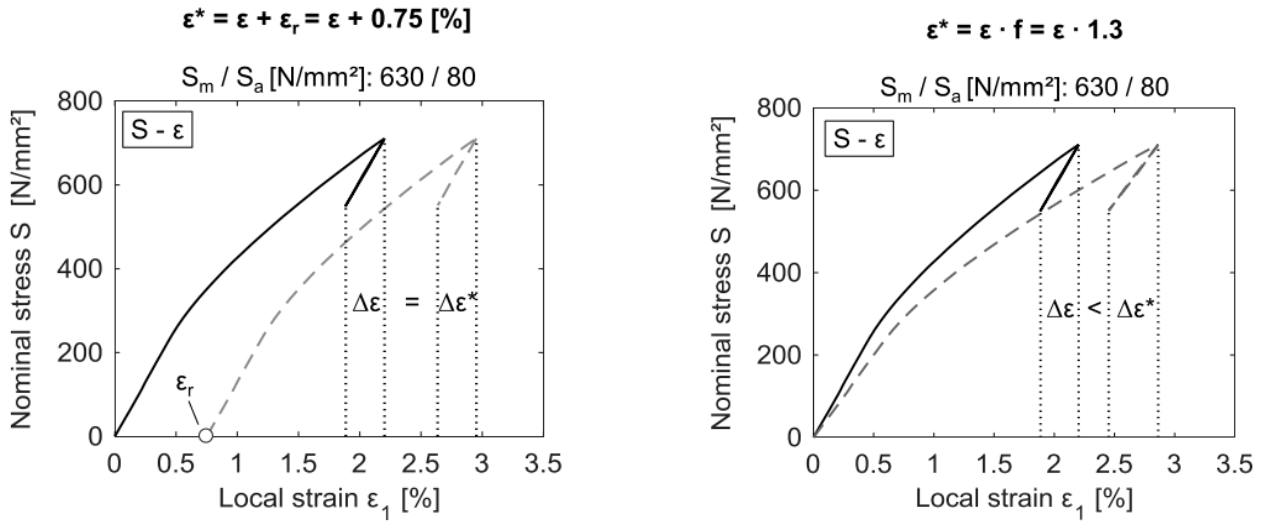
encompassing the loss of preload along with methods to overcome is being studied. This comes with regular updates to standards on the considerations for components and the ring flange itself, levels of preload for the safe functioning of these connections and the estimated fatigue life cycles, to name a few.

The idea of this research is to focus at the intersection of these two applications - hot-dip galvanization and preloading. Any detrimental impact observed at this intersection would mean that these issues can be aggravated during the operational phase in the presence of cyclic external loads and the effect of the environment. By identifying the mechanism and quantifying these effects we hope to make informed decisions regarding the design of larger components and their implementation. This will be done by comparing the combination of these effects in increasingly larger threaded fastener diameters. Conclusions based on these evaluations will further help the requirements considered necessary for future-proofing wind energy adoption as mentioned above. This also aids the objective of the larger Bolt and Beautiful project by providing insights for the deterministic bolt modeling. This approach will help us understand the trend of impact of galvanization on larger threaded fasteners and also quantify the extent to which it is advantageous or detrimental. Thus, through this research, we aim to answer

Chapter 2

Research Description

To aid the development of a deterministic model for bolt fatigue, we first intend in this research to understand the material parameters that will influence the performance of these bolts. The offshore environment is corrosive in nature to almost all materials. As a result, one of the tried and tested methods for corrosion protection of metallic components like bolts is by sacrificial anodic protection of the base material using a metal with higher electrochemical reactivity than the base material, in our case steel. The zinc layer serves two main protective functions as zinc corrodes (oxidizes) preferentially, protecting the steel from rusting even at exposed spots and the application of this layer provides barrier protection, physically separating the steel from the environment, preventing water and oxygen from reaching the steel surface and causing rust [3]. The low position of zinc in the galvanic series, supported by its low rate of self corrosion in common environment makes galvanization by zinc a preferable mode of anodic protection [55].



(a) Virtual strain model by Oechsner et al.(2015)[41]

(b) Factored strain model by Eichstadt (2019)[14]

Figure 2.1: Simplified engineering model for boundary layers

Researchers have conducted experimental and analytical investigations into identifying the impact of NT hot-dip galvanization of the lifetime of these fasteners mainly under cyclic loading conditions. The reduction in endurance limit as reported by standards (VDI 2230) is 20%, while experimental analysis has reported 25% lower fatigue strength compared to uncoated black bolts [17]. Microscopic analysis of intermetallic layers has thrown light on the process behind this effect, caused by pre-existing shrinkage cracks since the time of formation of these layers due to the brittleness of the phases in the steel substrate-zinc alloy surface layers, which act as fatigue crack initiation sites in the steel substrate - zinc interface due to stress peaks at the tip of these cracks. This is also observed in

the SEM image analysis of metric thread designation of 36mm nominal diameter (M36) bolt characterization by TNO, shown below. However, quantifying the effect numerically with the help of stress development at thread roots is a gap expressed by research in the past, with researchers answering this using simplified engineering models of introducing a boundary layer effect. Two methods have been previously employed, namely the virtual residual strain method by Oechsner et al. (2015)[41] (Figure 2.1a) and the factored strain approach by Eichstadt (2019)[14] (Figure 2.1b). Both these models incorporate the negative effect of zinc coating to the local loading conditions without actually considering a physical boundary layer. These researchers have also mentioned in their report a need for detailed model to understand the effect of galvanization. Therefore a major goal of this study is to incorporate these physical layers with the help of a background study on the material properties and damage characteristics of the galvanized zinc layer.

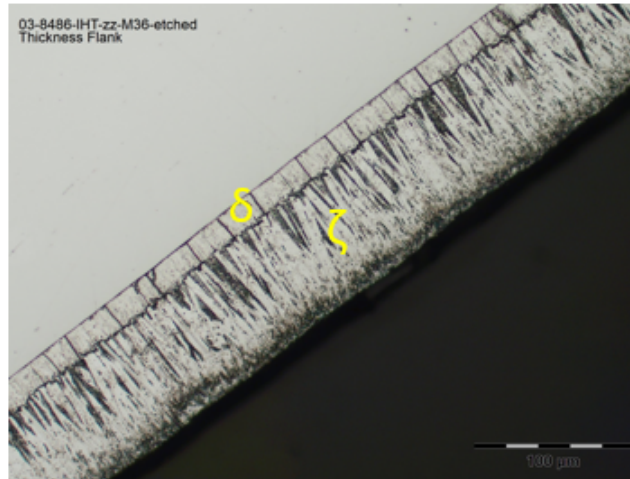


Figure 2.2: SEM image of an M36 coated stud. Mild etching done to show Zn-layer with phases δ and ζ . Noticeable cracks in δ phase.

The key to understanding the effect of hot-dip galvanization requires the analysis of the stress at the fatigue-prone thread root, which acts as a notch-like location for the initiation and propagation of fatigue cracks. This requires the comparison of galvanized and ungalvanized engaged thread specimens of similar geometry (M36) with the right material properties for the intermetallic phases involved and geometric values for the thickness of galvanization layers. Validating the results obtained from this numerical analysis with observations made in literature sources will throw light on questions regarding how the brittleness of these layers affect the local stress development at the engaged thread root.

Utilizing the verified results from the two-dimensional (2D) axisymmetric models, we move on to the three-dimensional model. The full three dimensional bolt modeling and analysis, full with thread pitch and angle, while also incorporating the galvanization layers is beneficial to mainly two things:: firstly this model will aid as a basis for further development of a deterministic bolt fatigue model, having already incorporated the galvanization layers and its effects on stress concentration. Secondly, the capabilities of local stress and strain redistribution along the helical thread during engagement will give us a better picture of the actual stress state at the location of contact at the first few engaged threads. The comparison will enable us to form an informed choice of the dimensional order of analysis to proceed with.

Following this, another major research question regarding the changing local stress behavior of increasing diameter of threaded fasteners will be answered. Theory suggest a geometric size effect which increases the sharpness of the notch-like thread root with an increasing diameter, which in turn increasing the stress concentration and creates a detrimental impact on the behavior and lifetime of these fasteners. By analyzing different fastener models from M36 to M80, we try to quantify the

stress-strain parameters while considering the galvanized zinc layer to identify if the incorporation of these layers benefit or negatively affect the local stress states. The understandings from this will benefit the research scope, giving insights into the effects it may have under a fracture mechanics approach.

The fracture mechanics approach is supported by the mechanical behavior of galvanized zinc layers, which is reported to be mechanically weaker than the steel substrate. Once again by comparing the variation in these values among increasing size of fasteners, we can form results-backed conclusions on the efficacy and behavior of large diameter preloaded fasteners with hot-dip galvanization. As part of this research we hope to conclude whether there is a positive or negative impact due to galvanization as the diameter of threaded fasteners increase.

To summarize, as part of the research we shall first identify the parameters contributing to the stress distribution at the engagement via an extensive literature study. The quantified parameters will then be applied to construct and analyze two dimensional axisymmetric models of both galvanized and ungalvanized threaded fasteners. This will serve as the first step of comparison to fully understand the effect of galvanization on the local stress. The observations and inputs from the two-dimensional model will be utilized to identify the evolution of stress at the thread root on three-dimensional (3D) models, to validate and understand the advantage or disadvantage of a higher dimension providing greater detail for our scope of research. This will be followed by the analysis being performed on models with increasing sizes so as to analyze the trend of stress development to evaluate the difference in the local stress state and the stress concentrations. Finally, we shall consider the behavior of the galvanization layers and their cracking behavior to quantify the effect it will have on the steel substrate using fracture mechanics' parameters. The research methodology given below in figure 2.3 explains this graphically.

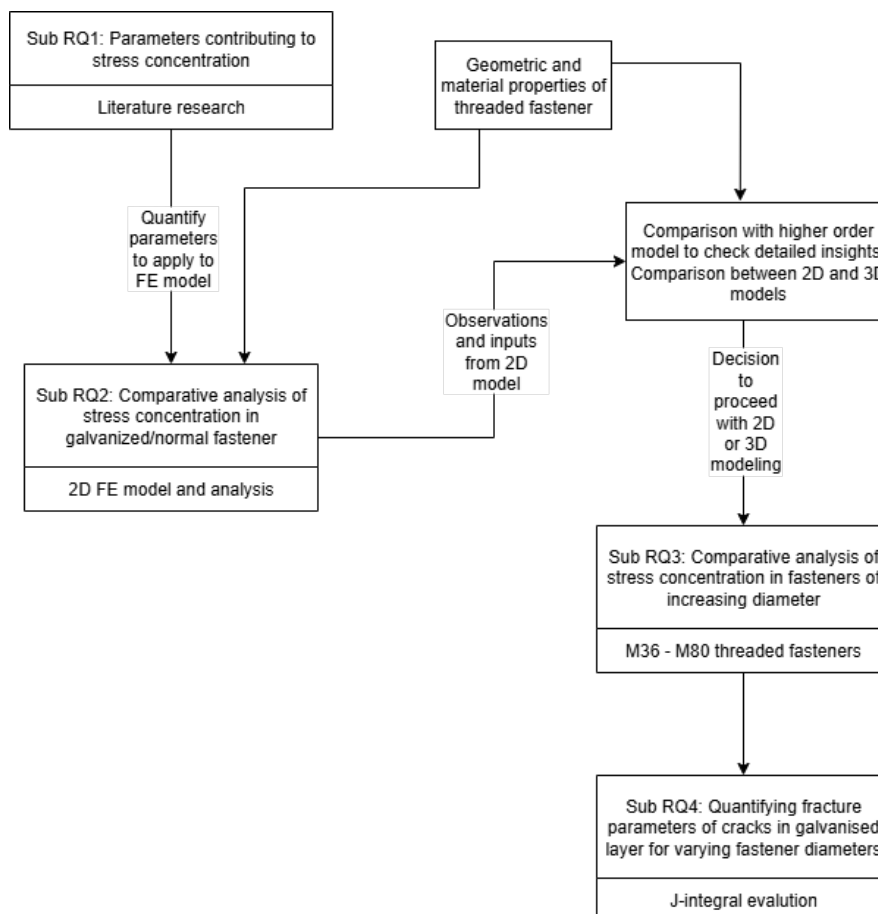


Figure 2.3: Research methodology

Chapter 3

Literature review

In this section, we shall look at the theoretical background of the research being conducted, with the help of literature sources and information obtained from other sources such as manufacturers and standards.

3.1 Production of threaded fasteners

Bolt-nut connections are important joining elements widely used in almost all engineering applications today. To a large extent, the efficacy of these connections depend on anti-loosening properties and high fatigue strength [40]. While a lot of studies from both structural engineering as well as mechanical engineering domains have focused on the anti-loosening performance of threaded fasteners, the fatigue aspects of these connections and improvements to them is still being developed, and this research also aims to support this development.

The manufacturing processes are in principle differentiated on the basis of whether the material is cut out from an original volume or formed into the required volume. The former is known as machining, where a controlled removal of material from a larger volume is done; the latter is known as forming, whereby metal parts are fashioned into the geometric dimensions required by mechanical deformation [33]. There is also a further differentiation within forming based on the temperature at which it is formed: they are cold and hot forming. As the necessary general dimensions of the fastener are achieved, the next step involves thread production. The production of threads is done by rolling, where the shaft of the fastener is rolled between two flat dies which creates the thread profile only by deformation of the surrounding material, thereby saving material. Figure 3.1a shows the process of thread rolling, and figure 3.6b shows the difference between a cut thread and a rolled thread. This process creates grain flow patterns as a result of dislocation of materials in threaded zones, as shown in figure 3.6b. With thread forming, the material is work hardened once again and the fiber pattern is not interrupted. Domblesky and Feng (2002)[12] in their parametric study showed material flow at different die penetration levels and discussed the strain contours which are lower in magnitude for the design profile compared to a profile with a different form, without rounding of the root. They also suggested the subdued effect of the blank diameter on the effective strain at thread root compared to other parameters like friction factor and thread form. It is important to notice the strain contours acting normal to the flow path represented in the study, throwing light on why thread roots are fatigue-prone critical regions.

Heat treatment of these fasteners is another critical procedure to ensure the microstructure is altered to ensure an increased hardness. As a usual practice which saves production costs, rolling is done before heat treatment due to which restoration of compressive residual stress occurs and no benefit to

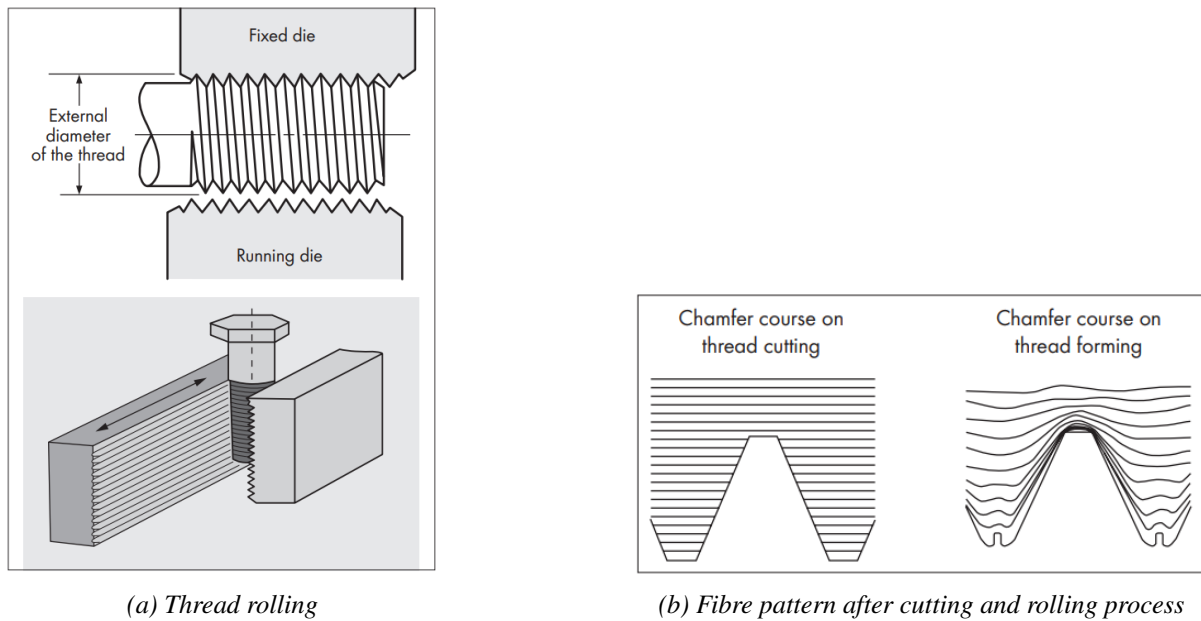


Figure 3.1: Characteristics of thread rolling

the fatigue resistance is observed. We shall consider this as one of the assumptions in our case study since it is commonly applicable to general connection standards.

An interesting point to mention as we talk about the production of threaded fasteners is the effect of the friction coefficient of the threads on the local stress distribution among engaged threads, which is governed by the rolling process. J.Braithwaite et al.(2020) [6] consider the effect of different friction coefficients by numerically evaluating the stress in engaged threads. The reduced friction coefficient is reported to improve the average stress in all the engaged threads, provided that the friction coefficient values of the external contact (nut-washer and washer-segment) friction coefficient values are equally small. Higher stress values at the threads beyond the first few engaged threads ensure an even distribution of the load, which is important in our case, as galvanization causes an increase in the coefficient of friction [9].

Another major point to be addressed here is the difference between fasteners, mainly the two types of external threaded fasteners - bolt and stud. Since we are discussing the application of preloaded fasteners mainly used in offshore ring flange connections, we shall consider the two types of external threaded fasteners manufactured by ITH Bolting Technologies, a major supplier of these bolting assemblies. Figure 3.2 shows the difference in components in each assembly.



(a) Bolt assembly configuration

(b) Stud assembly configuration

Figure 3.2: Types of ring flange connection assemblies in segment representation - IHF Fastener Systems

A bolt has a head on one end, designed to be inserted through one end of holes in assembled parts and secured with a nut. A stud is head-less straight shaft secured on both ends of the assembly by

nuts. As shown in figure 3.2b, the studs can be fully threaded or partially threaded as per requirement. Throughout this research, we have considered the analysis of a partially threaded stud since the material data available was for a stud-bolt. The boundary conditions in our global model setup (see Figure 4.1) considers a fixed boundary mimicking symmetry at the contact surface between segments in a ring flange connection. To keep up the symmetry throughout the setup, the partially threaded stud is modeled, considering a similar nut paired to the externally-threaded stud, with washer and segment on the other side of the boundary edge.

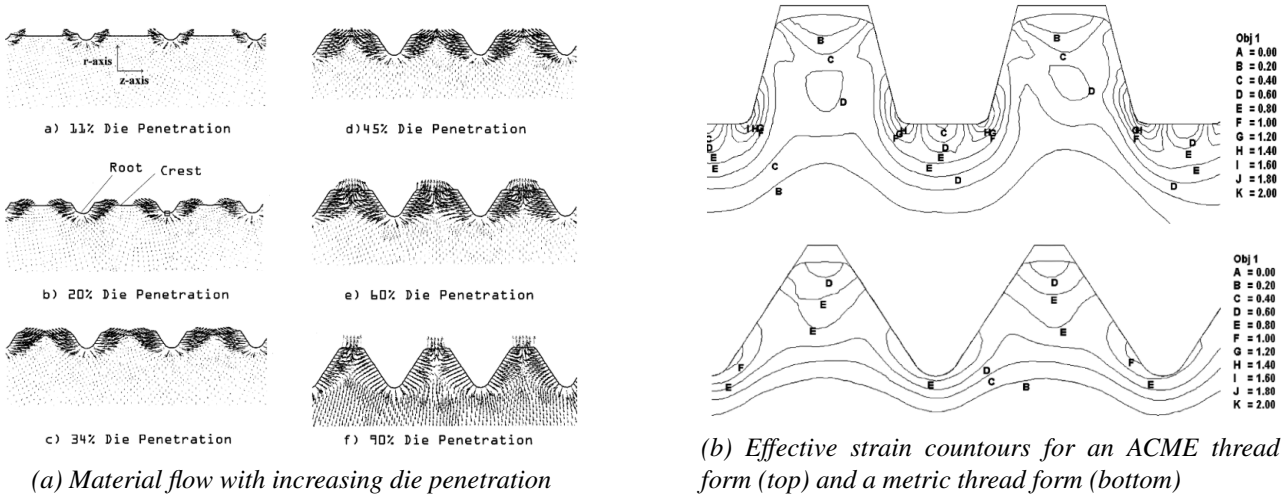


Figure 3.3: Results from parametric study - Domblesky and Feng (2002)[12]

A major characteristic of HV threaded fasteners is the increasing ratio of nominal diameter to the pitch (d/p) for increasing bolt diameters. Table 3.1 shows the d/p ratios for studs considered in our work. Even when the increasing ratio makes for a finer thread, it also leads to a sharper notch geometry which causes a increased stress concentration. This highlights the requirement of understanding geometric impacts on the stress-concentration, apart from the effect due to boundary layers, and will be discussed in our comparison of fasteners with different diameters.

Size of fastener	Pitch distance (mm)	d/p ratio
M36	4	9.0
M48	5	9.6
M64	6	10.7
M72	6	12.0
M80	6	13.3

Table 3.1: HV fastener sizes and d/p ratio

3.2 Preloading

Preloading refers to the tension created when a nut works with a bolt to ensure that two parts are held together, ensuring that the working load force would be borne by the connected flanges as well and not just the bolt assembly. Preloaded bolted connections are an important application in engineering structures today, spanning from piping and pressure vessels to ring flange connections of wind turbines supports [44]. This preload value ensures that fatigue failure and bolt fracture due to external forces do not cause a catastrophic failure [18], while ensuring that the contact stresses are not overcome at the design loads. Due to this preload, the variation in bolt stress is non-linear to the external loads, as shown in figure 3.4. Keeping in mind that external forces do not act as uniaxial tension or bending, but rather as a combination about various directions while being cyclic in nature, shows the importance of preload in maintaining a constant level of force in the bolt even in the presence of cyclic

external loads, providing fatigue endurance to the fastener. As seen in the image above, the bolt forces begin to increase non-linearly only when the flanges in contact begin opening, but still ensures that ultimate resistance of the connection remains the same even with preload application. Even though the performance of a bolt when tensioned to yield is best when considering its resistance to loosening and fatigue [46], standards only mention a limit to preload value of 70% the ultimate yield strength of the fastener. This is covered by numerical research conducted by El Bamby et al. (2024) [4], where it was reported that preloading up to 90-100% of the yield strength of the fastener causes a detrimental impact on the fatigue life of the bolts, especially at the fatigue-prone thread root where there already exists significant plastic deformation due to rolling. Even when a 100% preloaded connection has a flatter load transfer function graph and higher fatigue life, the effect of imperfections significantly influence the actual load on bolts, causing great uncertainty in actual bolt force at the ultimate tensile capacity of the bolt.

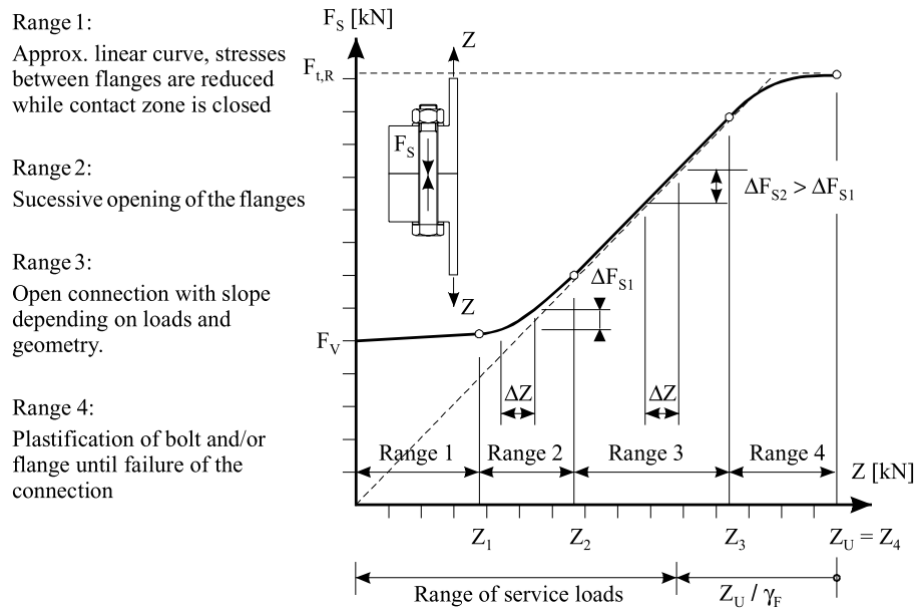


Figure 3.4: Bolt force vs. external force curve - Seidel and Schaumann (2001) [49]

The application of preload is done in engineering practice by different methods. For ring flange connections using HV bolts of large diameters, preloading is done using hydraulic tensioning. These devices stretch the bolt to a specified elongations, after which the nut is tightened against the flange, and the tensioner is released, leaving the bolt preloaded. The higher accuracy of preload level obtained by elongation of bolts is well-documented in literature, and therefore a preferred method for sufficiently large bolts [46].

3.3 Hot-dip galvanization

Hot dip galvanization (HDG) is one of the primary processes involved in coating steel articles with zinc for corrosion prevention measures, as it ensures quality at a low cost. In hot-dip galvanization (HDG), a protective zinc layer is formed by immersing steel pieces in a bath of molten zinc, thereby creating a series of steel-zinc alloy layers metallurgically bonded to the steel. The HDG process typically produces zinc coatings that are 45-200 μm thick. Therefore, the underlying steel is protected by two mechanisms: a physical barrier and electrochemical protection [2]. Figure 3.5 shows the steps involved in the HDG process.

The zinc coating makes the surface of a galvanized specimen different from an ungalvanized steel surface because of the difference in mechanical properties. Parameters such as coefficient of friction, stress-strain behavior, plasticity, and brittleness especially affect the local stress state in the case of

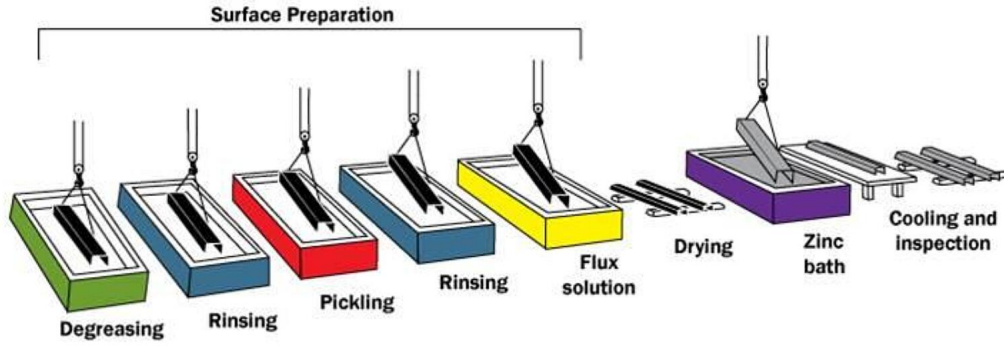
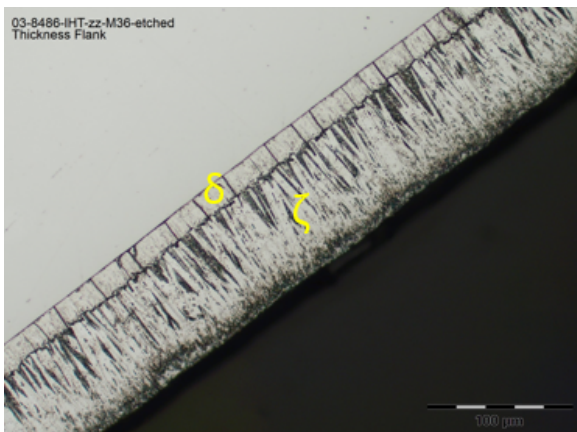
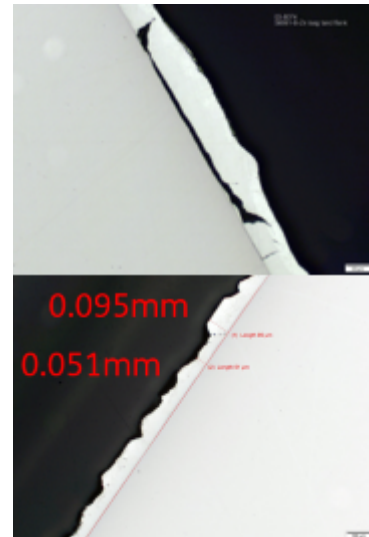


Figure 3.5: Hot-dip galvanisation process - American Galvanizers Association

engaged threads between threaded fastener connections. Zinc coating layers are easily damaged in severe plastic deformation under external pressure and sliding friction. Typical damages of the coating layers are cracking and powder-flaking [32], where the latter's degradation mechanism depends on the thickness of the Γ phase [47]. Since the electroscope images suggest the absence of a consistent layer of Γ inter-metallic phase, it is also noticed that cracking is a prominent failure, which is important to our study. The steel sample is subject to high temperatures during the process of hot-dip galvanization, which can have a negative impact of deterioration on the mechanical properties of high-strength steel items. Smak et al.(2021) [52] found that steel substrate with very high yield strengths (min. 1200 MPa and above) which were tempered at lower temperatures were affected the most, as their tensile and yield strengths considerably reduced after galvanization. Steel samples with yield strengths of 900 MPa and below had stable structural phases due to the tempering process at 550°C during manufacturing, and therefore did not have significant changes in their mechanical properties, except for hardness values as softening was observed irrespective of yield strengths due to a decreasing carbon content after the galvanization process.



(a) Galvanized zinc layer on unused M36 stud



(b) Galvanized zinc layer on two unused M72 studs

Figure 3.6: SEM images showing thickness of galvanized zinc layer (TNO)

As the literature has reported that no major differences in mechanical properties of the steel substrate occur after the process of HDG, our focus shifts to understanding the mechanical properties of the intermetallic phases produced by galvanization. This has been covered in detail in Chapter 4.

Based on the analysis of SEM images of hot-dip galvanized fasteners of M36 and M72 specifications, it was found that the thickness of galvanized zinc layer could be considered to be 75μm. It is

understood that the thickness of the layers depends on the chemical composition of the steel under consideration, which in turn also affects the strengths, yield and ultimate tensile, of the steel. This can be confirmed from the HDG coating thickness measurements in [51], which employ steel with similar mechanical properties. It must also be mentioned that the manufacturing process and quality control of the same also affect these measurements to a large extent. The manufacturer IHF with their StudBoltsTM and StretchBoltsTM are the major suppliers of fasteners used in ring flange connections of offshore wind turbines. The reliability of their processes supports our consideration of the constant thickness of the Zn layer, as supported by the SEM images for these fasteners from the manufacturer.

The presence of cracks in the brittle δ phase evident from the images is also reported in [14], [50] prior to loading of the specimen. These cracks cause a microscopic notch effect, leading to stress peaks at the boundary of the base material, which cause premature fatigue crack initiation. Crack initiation due to pre-damage of the base material by the liquid metal assisted cracking process could be disregarded as high temperature hot-dip galvanization is not done for large fasteners (M36 and higher) [41]. Oechsner and Schaumann (2016) [41] describes the influence of hot-dip galvanizing on the fatigue properties of steel. The major causes for this is mentioned as 1) brittle steel-zinc alloy phases, 2) cracks in zinc coating due to hot-dip galvanization, 3) crack which develop on these alloy phases due to cyclic loading and 4) penetration of zinc alloy phases into the base material. The correlation between decreasing fatigue strength and increasing thickness of zinc coating shows a detrimental impact beyond a thickness of 100 μ m. Glienke et al. (2023) [17] evaluated the fatigue performance of a large range of fastener diameters as part of developing detail categories for bolt assemblies. Part of the experiments were conducted on the IHF bolt assemblies of strength grade 10.9, which were pretensioned free of torsion. It was evaluated that the fracture in testing always occurred in the first load bearing thread, and the reduction in fatigue life of hot-dip galvanized bolts were attributed to microcracks in the steel-zinc alloy layers. Eder et al.(2018) [13] also mentions the effect of HDG on creating multiple crack initiation sites at the notch and the detrimental effect of thickness of the coating, through fatigue testing and numerical analysis. Throughout all these researches, a common conclusion is the requirement of a detailed numerical analysis approach considering the mechanical properties of these steel-zinc alloy phases, which will allow us to understand the occurrence of microcracks, its effect on crack initiation in the base material and further support the estimation of fatigue life of galvanized fasteners using efficient numerical approaches. The results of this study aims to throw light on these questions.

3.4 Finite element method

The design of connections or fasteners and understanding their behavior in highly-stressed conditions require a great deal of experimental preparation. Even then, in case of quantifying effects on a microscopic scale such as the local stress and strain at the location of thread root, it is still a tedious task when it comes to experimental setups, and rapid development in this front is happening currently. At the same time, the ability to include computational aids to analyze and understand these effects have also been developed with the rapid development in the technology age. The need to solve complex problems in elasticity and structural analysis, particularly in civil and aeronautical engineering in gave birth to finite element analysis (FEA) and modeling. The roots of FEA can be traced back to 1941. when Alexander Hrennikoff introduced a lattice framework for solving elasticity problems. In parallel, Richard Courant developed a method with a slight variation of using triangular sub-domains to solve partial differential equations, specifically for torsion problems in cylinders. Both approaches shared the essential concept of discretizing a continuous domain into smaller, manageable elements—a foundational idea for FEM. As a versatile computational method, FEM has matured today as an essential part of complex engineering system analysis and design, and is used to validate experimental findings and understand in detail the mechanism behind various engineering effects.

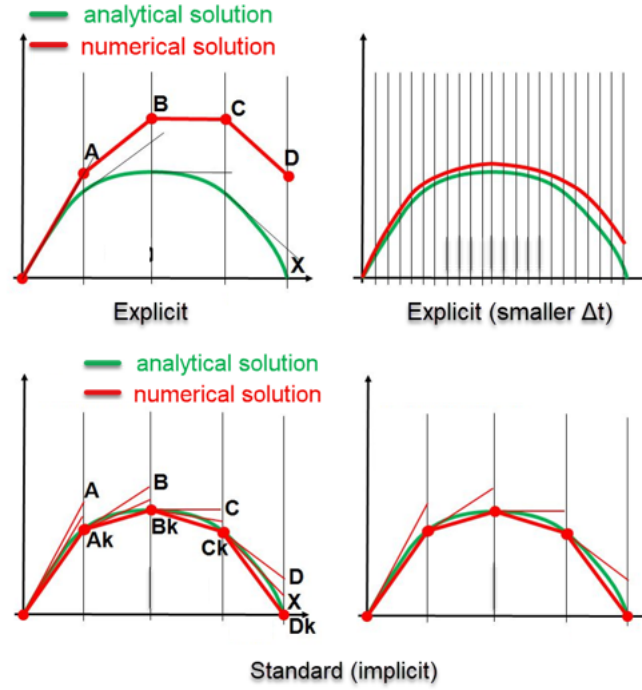


Figure 3.7: Different integration approaches used in explicit and implicit solvers

Today FEA has been commercialized and are used by all types of industries. In our research, we are using the ABAQUS FEA software suite developed by Dassault Systemes. This suite consists of Abaqus/CAE - the main user interface utilized for modeling, meshing and visualizing results. Abaqus provides two types of solver: the Standard solver and the Explicit solver. The Standard solver works with an implicit time integration approach, which is an iterative method used to ensure an equilibrium between internal and external forces at every time step, and reporting the results obtained from processing the differential equations forming the physical effect considered such as structural loading, thermal effects or pressure and more [31]. ABAQUS/Standard utilizes the Newton-Raphson iterative method to start with an initial guessed value and converge to the solution by iteration and monitoring the difference between consecutive estimates. The implicit solver approach is especially useful for smoothly evolving static or quasi-static, linear as well as non-linear problems. The Explicit solver employs an explicit time integration scheme, such as the central difference method, utilizing the parameters known from the previous step to the advance to the next step. The explicit solver does not require the iterative approach, thereby making it computationally inexpensive, but is highly dependent of the size of time steps used to ensure stability [31]. This can be seen in figure 3.7 where the explicit solution with small time steps are more consistent with the analytical solution. The explicit solver is more suited for highly non-linear or dynamic analyses or with models involving severe discontinuities. Even when our research on the local stress-strain state is of a geometrically complex fastener system, we have utilized the Standard (implicit) solver procedure for the analyses.

A general workflow of finite element analysis is as follows. A real life case of an experiment is first simplified or idealized into a physical model which can be represented on the FEM software. Next, this simplified physical model is defined with mathematical modeling attributes. They are features which are characteristic to that real life model. These include material properties, contacts properties, boundary conditions, loading conditions and the like. This is followed by discretizing the physical model, which is a major component of the finite element methodology. Discretization refers to the division of model body into an equivalent system of many smaller bodies interconnected at points common to two or more elements. The mathematical attributes of the full model is also applicable to these small elements. With the help of the previously mentioned solving scheme, the finite element program calculated the first set of displacement unknowns at the nodes of these elements. With the

help of constitutive equations, which are defined as attributes to the model, the first set of solutions are used to quantify the secondary unknown quantities, which are the stress and strains [22].

The advantage of commercial FEA packages such as ABAQUS is the freedom it gives to define the attributes for the physical model, such as the geometric domain, element type, material properties, element connectivities, physical constraints and contact properties. This is also partially disadvantageous since too many variables and their different values can have a great impact on the results obtained, and this shows the necessity of validating the numerical results with experimental outputs. In case of our scope involving modeling the engaged fasteners, the most important of these parameters affecting the validity of results were the material properties and contact.

We shall first discuss about contact configuration and definition which is important in our analysis. We shall start with the discretization of contact, which broadly varies between surface-to-surface contact and node-to-surface contact. The former discretization method enforces contact averaged over the element surface in contact, unlike the latter where the position of a node on the slave surface interacts with its projection on the master surface. The consideration of shape of both the slave and master surfaces ensures and optimizes stress accuracy, therefore recommending and considering surface-to-surface contact for all surfaces. The contact tracking algorithm comes next. When we define surface-to-surface contact discretization, we must also specify the sliding formulation which will track the relative position of nodes on the 'slave' surface. Firstly, we must decide whether the magnitude of sliding will be small or finite. The small-sliding contact assumes that there will be relatively little sliding between surfaces, therefore can be based on the linearized approximations of the main surface per constraint. The groups of nodes involved with individual contact constraints are fixed throughout the analysis for small-sliding contact, although the active/inactive status of these constraints typically can change during the analysis. Finite sliding allows arbitrary motion of surfaces. This is therefore computationally expensive as it updates the contact pair positions for every iteration. Since the contact in our case is predefined between the flanks of internal and external threads, and the relative sliding is small compared to the dimensions of the faces in contact, we shall use the small sliding formulation.

Modeling the inter-metallic layers to capture the effect of boundary layers is the general aim of this study. Therefore, we need to understand any special considerations to be kept in mind, so that the finite element analysis captures the effects of localized stress-strain. As mentioned earlier, researchers in the past have represented the effect of these boundary layers with the help of simplified engineering models interpreted analytically from experimental test data. But the research gap in identifying and understanding the exact effect on these inter-metallic layers, and the probable effect it can have on the substrate, was identified and we look forward to answer this in this research. From the background to considering the constitutive model of the effect of Zn layer on the steel substrate, results suggest that zinc coating has a definite effect on the steel substrate, but it could not be concluded whether there was an enhancement (positive) or reduction (negative) in the effect it had on steel substrate. Therefore, it was recommended not to neglect the zinc layer in a galvanized specimen, and its independent mechanical model must be established [32]. Few researchers report the advantage of using Cohesive Zone Modeling (CZM) with a predefined traction-separation law. This is advantageous when we require insights into effects such as delamination, but our scope is limited to local stress-strain effects due to thread engagement, and cracks forming perpendicular to the thickness of the zinc layers, which might cause micro stress peaks causing crack propagation into the steel substrate [20][32].

3.5 Fracture mechanics

The principles of fracture mechanics help us effectively quantify the issue of crack initiation and growth at hand. Conventional failure criteria has been defined for ductile and brittle materials. The von Mises criterion defines the yielding of ductile materials, while brittle materials experience frac-

ture without much plastic deformation, and criteria like the Coulomb-Mohr criterion is defined for the same [16]. These are macroscopic failure criteria which describes the onset of yield and fracture in ductile and brittle materials respectively. But it was understood early on that some failures, especially those of high-strength materials, could not be adequately explained by these design criteria. Alan Arnold Griffith observed that the discrepancy between observed strength of materials and their theoretical strength was attributed to the presence of discontinuities or flaws in the material. What is to be understood here is that fracture causes the formation of new surfaces, which requires spending energy irreversibly. Therefore quantifying this energy available at the tip of a crack will enable us to tell if a crack would propagate faster into a material in comparison to another crack.

Almost all materials which we consider in structural engineering has some amount of plasticity at the tip of a crack. The extent of plastic zone can be verified by analyzing the stress field around a crack tip, and comparing it to the yield strength of the material. This can be verified from our results which compare the von Mises stress plots equalizing beyond a particular depth from the crack tip in all fastener models. Theoretical studies [16] as well as manuals of finite element analysis [1] suggest the use of path independent J-integral as a fracture criterion, for elastic-plastic materials, supported by experiments and numerical analysis. It represent the amount of mechanical work or strain energy available per unit area of newly created crack surface, as the crack propagates. Therefore, this value measures the intensity of deformation field at the tip of the crack, which is directly related to the driving force for crack growth, and we shall consider the elastic-plastic fracture mechanics (EPFM).

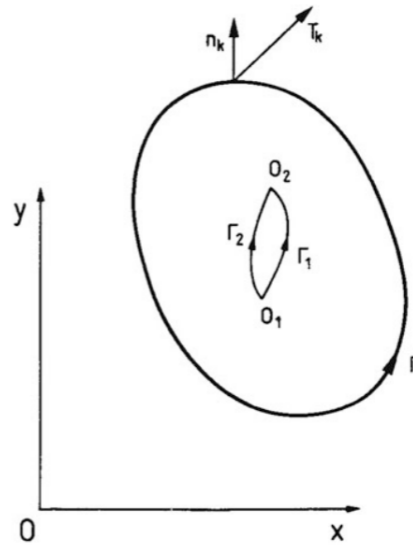


Figure 3.8: A representation of closed contour for J-integral calculation [16]

For a region R , consider Γ to be a closed contour bounding this region. The formula for J-integral is then given by

$$J = Q_1 = \int_{\Gamma} (\omega n_1 - T_k u_{k,1}) ds \quad (3.1)$$

where

$$n_1 = \frac{dy}{ds}. \quad (3.2)$$

and ω is the strain energy density and T_k is traction vector. For a closed contour, the value of J-integral is zero. But in the presence of a notch or a crack, the J-integral is calculated from an arbitrary point on one of the crack surfaces to another point on the other surface, defining another closed region bound

by the closed contour, as seen in image 3.9.

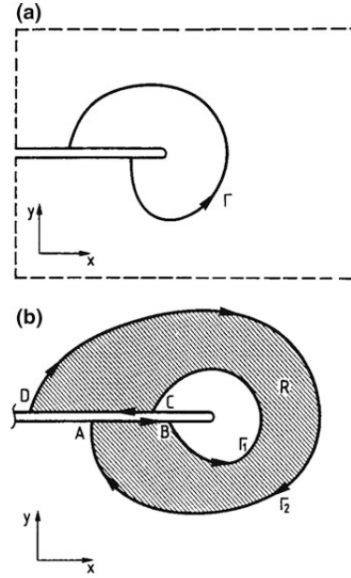


Figure 3.9: A representation of contour for J-integral calculation at crack tip [16]

For a mixed-mode stress field, as we notice in the stress distribution at engaged thread root in the subsequent analyses which is predominantly Mode I but also includes stress in Mode II, the J-integral value is governed by the stress intensity factors of the three modes, which in turn is governed by the stress state, initial crack length and geometric considerations of the thread geometry. In the equation below, $\eta = 1$ for plane stress and $\eta = 1 - \nu^2$ for plane strain.

$$J = \frac{\eta K_I^2}{E} + \frac{\eta K_{II}^2}{E} + \frac{1 + \nu}{E} K_{III}^2 \quad (3.3)$$

The applicability of this fracture criterion holds true only when the J-integral value is path independent, which is only possible when monotonic loading is considered, without any unloading. This is true in the case of axial preloading we have considered here, thereby making the comparison of results valid.

3.6 Summary

Here we shall summarize the input parameters considered in our numerical research, which is supported by results and observations from other experimental or numerical research conducted previously. Therefore this summary serves to identify the most important values utilized further in our numerical research, along with their sources.

Geometry		
Input parameter	Value	Source
Thread pitch	(in Chapter 4)	EN14399-4:2015 [15] upto M36, DAST-021 [10] for M48-M80
Other geometry parameters	(in Chapter 4)	ISO 68-1:2023 [27]

Table 3.2: Geometry parameters

Material		
Input parameter	Value	Source
Material properties of δ and ζ phases	Table 4.2, Table 4.3	Okamoto et al. (2013) [42], (2018) [43]
Material properties of steel substrate	Table 4.1	Specimen tensile test data - TNO

Table 3.3: Material parameters

Contact		
Input parameter	Value	Source
Friction coefficient - Galvanized surface	0.3	Collini et al. (2024) [9]
Friction coefficient - Ungalvanized surface	0.2	Shakeri et al. (2022) [50], Eichstadt (2019) [14]

Table 3.4: Contact parameters

Chapter 4

Two-dimensional analysis

After an extensive study involving understanding the state-of-the-art and various parameters applicable to this research, we move on to practical matters: starting with the numerical modeling and analysis of 2D axisymmetric models.

4.1 Geometry and model setup

The geometries of the threaded fastener under consideration is implemented according to ISO 68-1:2023 [27]. This is considered in accordance to the industry standard produced by a technical working group representing all parties of the supply chain for fasteners used in wind turbines. Looking at the basic and design profiles for metric screw threads, specifically for an M36 fastener having a 4 mm pitch, we see the difference with respect to the rounding off at the thread root. This inclusion came as a revision in 2023, prior to which only the basic thread profile was defined for both internal and external threads. It is understood that a curvature at the thread root minimizes notch effects, improving the fatigue life [37][39]. While the internal threads retain their flat design profile at the thread root to avoid interference and maintain the thread engagement strength by ensuring sufficient contact. The rounding off at thread roots is also a result of manufacturing feasibility as rolled threads inherently produce rounded roots due to the die geometry.

The introduction of galvanized zinc layer on the fasteners brings forth considerations for tolerances. As per ISO 10684:2004 [24], there are two different methods for mating threads of nuts and bolts after hot-dip galvanization, since the thickness of these layers are upwards of 40 μ m, and therefore requires special limits to accommodate such coatings. The first method uses oversize nuts of tolerance class 6AZ/6AX after coating mated with bolts or studs manufactured with threads to tolerance position g/h before coating. The second method consists of using external bolts or studs manufactured with threads undersized to tolerance class 6az before coating, to mate with nuts tapped to tolerance position H or G after coating. For all subsequent analysis we have considered the former - 6AZ/6g - as it would be beneficial in our comparison between stress concentration effects of ungalvanized and galvanized threaded studs to have the original dimensions of the steel substrate in the stud to be similar. As per Table 2 of ISO 965-2:2024 [25], the major diameter for an M36 external screw thread of tolerance class 6g is in the range of 35.94 mm - 35.465 mm before galvanization. Similarly Table 2 of ISO 965-5:1999 [26] specifies a minimum major diameter of 36.38mm after galvanization. The geometry considered for the two-dimensional model is checked to fit these ranges and limits.

For the thickness of hot-dip galvanized layer, we use data available from TNO on the characterization of M72 bolts and M36 studs obtained from IHT, a major supplier of fasteners for wind turbine supporting structures. Based on the scanning electron microscope imagery of galvanized fasteners, the

average thicknesses of zinc layer at the crest, flank and root locations are provided, along with their standard deviations. Based on this data, a standard thickness of 75 μm is considered for the zinc layer at all locations. As for the thickness of individual phases in the zinc layer, further visual analysis of the SEM imagery is considered. As shown in Figure 2.1, the thickness of the δ phase is considered 15 μm while the thickness of ζ phase is considered the remaining 60 μm .

Moving on to the global model setup, we shall first introduce all components considered in this model. As can be seen in Figure 4.1, the model consists of a threaded stud, a threaded nut, the washer and the segment. All these elements are considered symmetric about the vertical axis for this initial phase of analysis. The ease with respect to time and computation power, and the validity of results obtained in two-dimensional analysis when compared to a full three-dimensional analysis has been reported in literature[14], which support the initial study using an axisymmetric approach. The geometric properties of washer is obtained from [29], with a diameter of 37mm considered for the clearance hole and an outside diameter of 66mm. The geometric properties of the segment was considered according to [8].

The ring flange connection is the most common type of connections used for offshore wind turbine supporting structures. Previous numerical and analytical studies conducted to analyze various aspects of this connection has followed the segment approach for modeling. Literature sources consider the segment approach to understand effects ranging from load transfer between imposed loads and bolt force [8] to the effects of high preloading forces on ring flange connections [4] to the effect of manufacturing defects on lifetime of high-strength steel bolts [50]. Our consideration of studs for fastening provides the opportunity for physical symmetry about the contact surface between the top and bottom ring flange segment. Therefore the boundary condition is considered fixed about the contact surface at the bottom of the segment, as shown in Fig 4.1. The ENCASTRE boundary condition in ABAQUS is utilized to ensure rotational and translational fixity in all orthogonal directions.

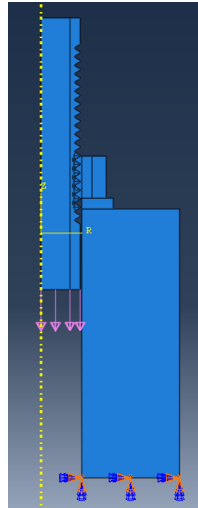


Figure 4.1: Snapshot from the two-dimensional model in ABAQUS showing the boundary conditions

To calculate the magnitude of preloading to be applied, the European Standard for high-strength structural bolting assemblies for preloading [15] suggests designs to allow preloading of at least 70% of nominal tensile strength of the threaded fastener, so as to obtain ductility predominantly by plastic deformation of engaged threads. The stud was loaded with a pressure applied to its lower cross-section. Eichstadt (2019)[14] reports that the local plastic strain at thread root developed when considering bolts subjected to rotational tightening are in similar order of magnitude when compared to axially preloaded fasteners.

4.2 Inter-metallic phases

A key output expected from the axisymmetric analysis of galvanized threaded fasteners is the effect of galvanization on the stress state at engaged thread roots. This is quantified on the basis of local stress and strain developed at these locations. This comparative analysis to the results from an ungalvanized fastener model will be reported and discussed subsequently, helping us understand the effect of galvanization on the threaded steel substrate.

The inter-metallic layers formed as a result of normal hot-dip galvanization is reported by various material researches. The coating layer of hot-dip galvanized zinc consists of thin layers of Fe-Zn inter-metallic compounds with decreasing Fe content as we go outwards from the steel substrate layer [42]

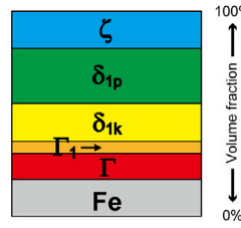


Figure 4.2: Schematic of inter-metallic layer in increasing order of Zn content from the steel substrate [42]

The applicability of these phases and transition between them is verified using the characterization of threaded fasteners. As specified in the scanning electron microscope images, the major phases present in the inter-metallic zone are the δ and ζ phases, with certain patches with pure Zn η -phase. The presence of these two phases in centrifuged, normal hot-dip galvanized specimen is also reported by [41], validating our consideration. Since the η phase is not consistent throughout the surface of the stud, this layer has been disregarded in the model.

The δ phase is one of the first formed layers, which then contributes to the formation of ζ phase through a peritectic reaction with liquid Zn, which is the reaction between a solid phase and a liquid phase to produce a second solid phase. The ζ phase produced through this reaction contains 5-6.2% by weight of Fe content [20]. As seen in Figure 4.2, the presence of two slightly different structures within the δ phase is reported by various researchers, with the δ_{1k} phase on the Fe-rich side and δ_{1p} phase on the Zn-rich side. However, studies have shown that the morphological structure is the only difference between the two, with the mechanical properties, which is of our concern, remaining the same [20]. The δ phase contains 7-11.5% by weight of Fe content.

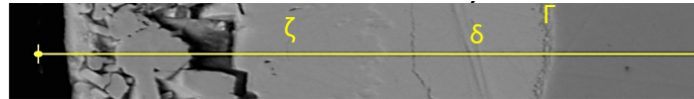


Figure 4.3: SEM image showing scale of thickness of each inter-metallic layer

The formation of Γ phase is also evident from the scanning electroscopes images, but the thickness of this layer is very minute compared to the other inter-metallic layers. In the numerical analysis of identifying local stress and strain, it is important to have all layers modeled consistently with respect to number of elements present in the through thickness of each layer. As a rule of thumb in , each layer must have at least two elements, and this guideline is rooted in numerical accuracy and physical representation of stress and strain gradient across thin layers, which is important to our research. These inter-metallic layers can exhibit steep stress or strain gradients through their thickness, especially under mechanical loading. Therefore one element would not capture these effects sufficiently and may lead to inaccurate results [34]. Having a poorly refined mesh can also create numerical integration errors at places where there is a change in material properties, which is the case with our

study, therefore requiring more than one integration point or element [7]. The thickness of Γ phase in all images analyzed is less than $5\mu\text{m}$, requiring a mesh seed size much smaller than what is deemed sufficient for convergence of calculated stressed and strains, as discussed subsequently. Therefore we have decided to forgo the Γ layer in the model.

4.3 Material models

The choice of material models to be considered was an important one to make so as to simulate the stress state during engagement as close to reality. As part of this study, we have made two choices with respect to material models: one for the steel substrate and the other for the inter-metallic Fe-Zn layers.

4.3.1 Material model for steel substrate

For the purpose of numerical analysis to replicate stress state as close as possible to reality, we have calibrated the actual specimen test data for an M36 studbolt of Grade 10.9 available from TNO. This was considered among three different choices about the material model. The second choice was to consider the elastic-plastic mechanical properties, calculated from the nominal mechanical properties for 10.9 grade fasteners available from Table 3 of ISO 898-1:2013 [28]. To interpolate the stress-strain graph in the plastic strain-hardening region, the Hill formulation is used, which is a simplification of the Ramberg-Osgood relationship, which is used in the absence of material-dependent parameters obtained from experimental testing. The Hill equation is described as

$$\varepsilon = \frac{\sigma}{E} + 0.002 \cdot \left(\frac{\sigma}{\sigma_{YS}} \right)^n \quad (4.1)$$

where n is the parameter for curve accuracy, given by

$$n = \frac{\frac{\varepsilon_{max} - \frac{\sigma_{UTS}}{E}}{0.002}}{\ln\left(\frac{\sigma_{UTS}}{\sigma_{YS}}\right)} \quad (4.2)$$

The third choice involved utilising stress-strain data available from strain-controlled constant amplitude cyclic material tests conducted by Oechsner et al. (2015). Cyclic material parameters required to process the experimental data to the Ramberg-Osgood regressions was available in Eichstadt's dissertation (2019)[14]. The converted true stress - true strain data plots are as shown below in Figure 4.4

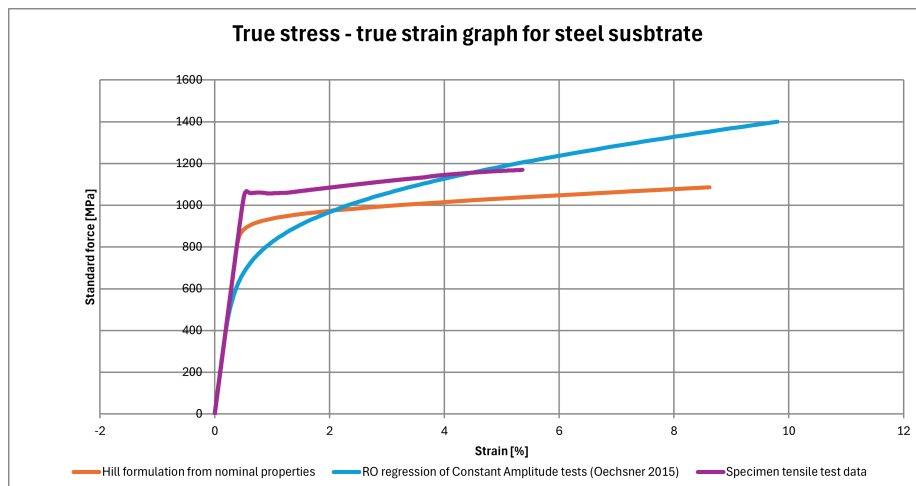


Figure 4.4: True stress vs true strain plot of steel substrate material model choices

In the end, the decision to proceed with the M36 specimen tensile test data was based on three factors. Firstly, the data was readily available with the team at TNO, making the processing of data easier. Secondly, the test data available was from an actual M36 stud bolt with TNO, making the applicability of this data most suited for the analysis at hand. Third, as the focus of this research is to understand the local stresses and strain under the effect of preloading the threaded fastener, the tensile test data was better suited for the scope of study compared to the data available from the CAT test.

With the help of material calibration option available in ABAQUS CAE, we import the test data available in their engineering form. This is first converted to its true form, followed by quantification of Young's modulus, which is given below.

Young's modulus (MPa)	Poisson's ratio (-)
205019	0.33

Table 4.1: Elastic properties of steel substrate

4.3.2 Material model for inter-metallic layers

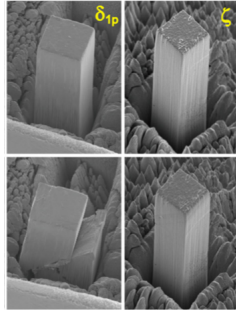
Focusing on the question we have at hand, the choice for a suitable material model for the inter-metallic Fe-Zn layers had to be so as to capture the tensile behavior of these layers at the engaged thread root during pretension. The brittleness of some of these inter-metallic layers is reported, albeit through nano-indentation tests. Typically, in the elastic region, the stress-strain response is the same in both tension and compression for most isotropic, homogeneous materials. Therefore, the modulus of elasticity is generally identical. The difference is evident in the plastic, or large deformation region. In case of tension, ductile materials exhibit necking, where deformation is localized to a small region with reduced cross section area, while brittle materials exhibit sudden fracture. Under compression though, materials typically do not neck and rather has an increase in loaded area due to barreling effect, thereby the ability to withstand higher loads without localised failure. The failure modes in case of compression is also different from that in tension.

Fatigue failure of bolts is reported as the most frequent cause for catastrophic failure of wind turbines, and the formation of cracks at the notch-like thread root followed by their propagation into the body of the fastener is a topic of focus for identifying the effect of galvanization on cracking of bolts and their fatigue performance [13]. Therefore, the tensile characteristics of the inter-metallic layers must be used to numerically replicate the failure mechanism.

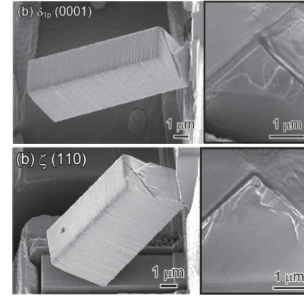
The material properties of inter-metallic layers have been reported by researchers in the past. Okamoto et al. has conducted extensive studies on the both the compression deformability by uniaxial compression tests [42] as well as [43] fracture toughness by micro beam bend testing. The brittleness of the δ phase is consistently reported by both these literature, while the ζ phase is comparatively ductile, even though a weaker layer as seen in the stress-strain plots. The ζ layer has the ability to attain plastic strains, signifying the deformability of this layer while the δ phase fails by fracture. The consistency of results reported by both these researches and its validation based on both compressive and tensile behavior makes it a good candidate for adoption in our study.

The material data obtained for the inter-metallic layer are given below in Tables 4.2 and 4.3.

The brittleness and fracture property of the δ layer is defined in ABAQUS using the ductile damage definition. The fracture strain is obtained from the stress-strain curves from [42], while the value for stress triaxiality is not mentioned in any of these studies. As reported by Yang et al. (2021) [54], the stress triaxiality governs whether the fracture would be by shear mode or void growth mode. Since



(a) Compression tests by Okamoto (2013)[42]



(b) Microbeam bending test by Okamoto (2018)[43]

Figure 4.5: SEM imagery of compression and bending microbeam testing by Okamoto et al.

δ phase properties	
Property	Value
Modulus of Elasticity (E) (GPa)	110
Yield strength (MPa)	1100
Poissons' ratio	0.33

Table 4.2: Material properties of δ phase [42][43]

ζ phase properties	
Property	Value
Modulus of Elasticity (E) (GPa)	82.4
Yield strength (MPa)	120
Poissons' ratio	0.33

Table 4.3: Material properties of ζ phase [42][43]

we are discussing here tensile fracture of the inter-metallic layers, it is suitable to consider a larger positive stress triaxiality. A value of 1.5 is considered following a convergence check.

The stress-strain curves of inter-metallic layers in their plastic region is given below.

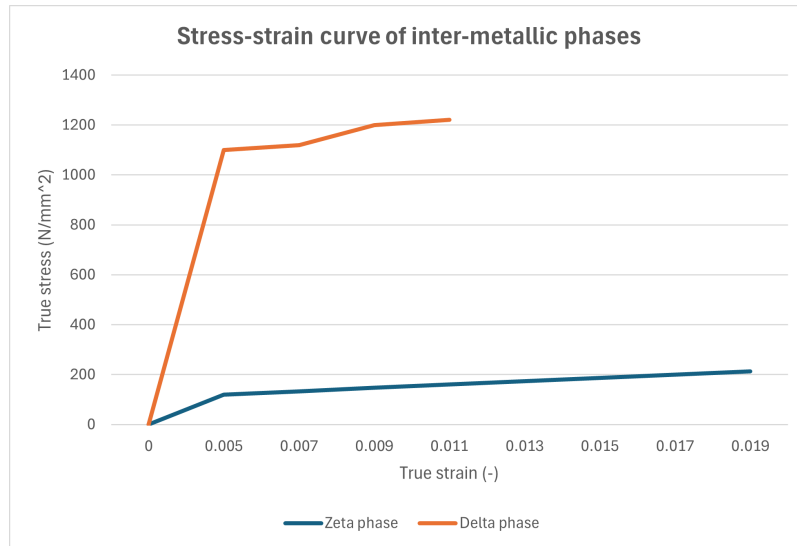


Figure 4.6: Stress-strain curve of inter-metallic phases as per Okamoto et al.[42][43]

4.4 Contact definition and thread interaction

When it comes to understanding the local stress and strains due to engagement of threads in fasteners, considering the right contact conditions along with interaction properties is indispensable to achieve optimum results. This needs to also be validated by experimental results or other numerical stud-

ies. In the case of the study, contact occurs between the engaged threads, the nut-washer and the washer-segment. Each of these contact and their properties will be discussed subsequently, with more emphasis on the thread contact.

The small-sliding formulation is considered for modeling the contact surfaces in ABAQUS/Standard. This allows efficient computation when the contacting surfaces undergo small sliding relative to their physical dimensions. The geometry of threads are designed in such a manner that slip or relative sliding is not prominent compared to the thread flank length in contact with each other. This formulation assumes that the nodes on the slave surface will interact with the same local area of the master surface throughout the analysis, which is true in our case.

The surface-to-surface discretization is considered here. This requires the identification of master and slave surfaces. It is general practice to have a rigid surface defined as the master surface and a deformable surface as the slave surface. In our study, both these surfaces have the same properties, therefore distinction between them is based on the stiffness of the structure that the surface is attached to. Thus, the external thread surface of the stud is considered the master surface, and the internal thread surface of the nut is considered the slave surface.

Another important consideration is the use of adjustment zones to control penetration of the slave surface into the master surface. In our analyses, we have specified a value of 0.0 as the depth of adjustment zone, implying that slave nodes which are overclosed (penetrating) in the initial configuration will be moved to be on the surface of the master node, thereby preventing convergence problems[1]. Due to the large control we have in terms of geometry in the two-dimensional approach, this does not come as a strict requirement, but this has been carefully enforced.

As for the contact property definition, the tangential and normal mechanical behaviors have been defined. The penalty friction formulation is considered for the tangential behavior, as we have the coefficient of friction (μ) for galvanized and ungalvanized surfaces. The friction coefficient between ungalvanized surfaces is assumed to be 0.2 from contemporary literature [50][14]. Experiments to quantify the friction coefficient for galvanized contact surfaces was conducted by Collini et al. (2024)[9], with values averaging at 0.3. To further elaborately consider the sticking and slipping conditions of the engaged threads, the critical shear stress limit is considered. As seen in Figure 4.7, the relationship is analogous with the elastic-plastic bilinear material behavior without hardening, where κ corresponds to the modulus of elasticity (E) and τ_{crit} corresponds to the yield stress. This critical value is the yield stress of the material in pure shear, which is $\sqrt{3}$ times lower than the tensile yield stress, as specified by the von Mises yield criterion.

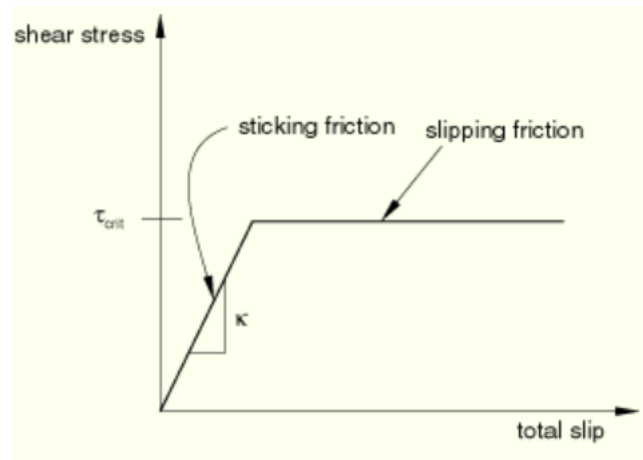


Figure 4.7: Shear stress vs total slip relation [1]

As for the mechanical normal behavior, the hard contact pressure-overclosure relationship is defined. This enforces the zero penetration condition based on the constrain enforcement used. Figure 4.8

shows the graphical representation.

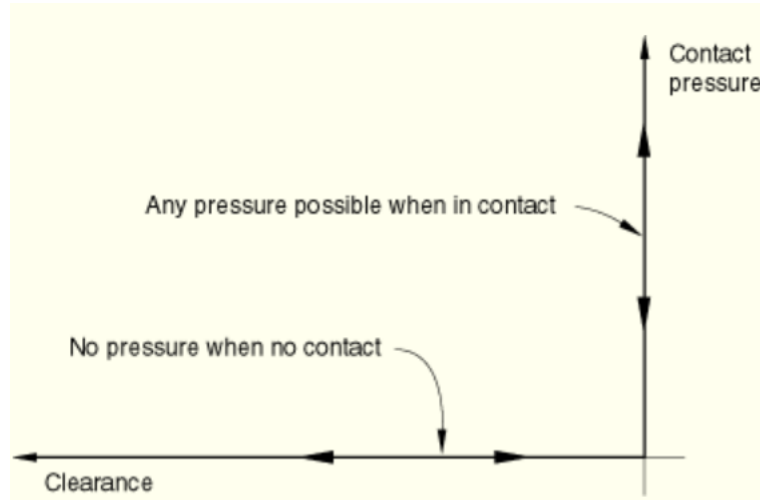


Figure 4.8: "Hard" pressure-overclosure relationship [1]

The direct method for constraint enforcement is considered, as it enforces the given pressure-overclosure behavior without the need of augmented iterations to calculate optimum contact stiffness. This was optimal for a two-dimensional model for solution accuracy. The toggle to allow separation after contact is turned ON for thread contacts, while for nut-washer and washer-segment contacts, they are considered to be in contact throughout to ensure the load path.

4.5 Meshing and sensitivity studies

Optimum and efficient mesh seed and element sizes to allow accurate numerical results while keeping computation times within efficient limits is important to our study. To this extent, mesh seed sizes are evaluated based on the geometric dimensions of the regions of focus in our study, followed by careful partitioning of parts and supported by a mesh convergence study for the same. The mesh seed considered at the thread root is 0.005mm, which was used for both the galvanized and ungalvanized models. The necessity of a fine mesh was confirmed after modeling the inter-metallic layers, each of size 0.015mm and 0.06mm. As we move away from the thread root to the core of the stud, the mesh seed is increased to 0.01mm, then to 0.02mm. Beyond the region of focus, at a distance of 2mm from the thread root, the seed size is kept at 0.2mm, and this is extended till the centerline of the model. Mesh seed consistent with the one described above is also applied to the ungalvanized model since it would aid effective comparison between local stresses and strains. Figures 4.9 and 4.10 represent the meshing applied to the galvanized fastener model. The washer and segments are meshed with a coarser global seed of 0.5mm.

To confirm the convergence of results with the mesh size considered, a mesh sensitivity study is conducted on the model. The model without galvanization layer incorporating linear-elastic material properties is considered in this study to negate the effect of thin boundary layer affecting the results when sufficient through thickness using mesh elements is not provided. The choice to have mesh sensitivity study conducted on the model with linear elastic properties is owed to the magnitude of change and convergence perceivable at the thread root radius. In case of elastic-plastic material behavior, we see in later discussions that the plastic redistribution brings the stress state at this region almost equal in all geometries of fasteners. This is also applicable to a changing mesh density, which does not report any major change with a decreasing mesh seed value. The table below shows the stress values calculated at the horizontal point at the thread root (corresponding to 0°). The graph in

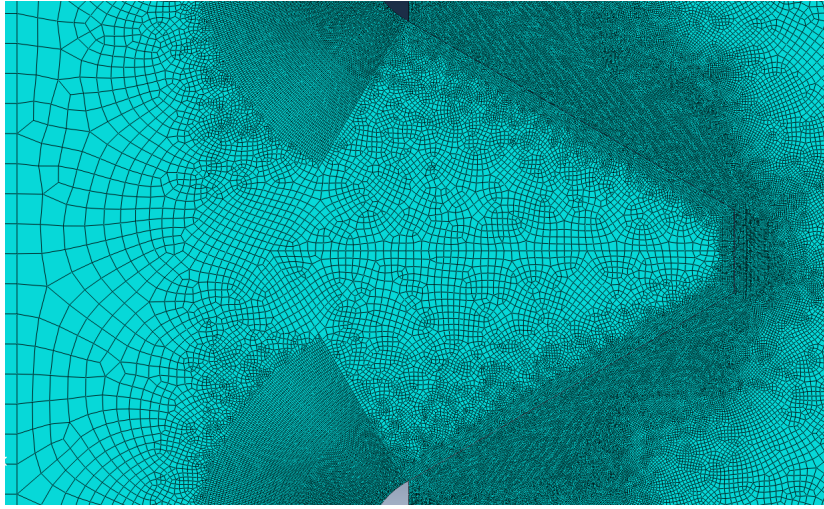


Figure 4.9: General mesh layout of first engaged thread

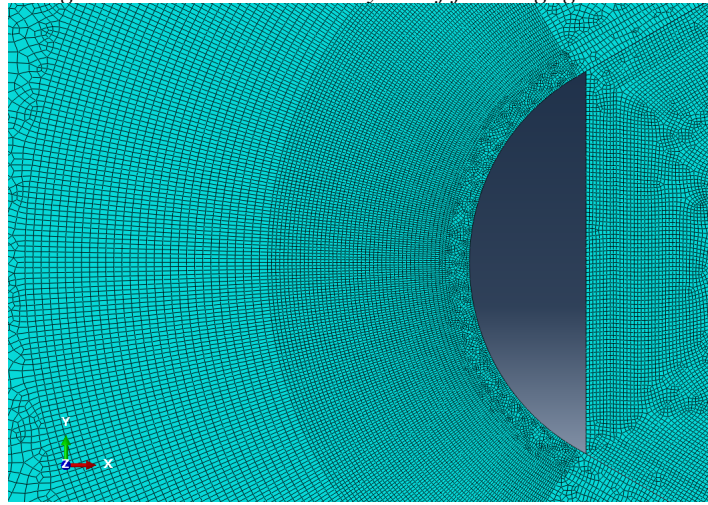


Figure 4.10: Mesh layout at thread root

figure 4.11 also shows convergence at 60 elements along the thread root radius, signifying that any mesh size smaller than 0.02mm is considered appropriate.

Mesh size (mm)	No . of element along thread root radius (= 1.2mm)	Principal stress (N/mm ²)
0.2	6	3211
0.1	12	3340
0.05	24	3783
0.02	60	3980
0.01	120	4050
0.005	240	4090

Table 4.4: Mesh sensitivity results

Based on these results, and keeping in mind the requirement of a minimum of two elements in the thickness of the thin δ layer, the decision to go ahead with a mesh size of 0.005mm along the thread root was made.

4.6 Results

The results from the analyses on two-dimensional models will be done in two parts: first we shall look into the results obtained from model consisting of elastic material model and then we shall cover data

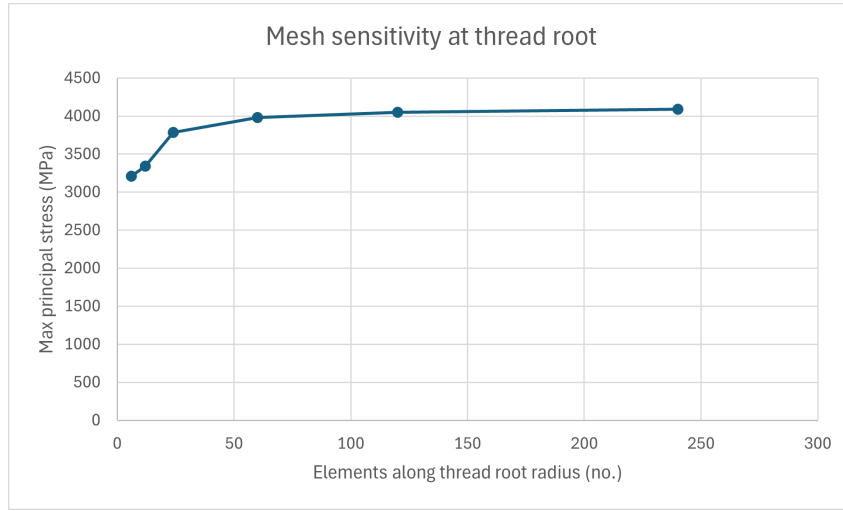
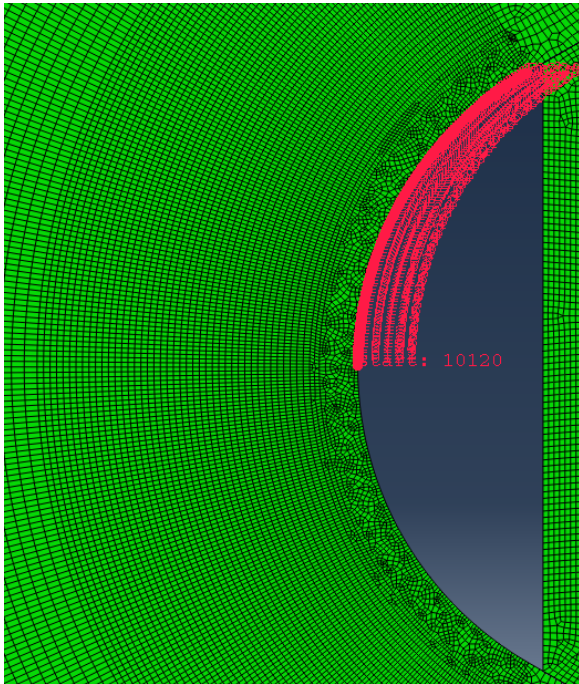
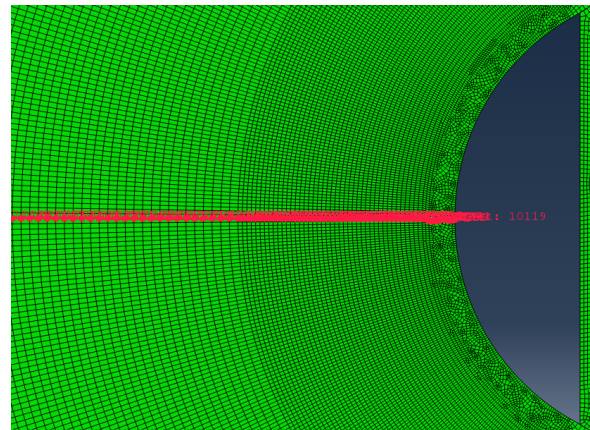


Figure 4.11: Mesh sensitivity plot showing convergence in values beyond 60 elements along thread root radius

obtained from the analysis of the model implementing elastic-plastic material properties, followed by a comparison in the next section. Before this, we shall defined the paths used to calculate and plot the values of stress and strain in the results below. Figure 4.12a defines the path along the thread root radius of the first engaged thread. The half thread root radius path is considered to understand the concentration of stress at an angle calculated from the normal. Figure 4.12b defines the path through the critical section at the first engaged thread root. The path starts from the point on the boundary of the thread root, which would be the lowest point at the first engaged thread root, to the line forming the central axis of the stud.



(a) Path along half thread root radius. Equal to 0.6mm for M36 stud



(b) Path through critical section at first engaged thread root

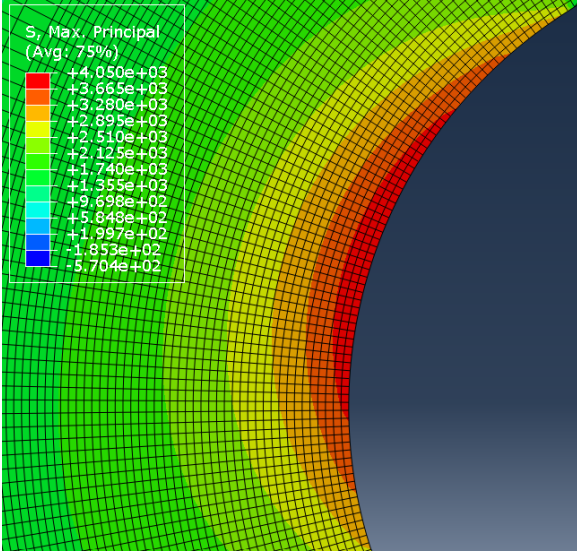
Figure 4.12: Paths used to present results at first engaged thread root

4.6.1 Linear elastic material conditions

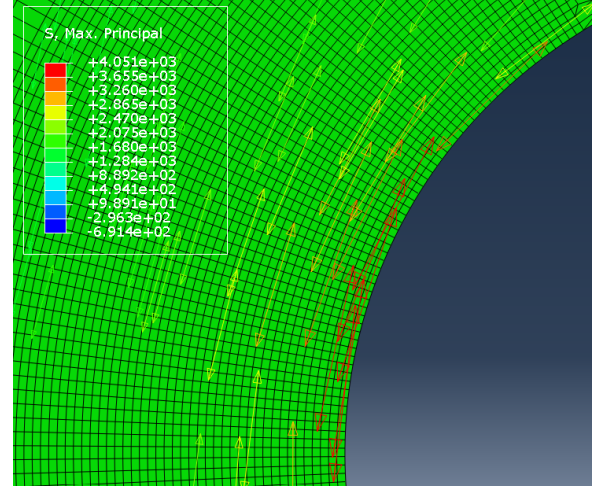
4.6.1.1 Ungalvanized fasteners

The stress concentration obtained from the linear elastic model is consistent with the results reported in numerical and analytical works for the first engaged thread root [14]. The maximum principal stress is 4050N/mm^2 , reported at an angle between 20° and 30° from the thread root normal as seen in

figure 4.13a and the peak value reported in figure 4.14. The stress concentration factor (SCF)(K_t) and plot of von Mises stress versus true distance into the critical section at notch-like thread root is given below. When compared to similar stress plots reported in literature (Wiegand et al. (2007)) shown in figure 4.15b, we can validate the results obtained here. As per results obtained from analysis, a linear elastic stress concentration factor of 6 is obtained at the first engaged thread root as seen in figure 4.15, similar to what is reported by [14].

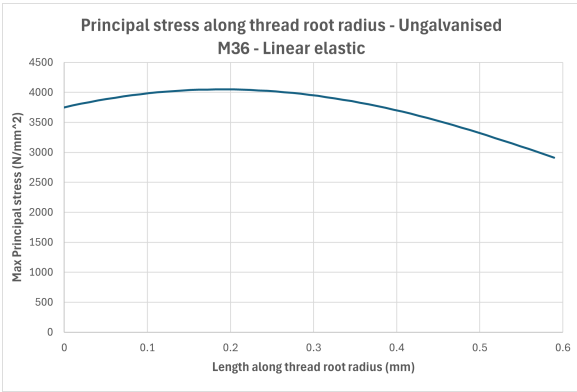


(a) Linear elastic principal stress at thread root for ungalvanised bolt

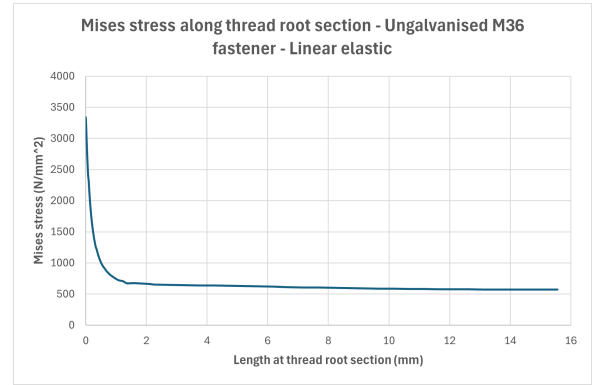


(b) Direction of principal stress is tangential to the thread root curvature

Figure 4.13: Principal stress plots from linear elastic ungalvanised M36 fastener model



(a) Stress plot along thread root radius

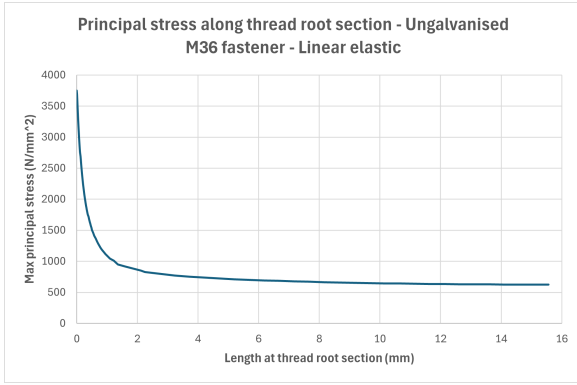


(b) Stress plot through critical thread root section

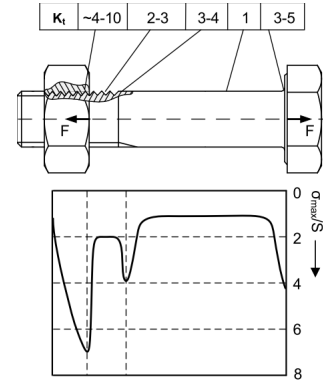
Figure 4.14: Stress plots from linear elastic ungalvanised M36 fastener model

4.6.1.2 Galvanized fasteners

The max principal stress in the model with galvanization layers is 2979 N/mm^2 , which is different from the peak stress in the ungalvanized model due to the presence of ζ inter-metallic layer on the boundary. Looking at the stress concentration plot across the critical thread root section in figure 4.16b, the peaks observed are a results of materials with varied properties on the boundary layer. Quite a bit of insight on the local stress and strain distribution is obtained comparing it to the plots available from ungalvanized fasteners. Specifically, if we look at the peak principal stress in the steel substrate in figure 4.16b, it is about $100\text{-}200 \text{ N/mm}^2$ more than when the steel substrate is not bound by the galvanization layers, corresponding to a linear elastic stress concentration factor of 6.2, whereas it is the other way around when we compare the von Mises stress in galvanized and ungalvanized bolt model for linear elastic material properties. Given that the Mises stress governs the start of



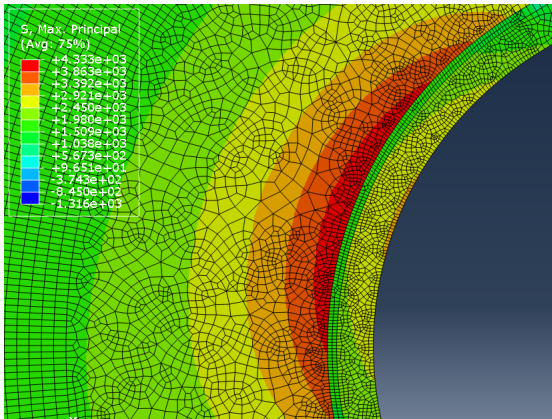
(a) Max principal stress plot along thread root section



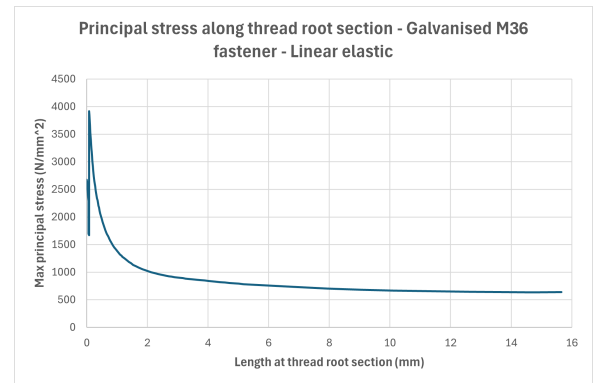
(b) Schematic stress distribution and usual range of SCF (Wiegand (2007))[14]

Figure 4.15: Comparison of linear elastic stress concentration between results obtained and theory

yield or permanent deformation under complex loading conditions, we could say that the presence of galvanized zinc layers are beneficial. But in reality, comparison must be made with the elastic-plastic material properties as plastification and redistribution, along with the brittleness of inter-metallic layers can affect the stress in the steel substrate, leading to increased chance of damage. However, it needs to be understood that material properties such as modulus of elasticity majorly govern the strain distribution along the thread root radius in these linear elastic models, along with geometric properties as a result of tolerances allowed by codal provisions for galvanized and ungalvanized fasteners. The comparison of stress plots between galvanized and ungalvanized threaded fasteners and discussion of the same is done in the next section.

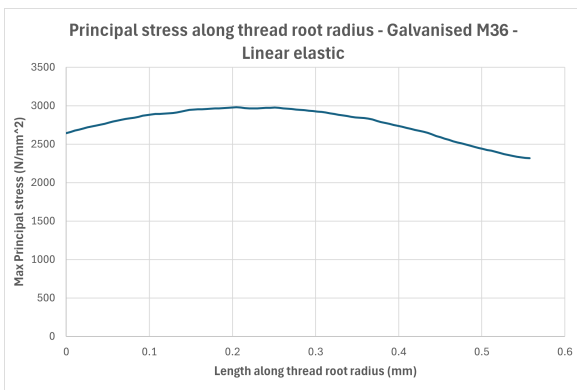


(a) Linear elastic principal stress at thread root for galvanized bolt

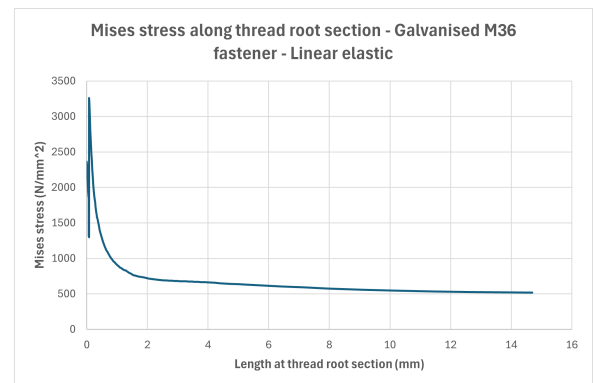


(b) Principal stress plot through critical thread root section

Figure 4.16: Stress plots from linear elastic galvanized M36 fastener model



(a) Stress plot along thread root radius



(b) Stress plot through critical thread root section

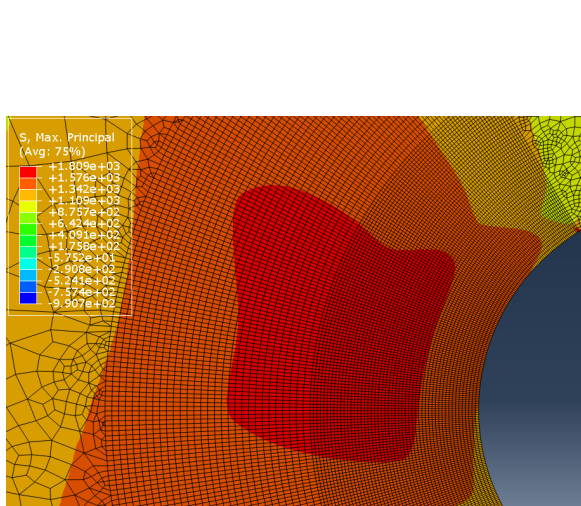
Figure 4.17: Stress plots from linear elastic galvanized M36 fastener model

4.6.2 Elastic-plastic material conditions

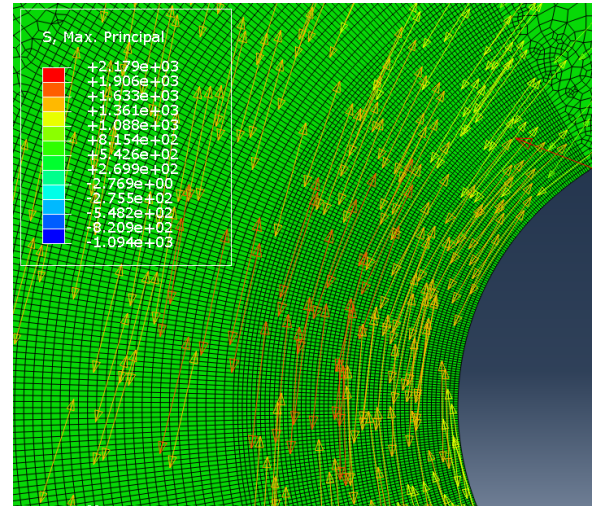
4.6.2.1 Ungalvanized fasteners

Based on the distribution of stresses in the elastic-plastic material condition for an ungalvanized fastener thread root, the redistribution of stresses along the root radius and into a plastic zone from the thread root edge is visible. This encapsulates the beneficial effect of redistribution by plastification, as mentioned earlier, providing support against catastrophic failure in the critical notch-like root. This effect, which causes a limitation of stresses under increasing strains, is known as the macroscopic support effect and is described in figure 4.20b. Under load, high elastic stresses develop at the notch root due to geometric discontinuities. Once the local stress exceeds the material's yield strength, plastic deformation occurs. By this mechanism, the effective notch radius is increased and the stress concentration factor is reduced. Stresses redistribute from the notch root to the bulk material, lowering peak stresses and homogenizing the stress field. This effect is visibly seen in our stress plot in figure 4.20a. It is also important to see how this mechanism changes with a change in geometric properties, which will be covered subsequently in the comparison with larger diameter specimens.

The maximum principal stress of 1353 N/mm^2 is seen at an angle from the thread root normal as discussed earlier, owing to the rounding off of the thread root beneficial against the undesirable stress concentration at sharp edges. The stress plot along the thread root radius also shows a flatter slope when compared to the linear elastic model, which is also as a result of the beneficial redistribution of local stress due to plasticity. Figures supporting these results are provided in 4.18-4.20.

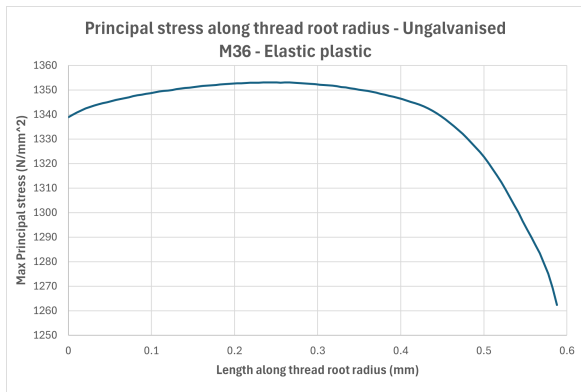


(a) Elastic-plastic principal stress at thread root for ungalvanized bolt

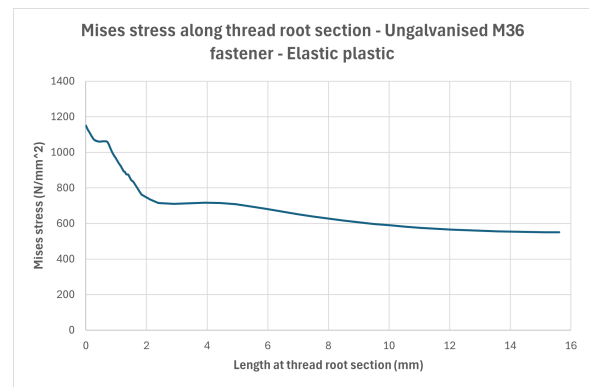


(b) Direction of principal stress is tangential to the thread root curvature even in elastic-plastic model

Figure 4.18: Principal stress plots from elastic-plastic ungalvanized M36 fastener model

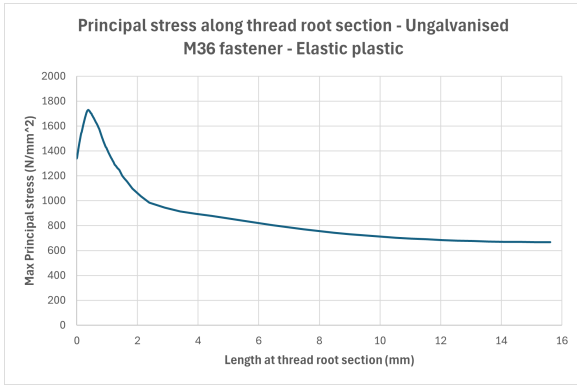


(a) Stress plot along thread root radius

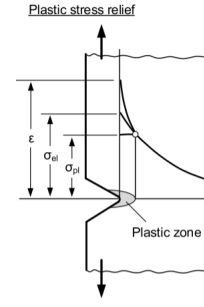


(b) Stress plot through critical thread root section

Figure 4.19: Stress plots from elastic-plastic ungalvanized M36 fastener model



(a) Principal stress plot through thread root section

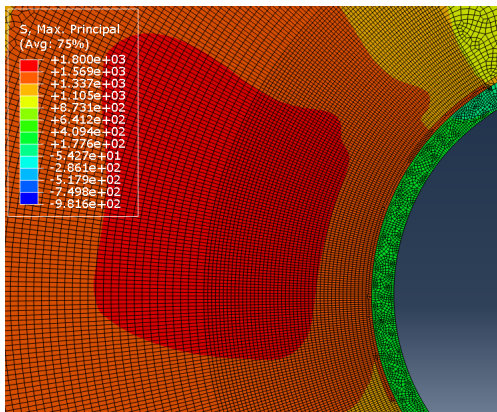


(b) Schematic showing macroscopic support effect by plastic stress relief (Vormwald and Seeger (2015))[14]

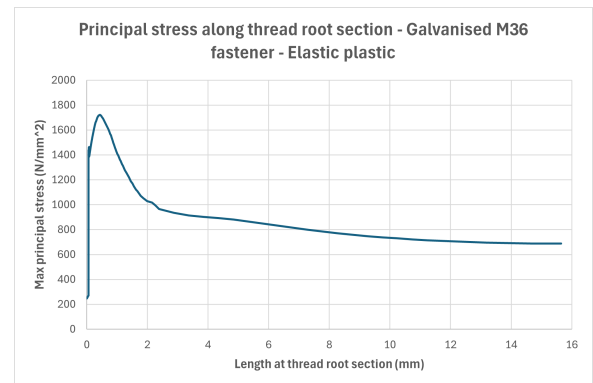
Figure 4.20: Comparison of stress plot between results and schematics available from theory

4.6.2.2 Galvanized fasteners

As per the stress distribution in the thread root region, we can see stark differences between the stresses at different inter-metallic layers and the steel substrate. As mentioned in the linear elastic results, the stress concentration at the steel substrate does not indicate any beneficial effect in terms of reduced stresses due to a protective galvanization layer. Rather the stress remains the same in both galvanized and ungalvanized models, if we compare 4.20a and 4.21b. But the material model included for the inter-metallic layers from [43][42] suggests that brittle δ layer already undergoes cracking at this stage. This is also evident from the total and plastic strain distribution plots at the critical notch section, where a clear dip in plastic strain developed is visible in the distance (0.06mm-0.075mm) spanning this inter-metallic layer (Figure 4.23a) and the scanning electron microscope images from used and unused bolts of various sizes in figure 4.23b. This was also evident from the flow curves obtained in figure 4.6, which shows high strength but low ductility of the δ phase and limited strain hardening capacity along with low failure strain, confirming brittle characteristics, while the ζ phase offers, albeit lower strength, higher ductility and a gradual yielding with extended ductility. The brittle nature of the delta phase may lead to coating cracking under mechanical loading, while the more ductile zeta phase can better accommodate deformation. This cracked zone can act as zones of stress concentration, potentially creating failure initiation sites which can lead to an enhanced crack propagation effect as discussed by various researches [13][50], and thereby reduce the lifetime under cyclic loads. The comparison of stress plots between galvanized and ungalvanized fastener models incorporating elastic-plastic material model is discussed in the next section.

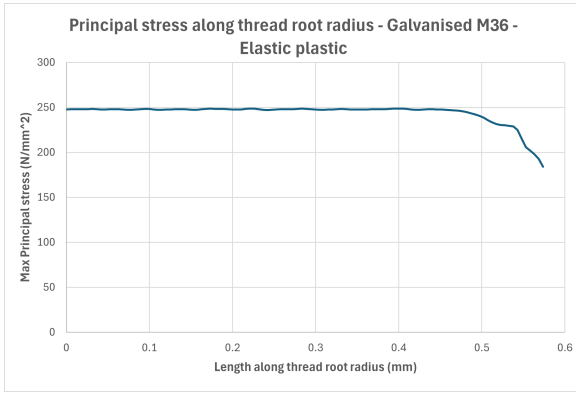


(a) Elastic-plastic principal stress at thread root for galvanized bolt

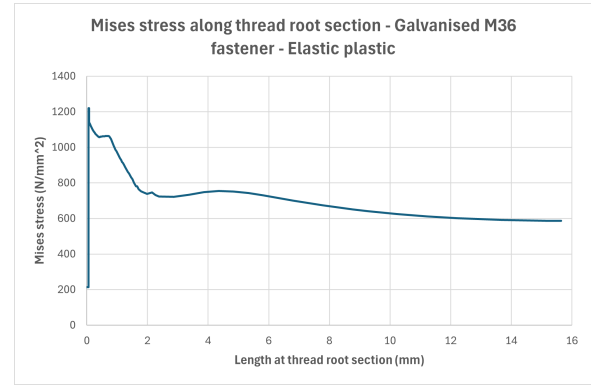


(b) Principal stress plot through critical thread root section

Figure 4.21: Stress plots from elastic-plastic galvanized M36 fastener model

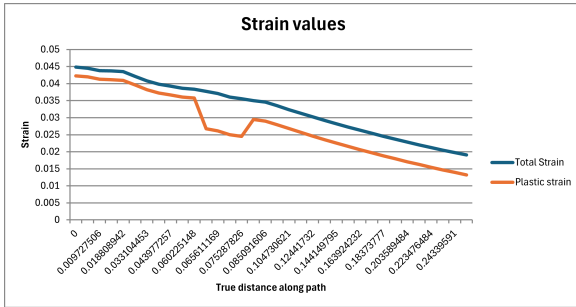


(a) Stress plot along thread root radius

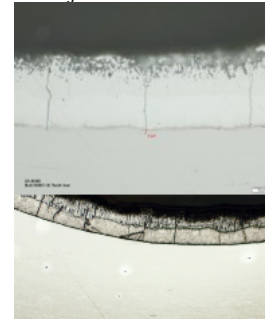


(b) Stress plot through critical thread root section

Figure 4.22: Stress plots from elastic-plastic galvanised M36 fastener model



(a) Total and plastic strains in the notch section. See the dip in plastic strain developed in the δ phase



(b) SEM images showing cracked intermetallic layers in unused (top) and used (bottom) fastener specimens

Figure 4.23: Brittle nature of inter-metallic layers

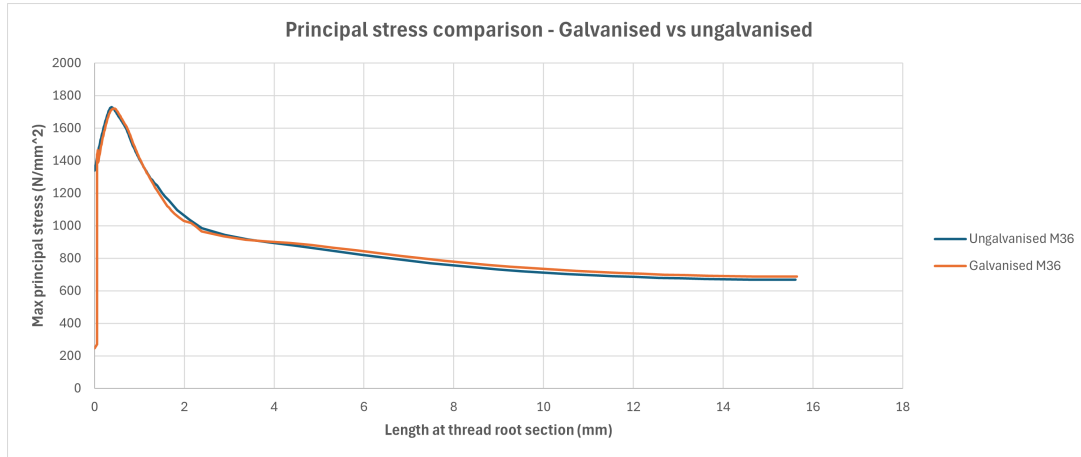
4.7 Discussion

Most contemporary research conducted numerically have focused on the local stress state and corresponding strains at the critical thread root section, either without considering boundary layer influences or by implementing it using engineering models which include the stress-strain behavior of the galvanized zinc layers deduced by analytically representing the reduced lifetime to failure in fatigue life experiments conducted on hot-dip galvanized bolts. Therefore, it is important to evaluate the validity of the models considered in our research with previous studies.

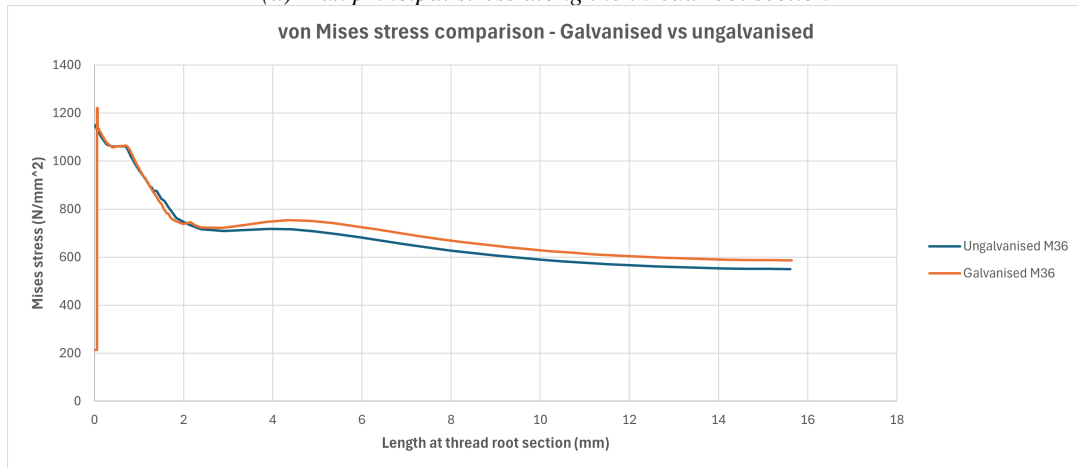
Results of the ungalvanized bolt model suggest the validity with respect to other numerical studies and theoretical literature. It is important for us to compare the results of the local stress between ungalvanized and galvanized fasteners, and this is shown in figure 4.24. The presence of a hot-dip galvanized zinc layer increases both the maximum principal and von Mises stresses at the thread root compared to the ungalvanized fastener. This increase can be attributed to the mechanical properties and geometry changes introduced by the zinc layer, such as increased local stiffness and potential stress concentration at the interface. The elevated von Mises stress in galvanized fasteners and the slightly higher stresses in the principal stress plot indicate a marginally increased risk of local yielding or crack initiation under the same loading conditions, which could impact the fasteners' fatigue and static strength performance.

As mentioned in section 5.6.2.2 and figure 4.23a, we see that the capacity of plastic strain developed by the δ layer is smaller than the ζ inter-metallic layer or the steel substrate. This means that the δ layer is much more brittle than the materials which bound it, giving opportunity for brittle failure at low strain levels caused by pretension and creating cracks in the galvanization layers. The brittleness of these layers is also highlighted in literature already mentioned in that section. By looking at the von Mises stress plot in the galvanized fastener model in figure 4.25, we see that inter-metallic layers have already reached their ultimate strength at preload level adjudged optimum for the performance of

these fasteners in ring flange connections. This means that brittle cracks would have already formed in these layer, up to the boundary between the steel substrate and the galvanized zinc coating. The effect of these microcracks is that it increases the local stress concentration at the crack tip, or at the surface of the steel substrate. This intensity of this stress governs the initiation and growth of crack into the steel substrate, which is the major cause of reduction of fatigue lifetime in threaded, preloaded fasteners, along with case individual attributes like cyclic load magnitude, mean stress, surface and geometric notch conditions [14].



(a) Max principal stress along the thread root section



(b) von Mises stress along the thread root section

Figure 4.24: Stress plots compared along the thread root section

A larger stress intensity (for linear elastic materials) or J-integral value (for elastic-plastic materials) would mean there is greater energy available for the crack to initiate and propagate in to the steel substrate, denoting a larger chance of these crack to cause failure under external, cyclic loading conditions. Therefore, from the comparison of local stress states in galvanized and ungalvanized fasteners, it can be concluded that there is a high probability of cracks being formed in the inter-metallic layers under preloading, and further analyses of stress intensity or energy available for crack initiation and propagation must be checked for difference among increasing fastener diameters. This will be conducted in subsequent sections.



Figure 4.25: Mises stress up to 2mm depth from the thread root boundary. Notice the zeta and delta layer values (first two plateaus) have attained ultimate tensile strength as seen in figure 4.6

Chapter 5

Three-dimensional analysis

After understanding the effects of galvanization with the help of a comparative analysis and refining the parameters by validating with respect to other numerical and experimental studies, we shall look forward in this chapter to applying the boundary layer model onto a three-dimensional segment model. To analyze the local stress and strains at the region of focus, i.e. the first two engaged threads, the global models involving the components of the connection (nut, stud, washer and segment) are analyzed. The deflections from this model are applied to a submodel with the thread engagement and intermetallic layers modeled. This is especially helpful due to the extremely small thickness of these layers and the fine mesh required for numerical results.

The consistency of local stress-strain values obtained in these two types of model is well documented in literature, such as figure 5.1. With increasing preload levels (in ascending order of curves from a to d), the local stress at the engaged thread roots tend to equalize as the difference between stress concentration at consecutive thread roots reduces. It is also noticed that the consistency in results reported from the 2D and 3D models increase. This can be understood looking at the causes and its subsequent effect of stress redistribution into the body of the fastener substrate due to thread root plastification. With increasing preload, there is increasing local strain values (corresponding to the spikes since in figure 5.1) but we also see equalizing local stress, which highlights the redistribution phenomenon. Plastification plays a beneficial role in redistributing the load evenly among engaged threads, reducing the risk of localized failure. Both numerical and experimental studies support that controlled plastification is a critical mechanism for safe and robust load transfer in threaded fastener assemblies [19].

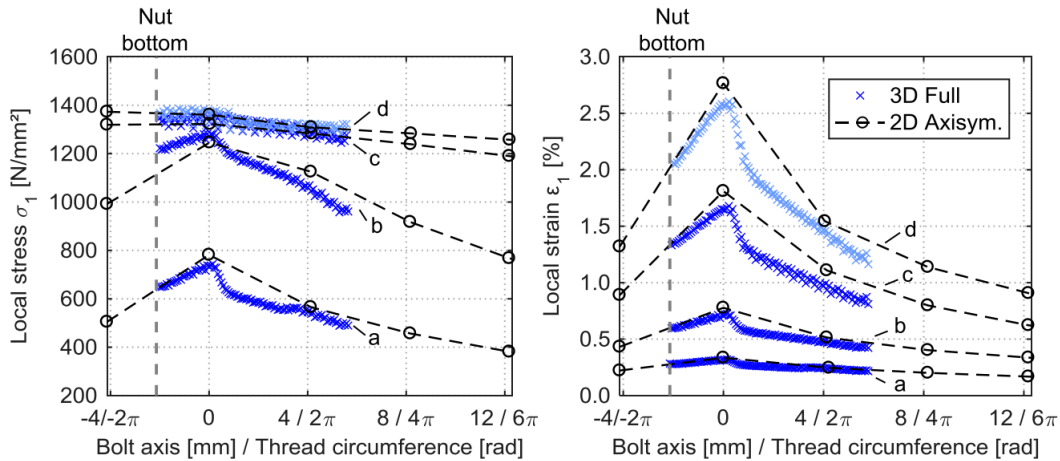


Figure 5.1: Local stresses (L) and local strain (R) inside the paired thread of an M36 bolt from calculation with 2D axisymmetric and full 3D model under elastic-plastic material behavior [14]

Curve	Nominal preload level (N/mm ²)
a	$0.2 \times R_{p,0.2} = 180$
b	$0.4 \times R_{p,0.2} = 360$
c	$0.7 \times R_{p,0.2} = 630$
d	$0.9 \times R_{p,0.2} = 810$

Table 5.1: Nominal preload levels corresponding to different curves in figure 5.1. $R_{p,0.2}$ corresponds to the nominal stress value at 0.2% plastic strain limit = 900 N/mm²

We shall see in this section if this holds true in our research case as well, if any additional improvements can be incorporated or if we can obtain additional insights from this comparative analysis, confirming our choice for research conclusions going ahead.

5.1 Model setup

The model is set up in similar ways to the two-dimensional axisymmetric model. The boundary conditions and loads remain similar to the two-dimensional model, with the fixed end specified at the bottom of the segment (in red) and the axial tension calculated to be 70 percent of the ultimate tensile strength of the threaded fastener applied as a pressure field at the bottom of the stud.

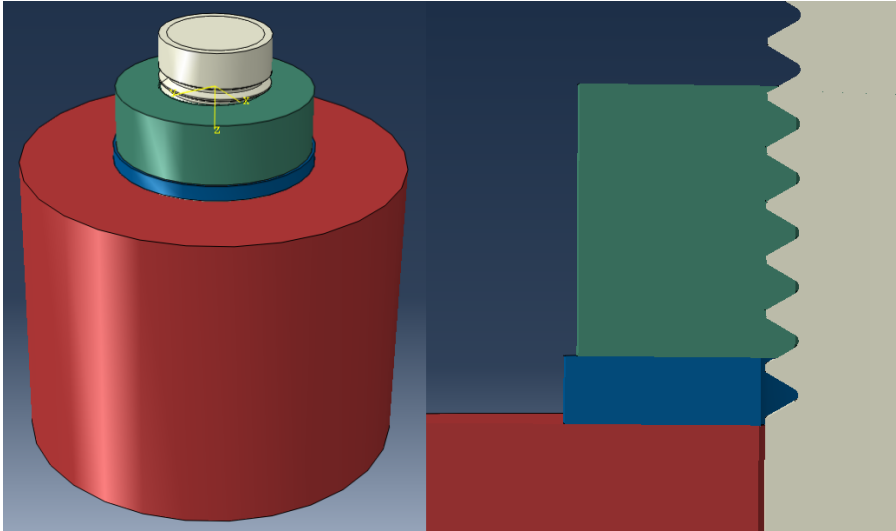
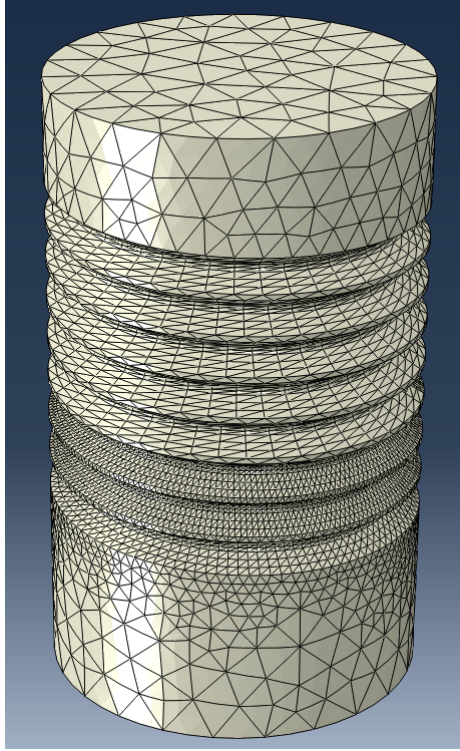


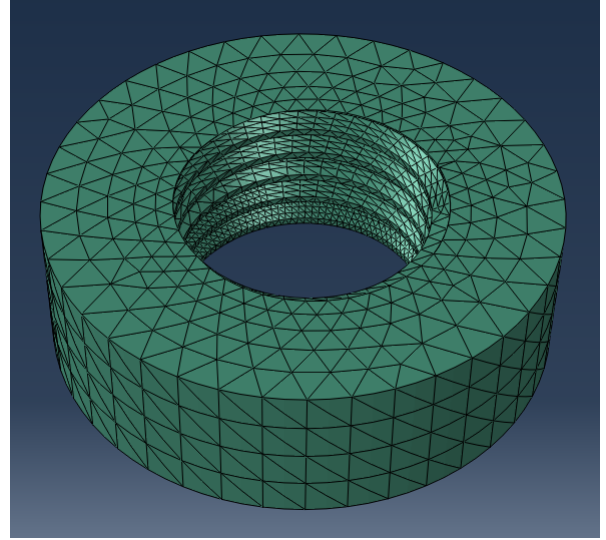
Figure 5.2: Global setup of the three-dimensional M36 model. The different colored parts signifies different components as seen in the two-dimensional segment model

Due to the highly intricate geometry of the helical thread involved in the full three-dimensional model, followed by the modeling and meshing of very thin inter-metallic layers, leads us to the first question we would like answers to. The necessity of a full 3D model for the purpose of optimally understanding the stress concentration at thread roots has been discussed by various research in the past[14][48]. It is understood that in the presence of pure axial loading (preload), the inclusion of continuous thread pitch does not provide any additional effect of a more efficient redistribution of local stress and strains. Yet, we have utilized the opportunity to see if any better insights into the local stress distribution can be seen by comparing the results from the 2D model to a full 3D model, as the understanding will enable us to evaluate the need of a three-dimensional model and also look into how we can implement a modeling method to include the effect of galvanization layers. Literature also suggests the advantage of including a full 3D local stress analysis in case of external bending on the fastener, but this is not in the scope of our study. The full three-dimensional model requires time and effort for an effective and optimum partition of layers, so as to get a consistent mesh, while at the same time keeping in

mind computation times required for running the analysis on parts with more than 100,000-200,000 elements. Using the ungalvanized bolt model and excluding the washer and the segment, we have been able to meet these criteria to get results required for the comparison.



(a) Mesh on 3D stud - M36



(b) Mesh on 3D nut - M36

Figure 5.3: Meshed parts of the full 3D model

The material models remain same as discussed in the two-dimensional model. In terms of the definition of contact, the explicit solver has the option of mechanical constraint formulation whereby the penalty contact method is chosen. The sliding formulation considered is the finite sliding formulation, which is different from that considered for the two-dimensional model since the assembly of components in the 3-D model might not have the same nodes on the slave surface interact with the same local area of the master surface throughout the analysis, mainly because of the coarser mesh considered for the global analysis and the effect of possible slip along the helical plane of the engaged threads. As for the contact interaction property, parameters have not changed from the two-dimensional model.

Optimizing the mesh size was necessary to sufficiently observe the localized stress in the first two engaged threads and to keep the number of elements within the computational limits. Therefore, the first two fully engaged thread roots and flanks have a mesh seed size of 0.5mm, and 2.5mm beyond this (Figure 5.3a). The shank edges of the stud, at the top and bottom, where there are no threads and only serve the purpose of boundaries where preload is applied, has a more coarser mesh of size 5mm. This mesh seed split and effective partitioning works well to capture relevant data for the purpose of comparing results between the model of different orders of dimension. An important point to mention here is the tetrahedral element type considered in the three-dimensional model. Given the complex thread geometry with the revolving helical pitch, it was not possible to have hexahedral mesh at the location of interest. The desirability of hex(-ahedral) mesh over a tet(-rahedral) mesh, in our particular case, owes to its reduced locking phenomena affecting the element stiffness and the superiority in contact modeling between engaged threads. Hexahedral elements show greater accuracy in high-strain gradient regions such as the thread root. Yet, the development of new element technologies to improve capabilities using numerical models, enables us to use quadratic tetrahedral elements to approach the accuracy of hexahedral elements, even when the solve time increases. We

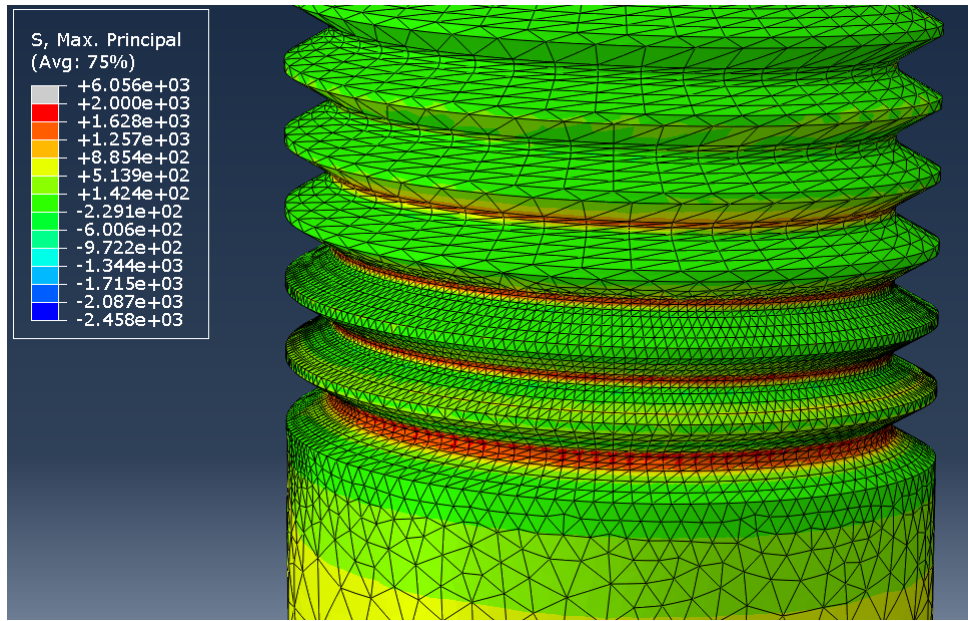
have considered 200,356 C3D10M elements in the model.

5.2 Results

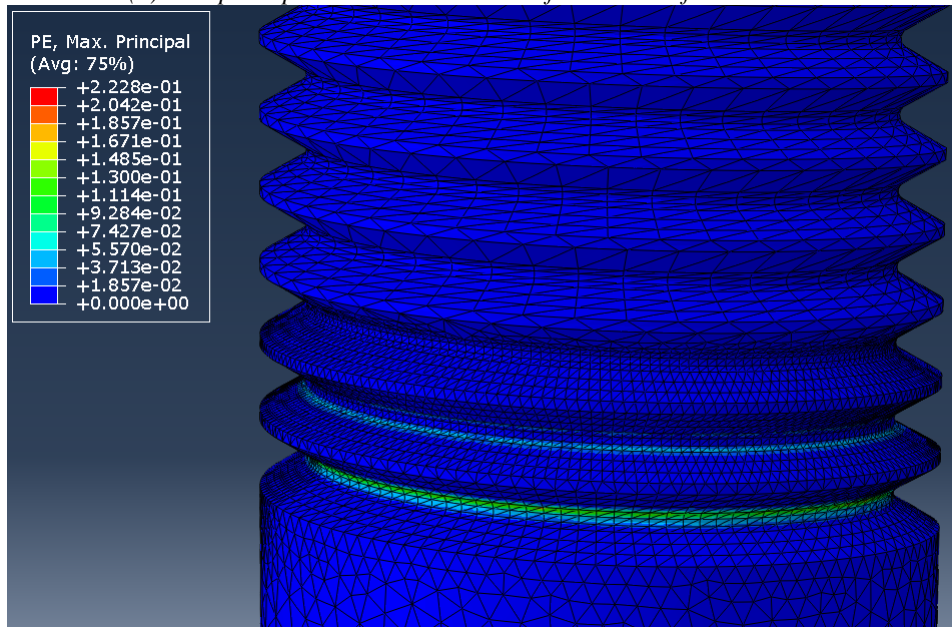
As a first check, we shall look at the general stressed state of the engaged threads. From figure 5.4, we can observe that the first two engaged threads show higher stress concentrations than the subsequent engaged threads, partially owing to a finer mesh in the first two engaged threads considered for optimal runtime and computation capacity, while being consistent with literature research such as mentioned above and theoretical sources confirming larger SCF at first two engaged thread roots. When compared to the trends observed in the 2D axisymmetric model, this shows considerable consistency but certain limitations regarding computational capacity and analysis time cannot be disregarded. Some are evident from the stress distribution at the first two engaged thread roots, which have a considerably higher stress peak as compared to the other engaged thread roots, which could be partially attributed to the finer mesh at these thread roots compared to the others. Yet, the comparison of stress plots reported in research compared to that reported by our results can be concluded similarly, keeping in mind the limitations mentioned above which could make a difference. If we look at the plastic strain distribution in figure 5.4, we see that the first two engaged threads have considerable plastic strain peaks which is the reason for the higher local stress concentration in these threads compared to others. This is a well-documented phenomena, with the plastification playing a beneficial role in redistributing the stress into the vicinity of the thread root region; a trend better observed in the axisymmetric 2D model showing development of redistributed plastic stress slightly away from the thread root boundary.

The verification in our analysis and results from three-dimensional full pitch model suggests conclusions similar to what has been reported in literature as mentioned in the beginning of this chapter, keeping in mind certain limitations which we shall see later. The image 5.4a shows stress distribution with peaks at the thread root, while we can also notice the reduction in intensity of stress concentration as we move further away from the first engaged thread root. The consistency in results between 2D and 3D models can be confirmed from the plot given below in figure 5.5. The orange points represents the principal stress values obtained from 3D model along a path created by the helical thread root, as shown in figure 5.6. The blue line represents the value of principal stress calculated at the first unengaged thread root, first engaged thread root and second engaged thread root, respectively from left to right of the plot. The red line suggests the location of the first engaged thread root in the two-dimensional axisymmetric model, corresponding to the location of start of engagement in the full three-dimensional model. Due to the helical pitch, points on the helical thread root path is considered to be partially engaged as there is not full engagement or contact between the flanks of the internal and external thread roots until this point, as can be confirmed in figure 5.7 and 5.8. The measure of distance on the horizontal axis starts from the point where path begins in figure 5.6a. The principal stress is compared here since the direction of principal stress along the thread root curvature is always tangential, as shown in figure 4.13b.

There are few critical points we must understand from these results. This is important when analyzing these results and evaluating the applicability of two-dimensional axisymmetric approach over the full three-dimensional approach to understand the local stress concentration effects. A combination of tetrahedral elements and larger mesh size compared to the two-dimensional approach are some of the reasons for the large scatter observed in the three-dimensional model, which will be discussed in the next section. Therefore, the comparison of stress concentration at the thread root level cannot be compared between the 3D and 2D models with complete certainty. The obvious advantage of continuing this research with the axisymmetric 2D approach is evident when the characteristics and the effect of extremely thin galvanized zinc layers, the dimensions of which are three orders smaller



(a) Max principal stress distribution in full 3D M36 fastener model



(b) Plastic strain distribution in full 3D M36 fastener model

Figure 5.4: Principal stress and plastic strain distribution in the engaged thread roots of full 3D model

than the geometric dimensions of threaded fasteners (length, nominal diameter, etc), needs to be quantified and understood. An ideal case for analysis would be to include all geometric parameters of the full 3D threads, including its pitch, taper and root properties, while including the galvanized inter-metallic layers, with the proper mesh density and element properties considered. This is unfortunately not possible at present, given the computation complexity and time constraint, and have therefore been included as a limitation to the study with recommendations for future consideration.

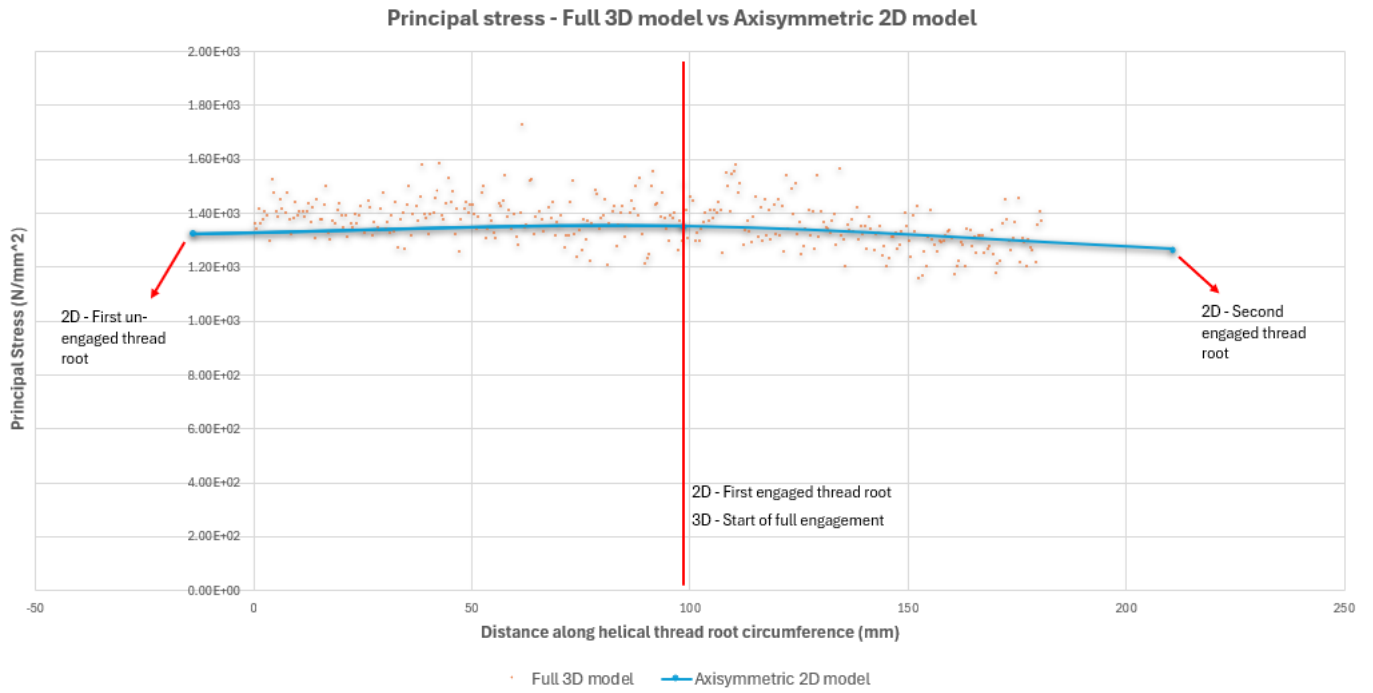
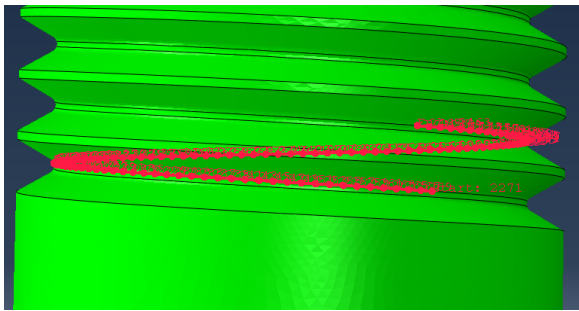
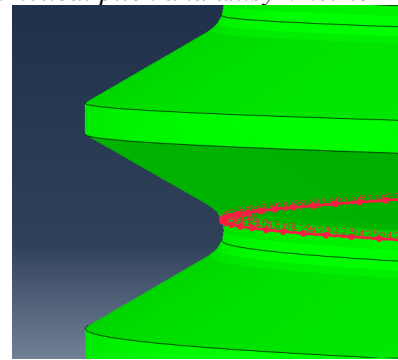


Figure 5.5: Comparison of stress plots between full 3D model with helical pitch and axisymmetric 2D model

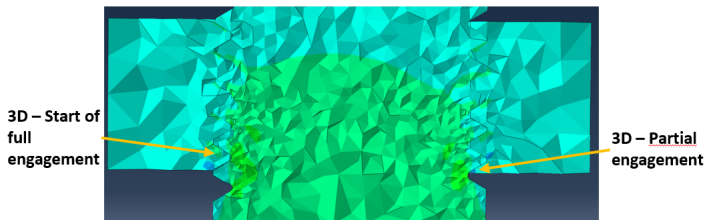


(a) Representative helical path considered for measuring local stress-strain values

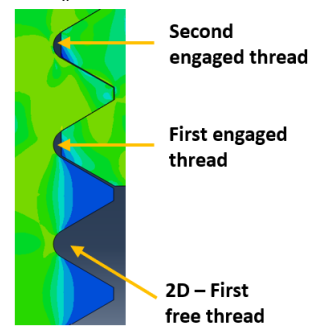


(b) Close-up at thread root showing orientation of path at 20-30 degree angle to the thread root normal

Figure 5.6: Path along which local stress is evaluated in full 3D model



(a) Difference between partial and fully engaged thread root in 3D model with helical pitch



(b) Engaged and unengaged thread roots from axisymmetric 2D model. Values from these location are plot in figure 5.5

Figure 5.7: Engaged threads in both models corresponding to locations mentioned in the comparison plot in figure 5.5

5.3 Discussion

As presented above, the consistency in results between the full three-dimensional model and the axisymmetric two-dimensional models highlight the efficiency of analysis results with the help of the

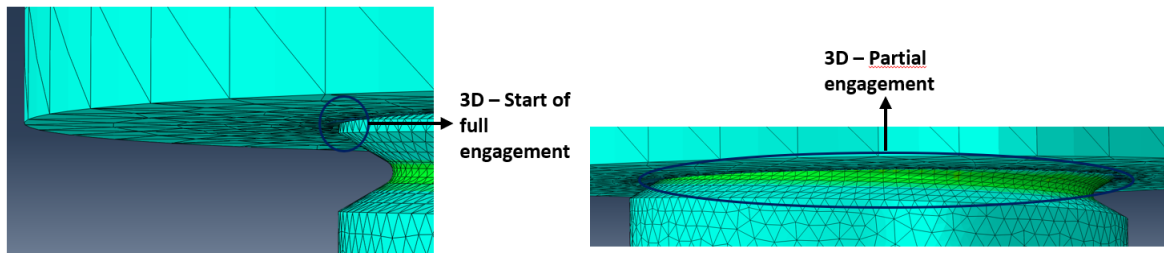


Figure 5.8: Point of start of full engagement and regions with partial engagement in full 3D model

axisymmetric model. The trend in stress values at the first engaged thread, and then the reduction as we go towards the second engaged thread root is reported by both sets of results.

A major point of discussion before we conclude the efficacy of a simpler 2D model would be to answer the scatter seen in the results from the 3D model. As mentioned earlier, the mesh size for the 3D model has been optimized keeping in mind the computational capacity and time available. To this extent, the mesh seed considered at the first two engaged threads in the 3D model is 0.5mm. Researchers in the past have concluded consistency in results using a finer mesh of less than 0.2mm[14]. It is found that the primary source of scatter in the 3D model results stems from inherent limitations in tetrahedral element formulations and their stress recovery characteristics. Typically, the stress calculation process in finite element analysis involves computing strains through differentiation of displacement fields, which occurs at integration points rather than at element faces or nodes. The results we would like to see is situated at one of the tetrahedral element (tet) elemental faces lying on the thread root, and these values are extrapolated from integration points to the element faces or nodes of the element. This extrapolation process introduces variability, especially when dealing with stress concentrations at geometric features like thread roots. The extrapolation accuracy depends heavily on element quality, aspect ratio, and local stress gradients. In threaded geometries, the complex stress fields around thread roots create conditions where individual tetrahedral elements may produce varying extrapolated stress values depending on their orientation and connection to neighboring elements. Research has also demonstrated that tet elements require significantly finer meshes to achieve the same accuracy comparable to hexahedral element (hex) meshes. But given the complicated thread root geometry, ABAQUS/CAE does not have the capability to hex mesh the sweeping, shifting geometry of the thread. Finally, the 3D helical thread representation introduces geometric complexities not present in the 2D axisymmetric model. Each tetrahedral element in the 3D model represents a slightly different geometric orientation relative to the helical thread path, whereas the 2D model treats the geometry as perfectly axisymmetric. This geometric variation, combined with the discrete nature of the tetrahedral mesh, creates natural variations in local stress states that manifest as scatter in the results. This geometric discretization introduces variability that is inherently absent from the continuous axisymmetric representation.

Despite the scatter in individual 3D data points, the agreement between the average 3D stress levels and the 2D axisymmetric results strongly supports the adequacy of 2D modeling for threaded fastener analysis, especially applicable to the modeling of physical inter-metallic boundary layers. The consistent trend captured by the 2D model demonstrates that it precisely represents the fundamental stress distribution mechanisms in threaded connections, similar to the results reported in literature [14], even when accuracy of these results are slightly affected by the computational constraints. The average agreement between these two results suggest that no physical phenomena is left not captured by the 2D model. The additional advantage of analyzing a two-dimensional model is the ability to have a better understanding of the redistribution phenomena we notice behind the critical thread root, the support effect offered by bolts and how it changes with increasing diameters. Another important point is the inclusion of physical galvanization layers, which is facilitated by two-dimensional modeling. These layers are in the order of 10-100 μ m. When we compare this to the general dimensions of

the fasteners, we see that a fine mesh is necessary to capture the stress-strain behavior of these layers and how it would affect the local state of stress at the thread root. Effective two-dimensional modeling allows us to have a mesh of 0.005mm seed size, while this is unattainable in three-dimensional models analyzed with general computing capacity. The applicability of results have been checked and verified in a submodel consisting of three-dimensional axisymmetric bolt model, which has been presented in the appendix. The results and comparison between this 3D axisymmetric model and 2D model also reports an increasing detail with increasing mesh density along with similar drawbacks from the comparison discussed above. Thus, subsequent analysis and comparison of bolt models of larger diameters will be conducted on two-dimensional models and will be reported in the upcoming chapters.

Chapter 6

Comparison of bolt models of larger diameters

The comparison of galvanized and ungalvanized fasteners of 36 millimeter nominal diameter (M36) gave us insights into the difference in local stress-strain states due to the presence of a galvanization layer as coating. Even when the thickness of this layer is minute when compared to the general geometric dimensions of the fastener, it had a great influence on the peak stress values and the redistribution of stresses which enhances the performance of these thread root notches under fatigue loading and stress concentration. These results give further impetus to see the effect on the local stress state for increasing diameter of fasteners.

Literature has mentioned the effect of thread root geometry acting like a notch, proving decisive for the fatigue strength of threaded fasteners. Eichstadt (2019) [14] has verified in his research that within the range of tolerances for metric thread geometry and engagement between internal and external threads, there is no significant impact on the stress concentration at the thread root. According to ISO 68-1:2023 [27] for metric screw thread profile dimensions and DAST 021 [10] for dimensions of HV bolts greater than M39, we understand that increasing diameters of threaded fasteners have increasing d/p ratio, which is the ratio of nominal diameter of the bolt to the thread pitch. This can also be seen in table 3.1. Numerical and experimental studies have shown that increasing d/p ratio leads to increasing stress concentration which leads to reduced fatigue endurance limit due to an increasing notch sharpness.

Apart from the increasing d/p ratio, the fatigue strength of these bolts are also dependent on their diameters. This is explained by size effect, defined by Kloos in 1976 in his paper titled 'Influence of the Surface State and the Sample Size regarding the Fatigue Strength'. This size effect can be subdivided into geometric size effect, statistical size effect, technological size effect and surface-technological size effect [36].

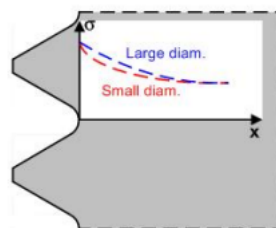


Figure 6.1: Stress distribution at notch and about thread root section for different nominal diameters [36]

The geometric size effect refers to the variation in stress gradients that arises with changes in component diameter. For notched components, it is critical to maintain geometric similarity with respect

to the notch geometry in order to isolate the pure geometric size effect. As illustrated in figure 6.1, the geometric size effect is evident in the case of bolt threads. For bolts with larger diameters, the stress gradient at the notch is less steep compared to bolts with smaller diameters. This results in a broader region subjected to high stresses in larger bolts, assuming the same maximum stress at the notch root. But in practical applications, the ratio between thread pitch and diameter does not remain constant but rather decreases as the diameter increases. Consequently, geometric similarity is not maintained across different bolt sizes. As a result, the observed differences in stress gradients for bolts of varying diameters are influenced not only by the diameter itself but also by variations in the stress concentration factor, which is affected by the changing thread geometry. Therefore, the influence of geometry on the fatigue strength of bolts cannot be attributed solely to the geometric size effect. Instead, it represents a combination of both size effects and notch effects, since the lack of geometric similarity introduces additional changes in the local stress distribution beyond those caused by size alone. It is therefore important to understand the difference in stress distribution due to difference in nominal diameters and thread geometry (pitch) separately, to analyze the effects properly. The technological size effect accounts for fatigue-relevant variations inherent in manufacturing processes. For bolts, both mechanical forming and heat treatment exhibit diameter-dependent characteristics. These processes induce distinct crystalline structures that directly influence fatigue behavior. Consequently, investigations targeting the technological size effect necessitate identical base materials and manufacturing methodologies across specimens. However, both material properties (e.g., grain structure) and manufacturing parameters inherently vary with increasing fastener diameter. This interdependence precludes the isolation of manufacturing-induced effects from dimensional changes. As a result, the technological size effect in threaded fasteners cannot be quantitatively assessed or reliably compared across different diameters, as material and process variables are intrinsically conflated with scale. The statistical size effect arises from the increased probability of damage-critical micro-structural defects occurring in larger components relative to smaller ones. This can be understood from the fact that geometrically larger threaded fasteners have a larger area of engaged parts (thread root, thread flanks, etc) which can have prior damage. Similar to the technological size effect, rigorous analysis of the statistical size effect requires identical material properties and manufacturing processes across all component dimensions under investigation. Similar to the technological size effect, material characteristics (e.g., grain structure) and manufacturing parameters inherently vary with diameter in fasteners. These variations prevent the isolation of statistically driven failure mechanisms from scale-dependent process influences. Consequently, statistical size effects cannot be meaningfully quantified or incorporated into fatigue assessments for bolts, as defect distribution cannot be made independent from diameter-dependent material and process variables. The surface-technological size effect accounts for inter-dependencies between boundary layer conditions (e.g., residual stress distributions), component thickness, and fatigue strength. These relationships are intrinsically governed by the specific production methodology employed. Once again, these surface characteristics exhibit scale-dependent behavior, but the influence of boundary layers are qualitatively understood from previous analysis is used to quantify the effect it might have on the lifetime of threaded fasteners.

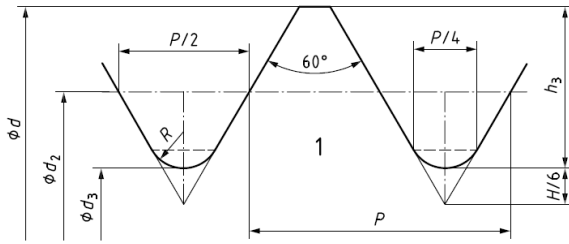
Due to the dependency of many of these effects mentioned above to their individual production processes and the scale of general dimension, we shall compare here the geometric size effect, and gain insights on the varied stress distribution behavior in fasteners of larger diameter. The need for larger supporting structures for offshore wind turbines in the upcoming years calls for equally larger connection components, and therefore our understanding of these geometric size dependent effects will be useful.

6.1 Model setup

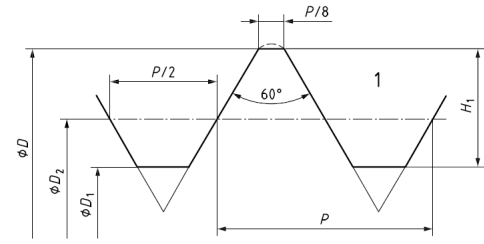
The comparison of threaded fasteners will be done for studs of 5 different nominal diameters: M36, M48, M64, M72 and M80. As per the conclusion in chapter 5, the comparison will be based on the stress distribution plots obtained by analyzing the axisymmetric models of these fasteners. ISO 68-1:2023 [27] gives the basic and design thread profile of internal and external threads based on the thread pitch value. ISO 14399-4:2015 [15] provides the pitch value for nominal diameters up to 36 millimeters. For larger diameters, DAST 021 [10] is utilized to calculate the pitch value. Table 6.1 gives the pitch values considered for different diameters.

Fastener specification	Pitch (mm)
M36	4
M48	5
M64	6
M72	6
M80	6

Table 6.1: Fastener specifications and pitch value



(a) Design profile of external thread



(b) Design profile of internal thread

Figure 6.2: Design thread profiles from [27]. Notice the fully rounded thread root for external (stud/bolt) thread. '1' represents the body of the bolt/stud and nut respectively

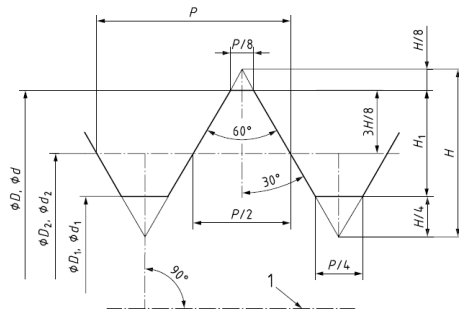
$$H = 3^{0.5} P / 2 = 0.866025404 P$$

$$H_1 = 5H/8 = 0.541265877 P$$

$$3H/8 = 0.324759526 P$$

$$H/4 = 0.216506351 P$$

$$H/8 = 0.108253175 P$$



(a) General thread geometry parameters and their locations. '1' represents the axis of screw thread

Pitch	h_3	R	$R_{1\min}$
P	$(17H/24)$	$0.14434 P$	$0.125 P$

(b) Thread geometry parameters for design profile in fig 6.2

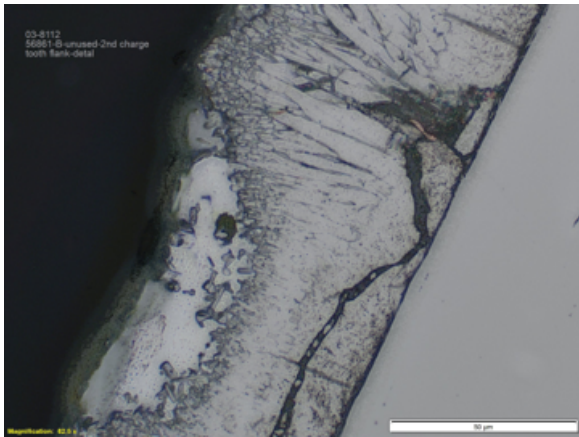
Figure 6.3: Thread geometry parameters and their dependence on pitch value

The design profiles of the internal and external threads are given in figure 6.2, along with the formulae for other geometric parameters of the thread in figure 6.3. A standout point to notice here is how the thread geometry parameters are dependent only on the thread pitch, which is in turn different for different diameters. But the pitch for M64-M80 threaded fasteners are the same. Therefore the

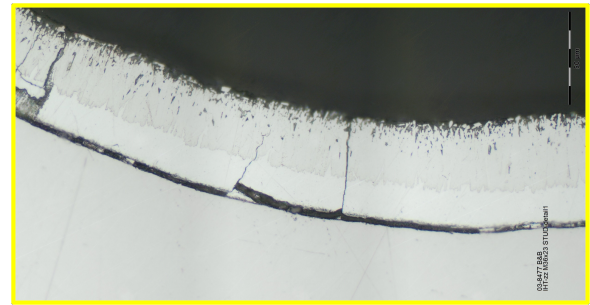
comparison will help us uncover how the stress distribution varies with respect to pitch and nominal diameter individually.

The model is set up similarly to the 2D axisymmetric M36 model in figure 4.1. Throughout this section, we will compare the models with elastic-plastic material properties, with the inclusion of galvanized zinc layers. Previous studies have shown that comparison of bolts of larger diameters have been done based on their linear elastic SCF values which shows that there is a modest increase in values at larger bolt diameters [14]. Therefore, here we would like to evaluate the effect of redistribution of stress from the fatigue critical, notch-like first engaged thread root into the body of the fasteners. By evaluating the model based on the actual mechanical properties of the material, we not only understand the concentration of stress at the thread root, but also the dependence of phenomena such as stress redistribution on the geometric properties of fastener.

The parameters considered in the model remains the same as the considerations mentioned in chapter 4. These considerations are also discussed in appendix B. The mesh convergence and sensitivity study was conducted for the M36 fastener, and it was found that a mesh seed size of 0.005mm was necessary at the critical thread root. Based on comparison of stress state at this thread root for larger diameters, and the similarity in loading conditions, transfer of loads and stress gradients, the same mesh seed size was considered for larger diameter models as well.



(a) Thickness of galvanized zinc layer in M72 bolt



(b) Thickness of galvanized zinc layer in M36 stud

Figure 6.4: SEM images from TNO showing consistent thickness of galvanized zinc layer irrespective of size of threaded fastener

As seen in the SEM images above, the thickness of layers in M36 and M72 are in the same range. ISO 10684:2004 [24] is the standard governing hot-dip galvanization of fasteners. It suggests that the minimum local coating thickness of zinc should be 40µm and the average coating thickness of a batch of fasteners should be 50µm. Apart from this, the maximum coating thickness of based on the pitch value is also provided, as shown in table 6.2. Some standards also suggest that the thickness of coating is directly proportional to the duration of corrosion protection expected on a steel article and its size. Therefore, it could be understood that an M36 stud might have a smaller coating thickness compared to an M72 stud. But in the large list of bolt diameter range, both M36 and M72 (and any other large HV bolt for that matter) are expected to fall within the standardized range if processed together. For comparative purposes, the fasteners manufactured by the same company, undergoing similar manufacturing processes is considered here, ensuring consistently equal thickness of these layers and aiding in the comparison when understanding if galvanization has a different effect on studs of larger diameter.

Pitch (mm)	Maximum coating thickness (μm)
4	110
4.5	113
5	118
5.5	121
6	125

Table 6.2: Pitch and corresponding maximum coating thickness in HDG fasteners

6.2 Results

The geometric size effect requires to be compared to understand the difference in effects between varying diameters. Therefore, in this section we shall compare the stress distribution diagrams of different sizes of fasteners, along with the Mises and max principal stress plots and strain plots. These are in similar lines to results discussed in chapter 4. Apart from this, we shall also compare stresses obtained in the axial and radial direction of the threaded fastener. This comparison is important since forces in these two principal directions not only contributes to the stress concentration, but the difference in contact surface areas between different diameter fasteners introduce different values of axial and radial stress at these critical regions. During axial pretension, the engaged flanks of internal and external threads transfer stresses. These flanks are inclined and therefore will have two force components - axial and radial. These components cause further tensile stresses that increase the range of stress under cyclic loading and aggravate the fatigue cracking effect. At this stage it is also important to mention that all stresses are calculated at the first engaged thread root about the section, with the path defined as in figure 4.12b, starting from the outermost point on the thread root edge all the way to the central axis of the bolt. The stress distribution about the thread root radius is not considered since the effect due to change in geometric size is more pronounced along the critical thread root section, and comparison with larger diameters will not result in any important insights because the stress along the thread root circumference depends on the inter-metallic ζ layer and we cannot evaluate the difference with respect to fastener geometry.

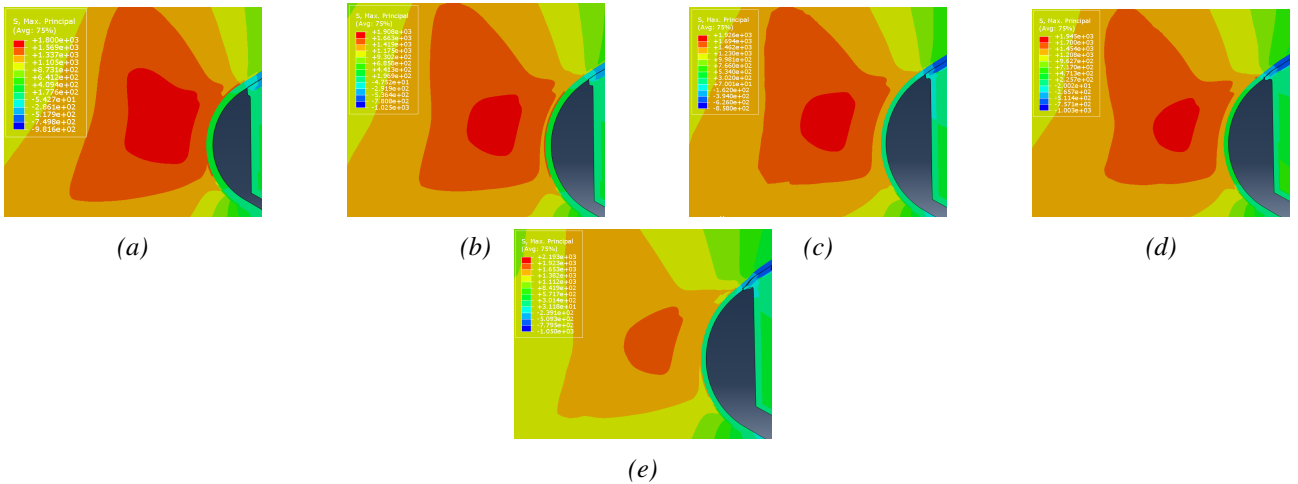


Figure 6.5: Comparison of principal stress distribution at critical thread root for fasteners of different diameters. a - M36, b - M48, c - M64, d - M72, e - M80. Visual comparison suggest identical stress distribution

As the first parameter of comparison, we shall see the plots of max principal stress in all fasteners. The direction of maximum principal stress is tangential to the curvature of the thread root, and therefore comparison of these results will give conclusive evidence on the stresses which cause cracking mechanism at the thread root.

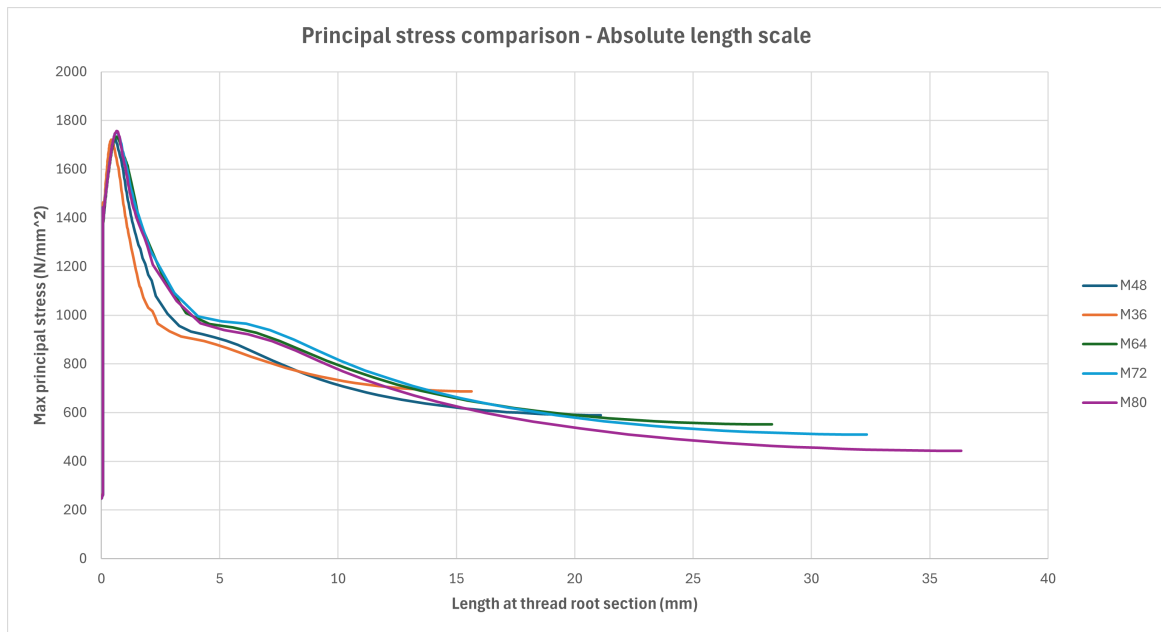


Figure 6.6: Max principal stress plots on the absolute length scale at the critical thread root section

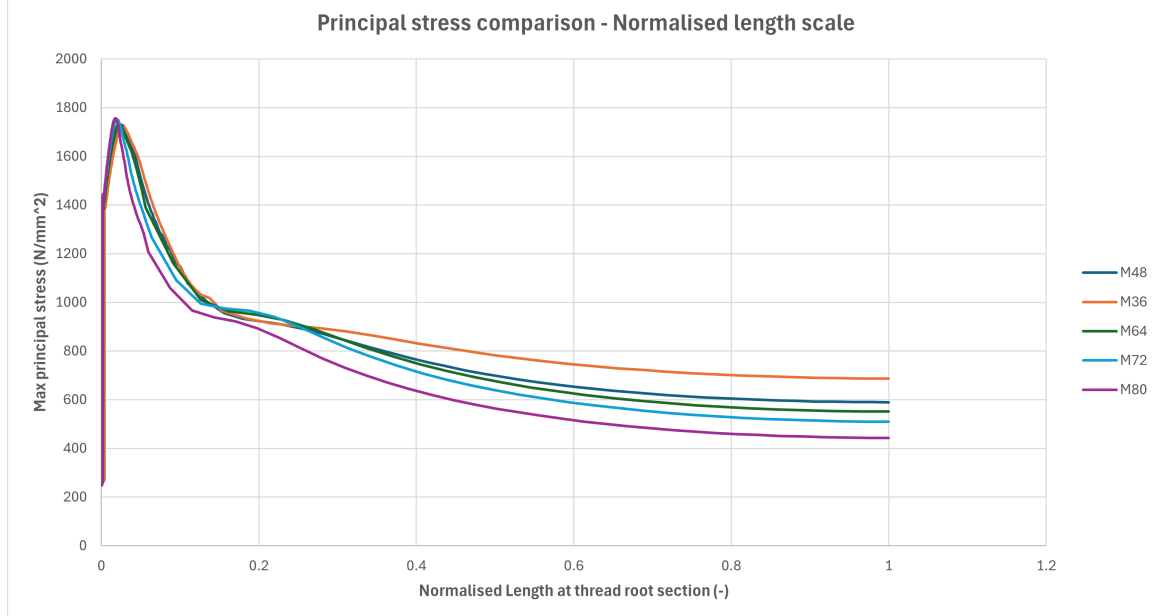


Figure 6.7: Max principal stress plots on the normalized length scale at the critical thread root section

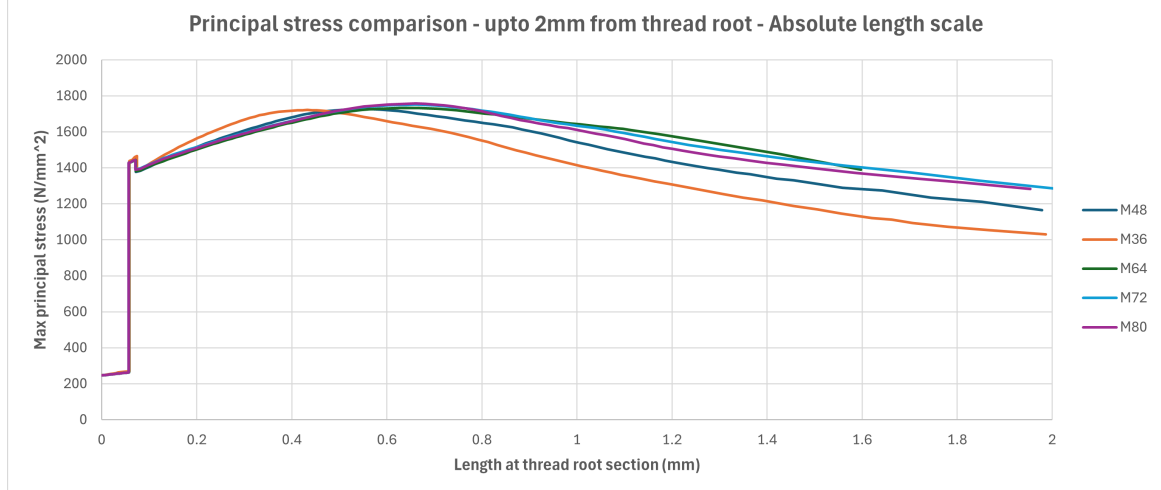


Figure 6.8: Max principal stress plots up to 2mm from the critical thread root section edge

Across the range of bolt diameters analyzed, the peak principal stress at the thread root increases as the fastener diameter increases. The tabulated results in table 6.3 show a roughly 2% consistent increase from M36 to M80 fastener. This trend highlights the geometric size effect mentioned in the preface of this chapter, where larger fasteners experience slightly higher peak stresses at the thread root under equivalent loading conditions. The position of the maximum principal stress also moves closer to the thread root boundary as the diameter increases. The normalized distance from the thread root boundary to the stress peak decreases from 0.0277 for M36 to 0.0182 for M80, seen in figure 6.7 and in table 6.4, suggesting that the region of highest stress concentration is more localized near the critical thread root boundary in larger diameter fasteners. This potentially increases the susceptibility to fatigue failure in the presence of a pre-existing crack and accelerated crack propagation due to higher localized stress.

Bolt size (-)	Peak principal stress (N/mm²)
M36	1721
M48	1728
M64	1734
M72	1751
M80	1757

Table 6.3: Fastener size and peak principal stress values.

Bolt size (-)	Distance of peak from root boundary on the normalised length scale (-)
M36	0.028
M48	0.026
M64	0.023
M72	0.020
M80	0.018

Table 6.4: Distance of peak from root boundary for various fastener sizes

The comparison of the normalized principal stress distribution about the critical section indicate that the overall shape of the stress profile is not affected by thread pitch as much as the nominal diameter. Thread pitch and nominal diameter are independent parameters, according to the codal provisions for metric thread profiles. Most contemporary research compares these geometric effects on stress concentration based on the d/p ratio, which makes it harder to evaluate the effect of each of these parameters separately. From our analyses of max principal stress, we understand that even when three stud models (M64, M72 and M80) have the same thread pitch value, their principal stress distribution varies slightly, as visible in the normalized length scale as well as at the local region up to 2mm from the thread root edge. As figure 6.8 shows, the comparison of stress variation up to a depth of 2mm from the thread root boundary is done since 70% of stress variation happens in this region, as is evident from the stress plots in figure 6.6.

The results also show a reduced support effect in larger fasteners, which hinders the redistribution of plastic stresses into the body of the fastener. This means that as diameter increases, the ability of the fastener body to absorb and redistribute stresses away from the highly loaded thread root diminishes. This is the reason for the higher peak stress values and the location of peak stress being closer to the edge. The consistency of trends observed in all these plots, along with the initial comparison in chapter 4 to other numerical studies provides confidence in the robustness of these numerical results. This also emphasizes the importance of using normalized scales for meaningful comparison across different bolt sizes. Another salient point we can notice in the principal stress comparison plots, in both absolute (Fig. 6.6) and normal (Fig. 6.7) scale, is the reduced stress levels towards the body

centre of these fasteners as the diameter increases. This is due to the thread geometry effects, which shows larger concentration of higher magnitude stress near the thread root region, which effectively reduces the stress level at the center as the stress is subject to balancing and distribution throughout this section. We quantify this by calculating the width over which the principal stress reduces to 1000MPa, beyond which the rate of stress reduction is substantially less as seen from the graphs. The table 6.5 shows that the width of loaded region from the thread root boundary reduces with increasing diameter of fastener, signifying a reduced redistribution phenomenon which causes smaller but highly stress regions in the vicinity of the thread root. Therefore an increased stiffness of larger diameter fasteners due to larger physical dimensions along with the stress distribution at the thread root region due to the geometry at this critical region causes the difference in stress distribution, which we especially see about the body center of these fasteners.

Bolt size (-)	Width of stressed region from thread root boundary (on the normalized scale) (-)
M36	0.1429
M48	0.1356
M64	0.1336
M72	0.1247
M80	0.1150

Table 6.5: Width of stressed region from thread root boundary on a normalized scale

Next we shall compare stress in various diameter fasteners based on their von Mises stress plots, again calculated in the path defined across the critical thread root. Von Mises stress integrates tensile, shear, and bending stresses into a single equivalent value, critical for assessing multi-axial loading scenarios, and the von Mises stress validates whether combined stresses exceed the material's yield strength, preventing plastic deformation or fatigue failure.

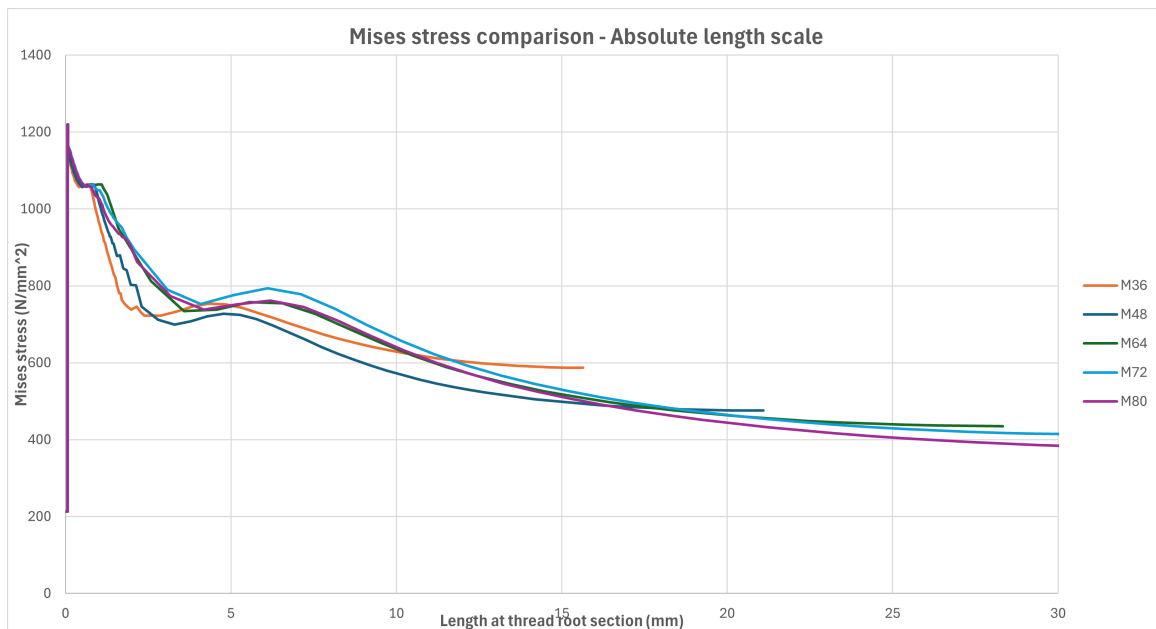


Figure 6.9: Mises stress plots on the absolute length scale at the critical thread root section

All fasteners, regardless of diameter, exhibit a sharp initial peak in von Mises stress at the immediate vicinity of the thread root, followed by a rapid decay within the first millimeters as seen in figure 6.9. This behavior signifies the critical nature of the thread root as the primary site for stress concentration and potential failure initiation. The similarity in this initial peak across sizes suggests that the local geometry at the root dominates the stress response, even as the overall bolt diameter increases. The

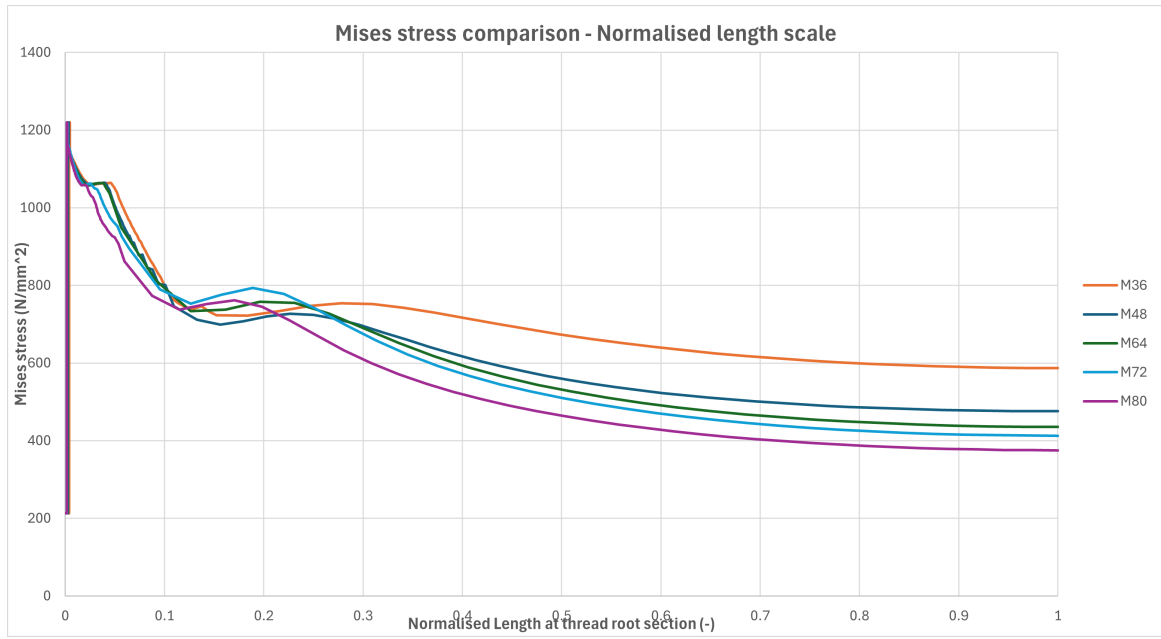


Figure 6.10: Mises stress plots on the normalized length scale at the critical thread root section

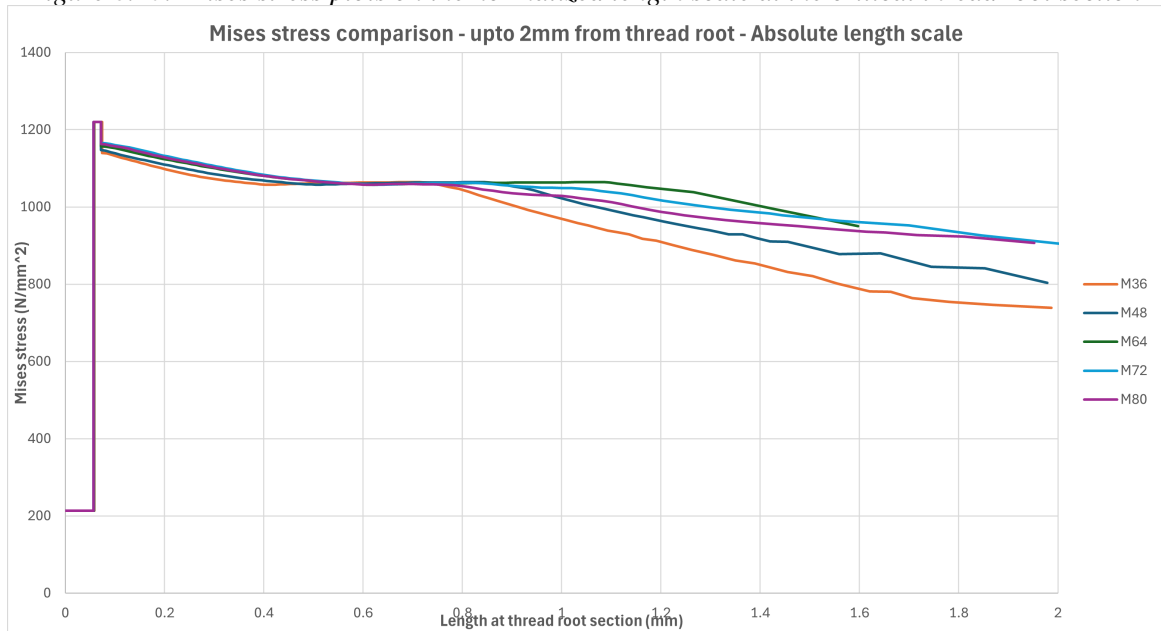


Figure 6.11: Mises stress plots up to 2mm from the critical thread root section edge

plateaus correspond to the inter-metallic layers, as we already discussed in the comparison between galvanized and ungalvanized fasteners. This similarity in peak values shows a consistent yielding criterion of cracks formed in the galvanized zinc layers across different fastener sizes, effects of which needs to be evaluated further. While the initial decay is steep for all sizes, larger fasteners (M64, M72, M80) show a more gradual reduction in stress beyond the first few millimeters compared to smaller ones (M36, M48). This indicates that a greater volume of material remains at higher stress levels further from the root in larger diameter threaded fasteners, which reduces the volume of substrate material available for redistribution of plastic stress. This causes unwanted plastic deformation under the presence of an external cyclic loading which may have implications for fatigue life and crack propagation resistance.

The absolute scale plot reveals that fasteners with similar pitch (M64, M72, M80) have overlapping stress distributions, highlighting the dominant effect of thread geometry, which is in turn governed by the thread pitch, which was not seen in the principal stress comparison done previously. Therefore comparison of the von Mises stress distribution enables us to quantify the difference in stress distri-

bution with changing thread pitch values, and also shows us the importance of considering the thread pitch and thereby the profile in design, especially when scaling up sizes. The observed trends suggest that simply increasing fastener diameter does not proportionally reduce peak stress at the critical thread root. Therefore, geometric optimization and material properties must be chosen with regards to the fastener size to ensure efficient material utilization and to improve the mechanical performance of these fasteners.

Now we shall see the comparison of stress plots of various diameter fasteners in their axial direction. These are stress developed in the direction of applied preload.

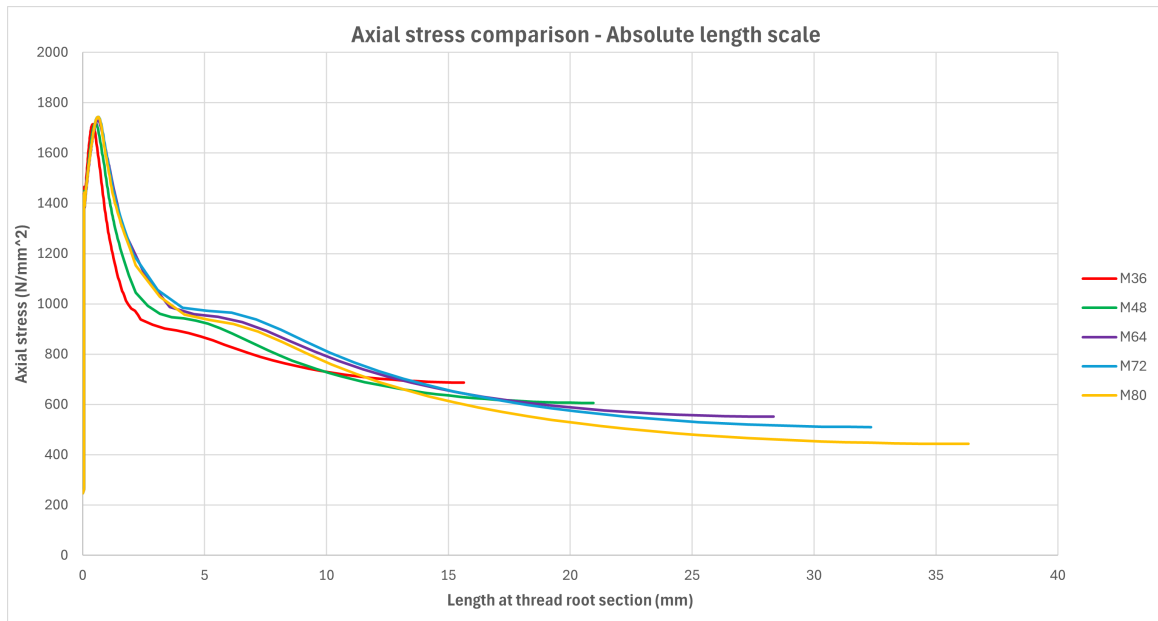


Figure 6.12: Axial stress plots on the absolute length scale at the critical thread root section

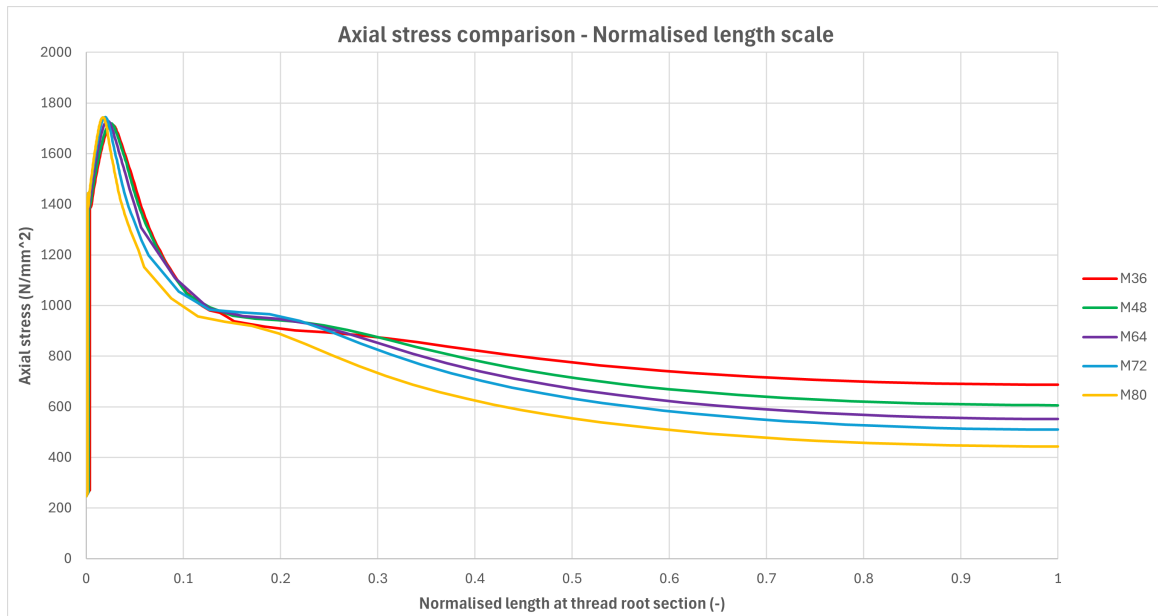


Figure 6.13: Axial stress plots on the normalized length scale at the critical thread root section

From the first look of the stress plot, it can be understood that the axial stress plot is similar to the maximum principal stress plot. Therefore the insights obtained from these plots are similar to the ones mentioned previously in case of the max principal stress comparison. We can see that the peak stress is slightly more in larger diameter fasteners, attributed to the relatively sharper notch with increased



Figure 6.14: Axial stress plots up to 2mm from the critical thread root section edge

d/p ratios for larger diameters. An observation made from figure 6.12 is the gentler stress gradient in larger fasteners. The slower reduction of axial stress with distance from the thread root suggests that the fatigue-critical volume is larger in bigger fasteners, potentially increasing the probability of sub-surface crack initiation and growth when subjected to high cyclic stress over a greater region.

When comparing the normalized stress distributions, it becomes clear that the mechanical size effect is seen as a shorter normalized width of high-stress region for larger fasteners. This means that, proportionally, the most critical zone is more localized in larger bolts, but the absolute length over which high stresses persist is greater. This difference when comparing two plots on different scales is important for understanding both local crack initiation risks and the potential for longer cracks to propagate in large-diameter fasteners. The data also suggests that for larger fasteners, increasing the number of engaged threads can be beneficial since it helps distribute loads more evenly across multiple engaged threads, thereby eliminating the presence of a highly stressed region near the first engaged thread and improving fatigue performance. The broader region of high axial stress in large-diameter fasteners highlights the need for greater quality control focused on the thread root and adjacent material. Surface treatments, improved thread root radius and non-destructive testing (NDT) evaluation should aid this.

For our last comparison, we shall look at the stress plots of radial stress distribution in different fasteners. Due to the engagement of threads, there is compressive stress normal to the flank of the external (stud) thread, which can be resolved into two components in two orthogonal directions - axial stress in the direction of stud axis, and radial stress perpendicular to the axis of the stud. This radial stress at the face of engaged thread flank is compressive in general. Due to the geometry at thread root where stress concentration occurs, the radial stress tends to be tensile about the thread root circumference, which can be confirmed from the stress distribution plot below in figure 6.15. Positive radial stresses are concerning from a fracture mechanics perspective since they promote an opening type crack initiation at the thread root surface.

Radial stresses can be noticed to be about one-third of the peak axial stress highlights the significant role of radial stress in the overall multi-axial stress state at the thread root. Although axial stress remains the primary driver for load transfer and crack initiation, the radial (tensile) component is crucial because the combination of high local tensile stress and a broader affected volume in large-

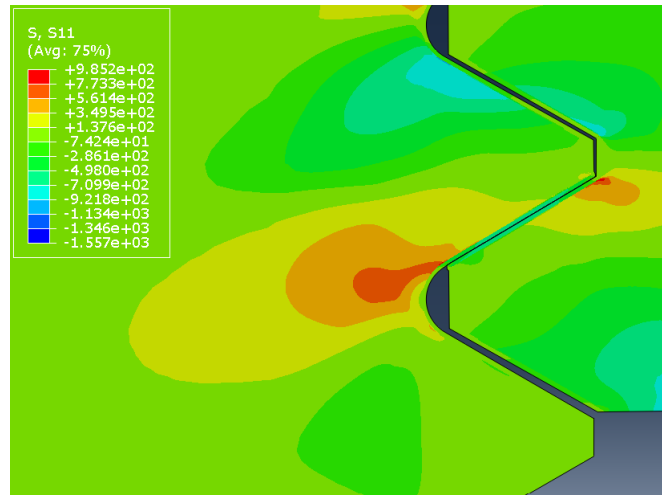


Figure 6.15: Radial stress distribution at critical thread root - M36

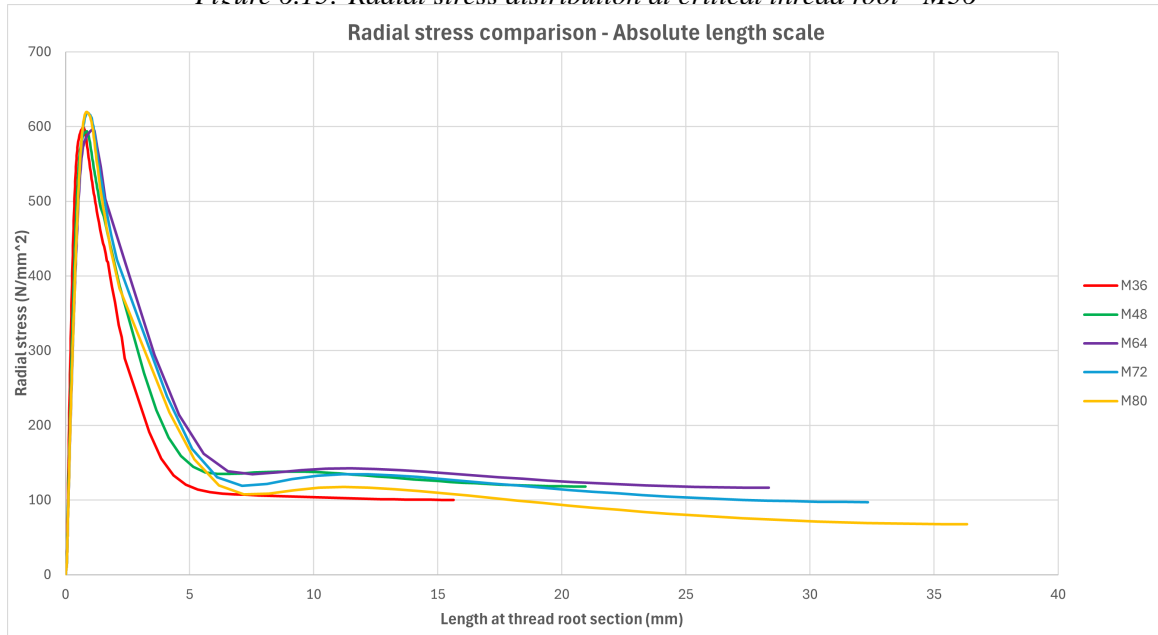


Figure 6.16: Radial stress plots on the absolute length scale at the critical thread root section

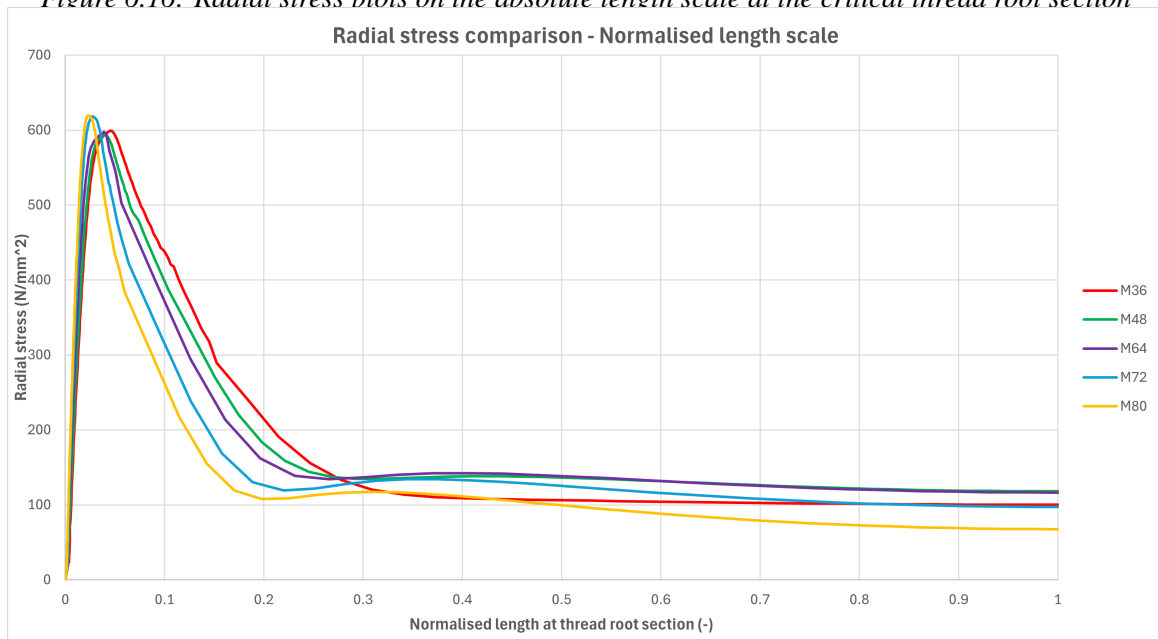


Figure 6.17: Radial stress plots on the normalized length scale at the critical thread root section

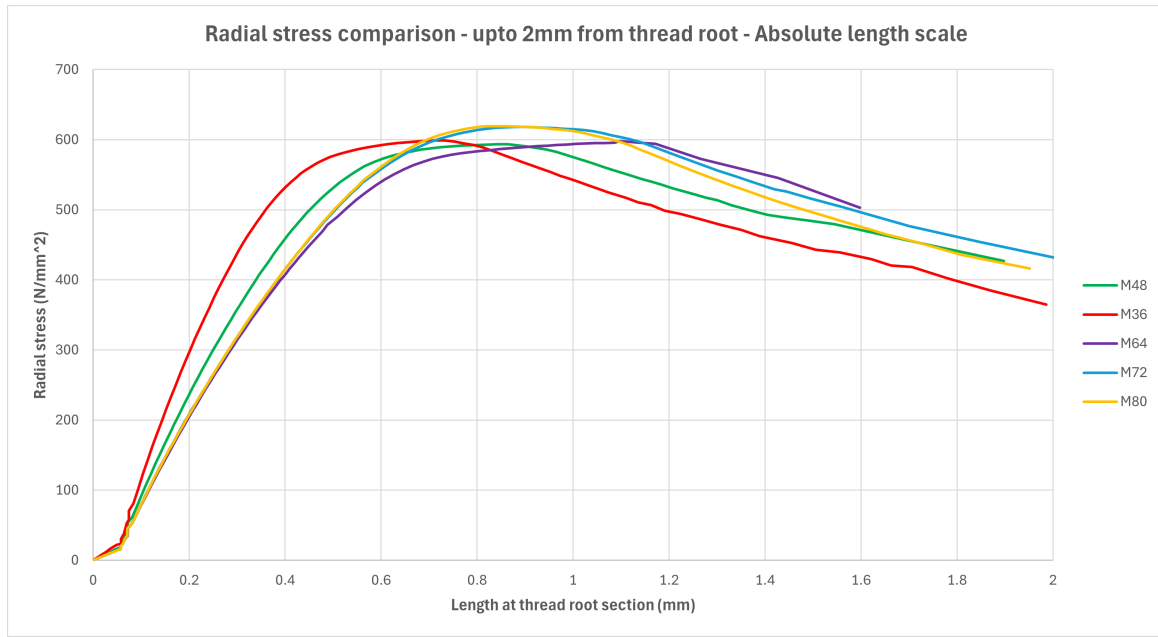


Figure 6.18: Radial stress plots up to 2mm from the critical thread root section edge

diameter bolts may necessitate more conservative design margins to ensure long-term reliability.

6.3 Discussion

The aim of the comparison was to understand any detrimental effects which would aggravate the stress state at the critical thread root section of large-diameter threaded fasteners. As discussed in the results, we have been able to report conclusive findings which suggest higher and more localized stress concentration at the thread root for increasing fastener diameter, with significant effects on fatigue life and failure risk.

The analyses confirm that as the fastener diameter increases from M36 to M80, the peak principal stress at the thread root also increases, though the rise is modest. With this shifts the peak stress closer to the thread root boundary, indicating a more localized highly stressed region. This increases the risk of failure due to fatigue in the presence of external cyclic loading, and pre-existing cracks, which is noticed in the inter-metallic layer and also due to the Mises stress reaching the yield limit in these materials. The stress intensity in the critical region will accelerate crack initiation and propagation. The majority of stress variation—up to 70% occurs within the first 2 mm from the thread root boundary, highlighting the importance of this region for fatigue and fracture analysis. Normalized stress plots show us that even when the trends in stress looks comparable, salient points such as stress peaks and stress gradients varied with different pitch and nominal diameters, which poses the question of considering geometric optimization for each fastener size. The von Mises stress plots show a sharp peak at the thread root, followed by rapid decay within few millimeters. The gradual decay notices in larger fasteners shows a greater volume of highly stressed material further from the root edge, reducing the region available for redistribution of plastic stress. It is also important to notice fasteners with similar thread pitch values having overlapping Mises stress distribution, highlighting the dominant effect of thread geometry on multi-axial stress states. This is also contributed to by the tensile axial and radial stress, where we notice similar trends of increasing values for larger diameter fasteners. These findings suggest that, for large diameter fasteners, special attention should be given to the thread root geometry, surface finish, and potential for surface defects, as the risk of failure initiation at or near the thread root increases with size.

From a fracture mechanical point of view, the results suggesting greater localized stresses in larger fasteners are particularly concerning. When we look back at the direction of max principal stress in chapter 4, we see that they are parallel to the axis of the bolt at the thread root, which is also the direction of applied preload. This suggests the direction of potential crack propagation at the thread root to be perpendicular to axis of the fastener. The increasing tensile stresses reported all throughout this chapter with increasing size suggest that they promote crack initiation in Mode I, which is the tensile or opening mode. The intensity of the crack initiation at the tip of a potential crack due to the brittle, cracked galvanized zinc layer, can only be verified with the help of fracture mechanics' parameters such as J-integral values for elastic-plastic material properties under monotonic loading. Therefore, the upcoming section will consider the difference in these fracture parameters at the tip of a crack considered in the inter-metallic layer. This will further enable us to verify and conclude if larger diameter bolts needs further considerations to make it safer, and recommend on what can be done to ensure similar levels of reliability among different fastener sizes.

Chapter 7

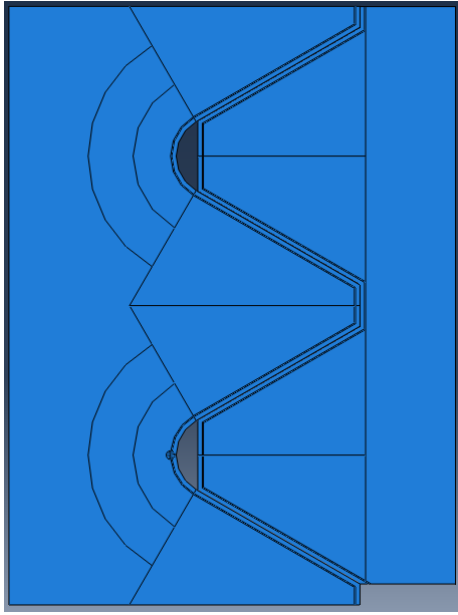
Comparison of bolt models with cracked galvanization layer

From the previous sections, we could conclude two things: firstly we validated the observations that some part of the galvanized zinc layer is brittle, and their Mises stress state at 70% preload caused cracking effect in these layers with the help of numerical analysis. Secondly, we saw that different fastener diameters have different locally stresses state, with variations in their peak values, the location of these peaks with respect to their distance from the root edge and the volume of highly stresses area in the locality. In this chapter, we shall see the effect of cracks in these galvanized zinc layers on the steel substrate of varying size. The presence of cracks perpendicular to the thickness of galvanization layer is observed in SEM images as well as previous research. By modeling such a crack at the thread root, and understanding the varying crack tip characteristic at the boundary between steel substrate and inter-metallic layer will be beneficial. By numerically quantifying the energy available to initiate and propagate cracks in the steel substrate, we can conclude if the effects of brittle cracking in inter-metallic Fe-Zn layers are different for varying fastener diameters. The dependence on the geometric variation in these thread profiles can also be checked to compare and see the difference.

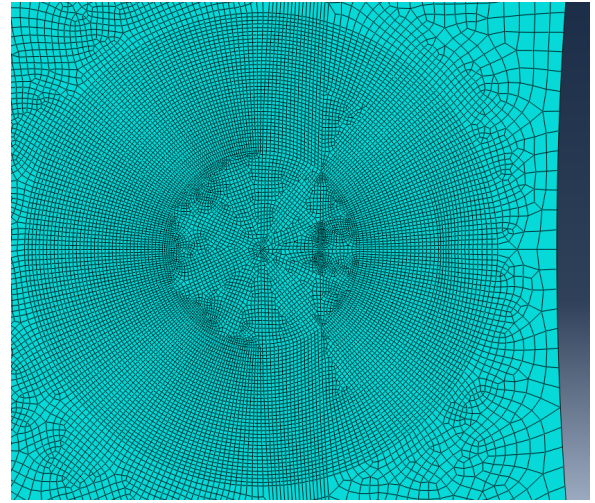
7.1 Model setup

Based on the previous analysis and discussion of axisymmetric models of varying diameters, we have prepared models for different fasteners. The analysis of effects due to J-integral around the crack tip zone requires a finer mesh, and therefore a larger number of mesh element. Keeping optimization in mind, we have considered sub-models of the original axisymmetric model. This sub-model includes the first and second engaged thread roots, as seen in figure 7.1a. The properties with respect to materials and contact have been kept unchanged. A mesh seed of 0.001mm has been considered in the crack tip region, keeping the mesh seed size in other regions consistent with the original model.

As we zoom in to the pre-defined crack, we see that the crack spans the thickness of the inter-metallic layers. This is representative of the cracking pattern observed in SEM images and also from the von Mises plot analysis, showing failure of these layers. Various crack modeling techniques are available in ABAQUS. Here we shall use the crack definition using an embedded seam and then perform a contour integral analysis. The seam will split as the analysis proceeds, as seen in figure 7.3. The fracture criterion parameters such as J-integral and stress intensity factor (for linear elastic fracture mechanics (LEFM)) can be requested from the software output. As seen above in image 7.2, the region in red represents the crack front and the point represents the crack tip. The rings around the crack front region are the contour integral surfaces defined.

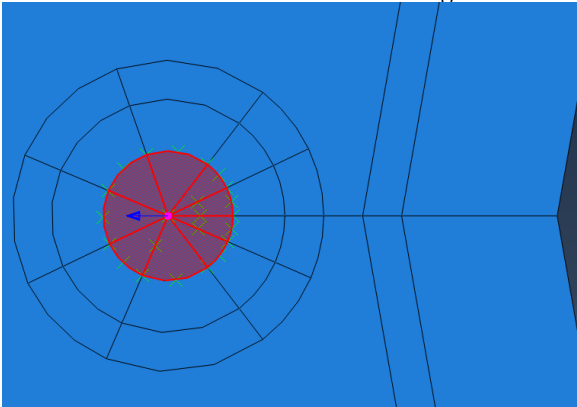


(a) Sub-model consisting of crack region at first engaged thread root

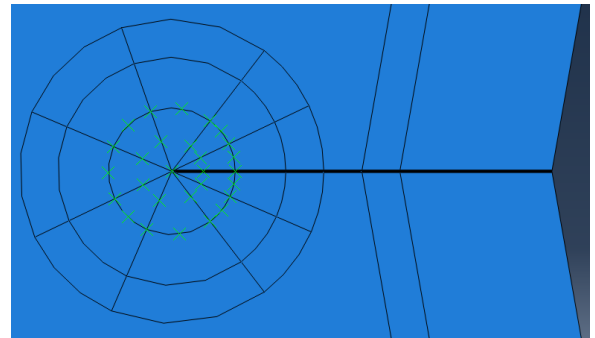


(b) Mesh pattern about the crack tip with quad-dominated elements [1]

Figure 7.1: Crack sub-model and mesh



(a) Spider-web partitioning around the crack tip for contour integral



(b) Crack seam represented by the black line

Figure 7.2: Crack definition and parameters to be defined for contour integral analysis

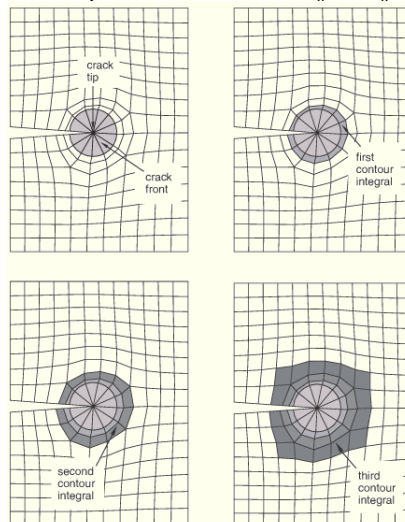


Figure 7.3: Definition of contour integral analysis parameters in ABAQUS/CAE [1]

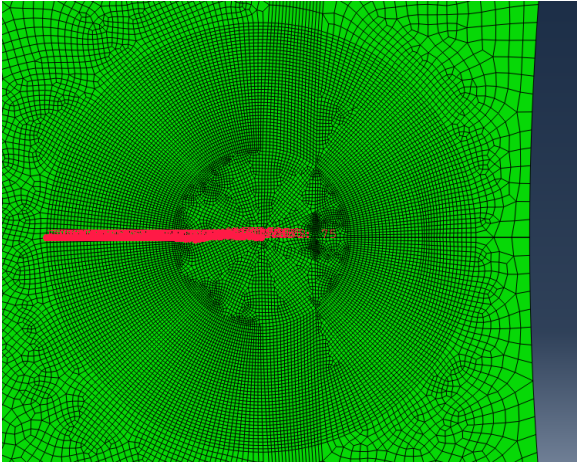
The initial angle of crack is considered to be normal to the thread root, incline at 0° . This has been defined based on the stresses obtained at the thread root which we have seen in previous chapters. The

maximum principal stress along the thread root circumference was found to be consistently tangential, implying that the crack formation would propagate perpendicular to this maximum principal stress, as per the criterion. This is also supported by the dominant axial stress in this region, which makes Mode I (tensile) dominant and initiating crack perpendicular to the bolt axis. Research has reported that the initial angle of crack will affect the value of stress intensity or J-integral [50]. Therefore, we have considered the orientation of crack to be consistent for the sake of comparison between increasing fastener diameter models.

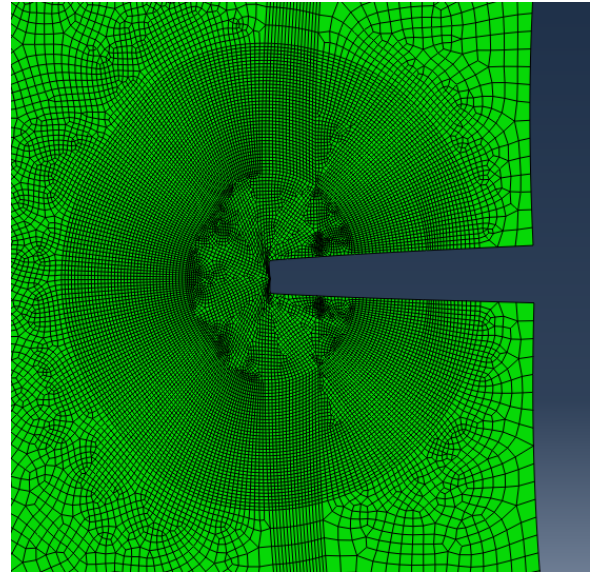
7.2 Results

At the crack tip, the presence of stress singularity prevents us from directly comparing the values per different fastener sizes. The stress intensity factor (K) for LEFM and the J-integral values for EPFM characterizes the stress singularity field and thereby the stress concentration at the crack tip region. Therefore, a direct comparison of stress plots for various fasteners will not portray any valid results. Yet, we can obtain insights such as the equalization of stress fields beyond the contour regions signifying the validity of our results.

The results from the sub-model are analyzed in this section. For this we shall first define the path about which we shall calculate the stress results. Given below in figure 7.4 is the undeformed and deformed shaped of the region in the immediate vicinity of the crack for an M72 fastener.



(a) Undeformed crack region and path considered for stress plots



(b) Deformed crack region and its vicinity

Figure 7.4: Undeformed and deformed crack region at the first engaged thread root - M72 fastener

The results are plot from the crack tip to the outermost contour of the crack region. As we can observe from von Mises plot values, the stress obtained from all fastener models fall below the yield stress limit of the steel substrate material, signifying the validity of the defined outer contours. We can also see the equalization of stresses beyond the vicinity of the crack tip, which would be useful in quantifying the far-field effects and calculating J-integral values. Even though we cannot compare the stress values at the crack tip due to singularity effects, the value highlights the concentration of stress at the crack tip, which can cause drastic effect in the presence of a material flaw like a crack and external loading. The identical profiles of max principal and axial stress distributions suggest that the crack predominantly experiences Mode I opening, suggesting the propagation of crack perpendicular to the axis of the fastener.

This leads us to the comparison of J-integral values for these models of increasing fastener diameter. The table 7.1 gives the values of J-integral calculated around the crack tip region in different models.

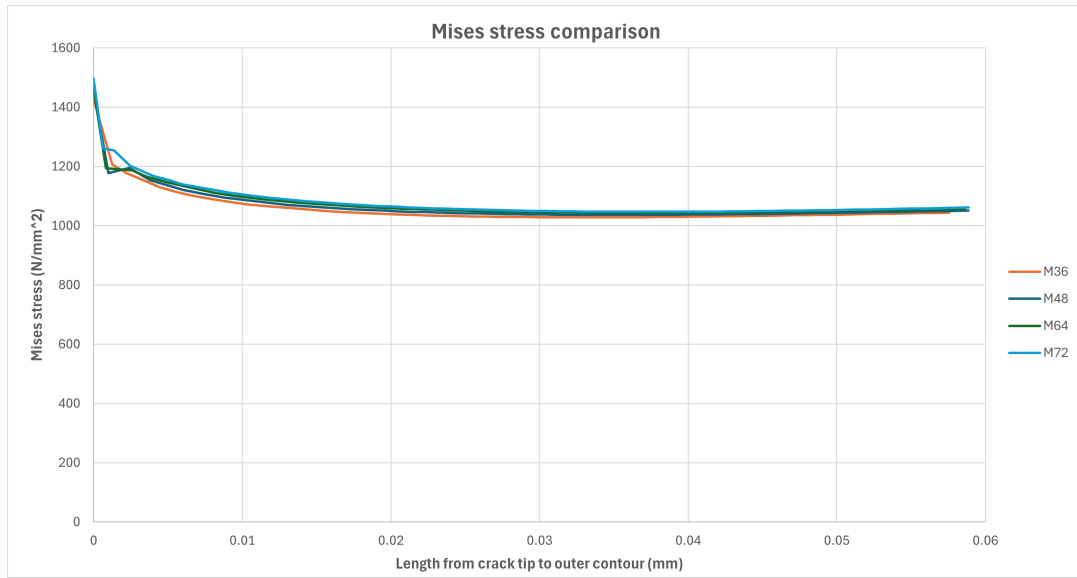


Figure 7.5: von Mises stress comparison along predefined path from crack tip

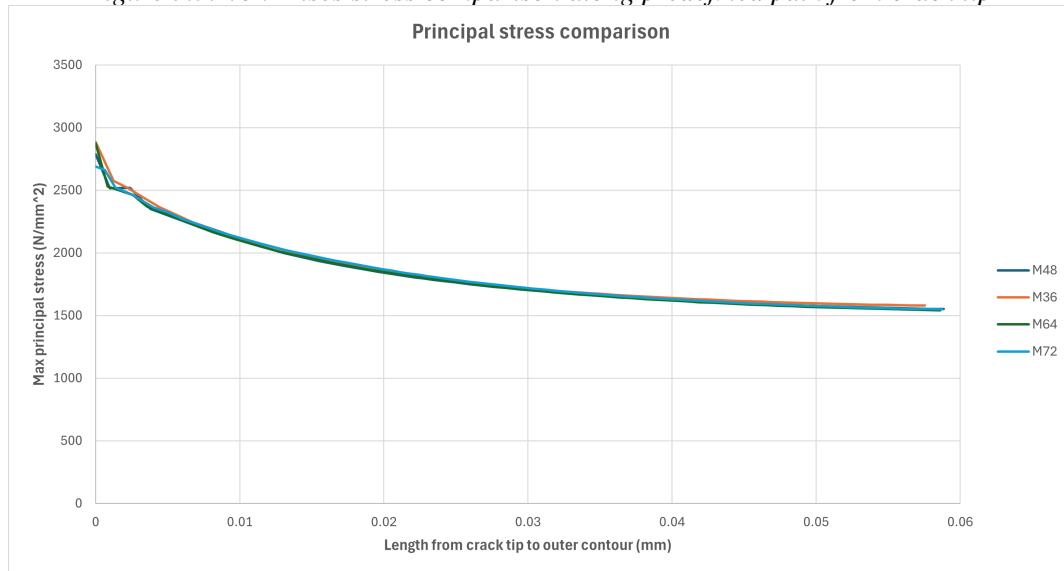


Figure 7.6: Max principal stress comparison along predefined path from crack tip

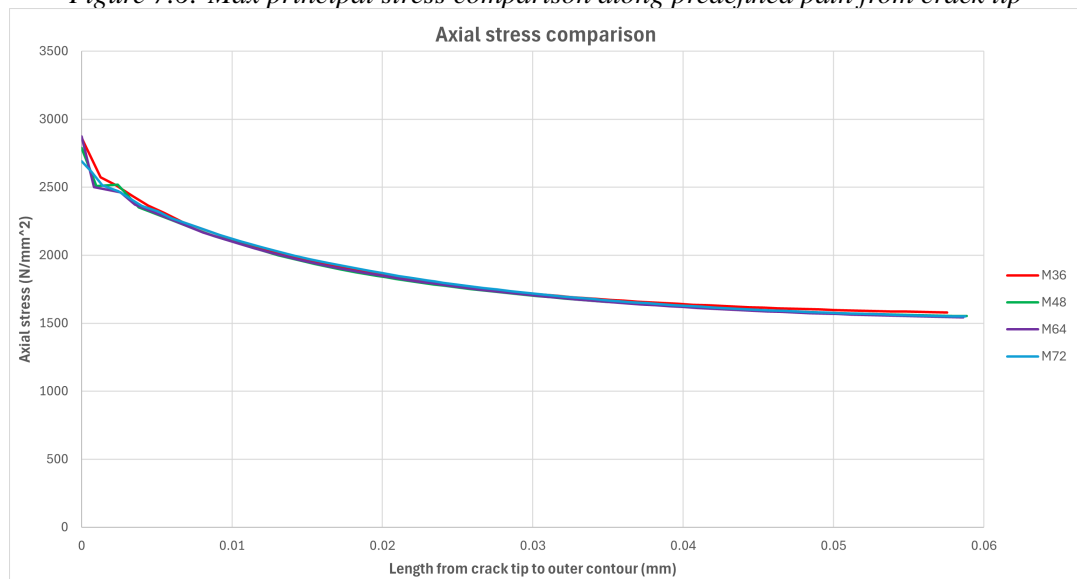


Figure 7.7: Axial stress comparison along predefined path from crack tip

The initial crack length and the geometric orientation of cracks in all these models are consistent.

Fastener	First integral	Second integral	Third integral	Fourth integral
M36	9.70	9.70	9.70	9.71
M48	11.40	11.41	11.41	11.41
M64	13.03	13.04	13.04	13.04
M72	14.61	14.61	14.61	14.61

Table 7.1: *J*-integral values (J/mm^2)

From the results, our first observation is the fact that *J*-integral values increase with increasing diameter, highlighting the global energy considerations that are different from local stress state discussed at the crack tip region earlier. The stress plots show great consistency across bolt sizes. When checking The principal stress plot, in the direction of axial preloading, suggest similar crack initiation mechanism in the steel substrate, irrespective of diameter. The non-dependence of stress values on the *J*-integral values suggest that the size of plastic zone and stress singularity is dominated by material properties rather than geometry. Further conclusions will be discussed subsequently.

7.3 Discussion

The comparison of stress plots and the values of *J*-integral obtained for different diameters of fasteners gives us few interesting insights which we shall discuss here. The standout observation here is the distinction between local crack-tip stress field suggesting consistency between increasing diameters of fasteners and the global fracture driving force parameters defined by the *J*-integral. In larger diameter threaded fasteners, the constraining effect which prevents plastic deformation at the tip of the crack is seen based on the higher volume of stressed area in the direct vicinity of critical thread root. This reduced plastic flow freedom is one of the reasons for an increasing crack-tip constraint, as larger specimens contain more material volume at high stress.

The *J*-integral values represent the energy available per unit crack extension. Increased structural stiffness in larger fasteners leads to higher energy storage. A larger *J*-integral value also suggest a larger plastic zone around the crack tip, which was noticed from our stress analysis indicating slightly larger stresses at crack tip for larger diameters. Theory also points towards a larger positive stress triaxiality measure when the notch is sharper, which is the case with increasing *d/p* ratio with increasing diameter. The stress is concentrated in a smaller area when the notch radii is smaller [5]. From the above results, we can conclude that crack initiation is governed by local stresses and material properties, therefore size-independent. While the crack propagation resistance increases with size due to constraint effects mentioned above.

Chapter 8

Conclusion and Recommendations

8.1 Conclusions

The work covered in this thesis set out to systematically investigate the impact of hot-dip galvanization on parameters which govern the behavior of large, preloaded threaded fasteners. Understanding the effect of hot-dip galvanization and the quantification of parameters such as the local stress distribution, fracture behavior and their variation with respect to geometry of fasteners were of particular focus, and they have been well-recorded and presented in this research report. The research was motivated by the growing trend towards larger wind turbines and the corresponding up-scaling of structural fasteners, which has introduced new challenges in ensuring both corrosion protection and mechanical reliability under demanding service conditions. Research conducted previously and later implemented in standards used today have confirmed that while hot-dip galvanization remains important for protecting steel fasteners from aggressive marine environments, it also introduces a layer of complexity to the mechanical performance of these components, as these inter-metallic layers are brittle compared to the substrate. Due to the size of these layers, the behavior of these brittle layers were not captured in any contemporary studies, both experimental and numerical. In experimental studies, the reduced lifetime of galvanized threaded fasteners under cyclic loading has been well discussed and implemented in codal standards, with theoretical explanation of why this behavior is seen. In numerical studies, the behavior has been discussed by trying to replicate the behavior and lifetime of threaded fasteners in cyclic loading experiments, and thereby analytically estimating the stress-strain properties of these layers, without actually modeling the physical boundary layers. Our study has tried to bridge this gap, mentioned in contemporary literature, with the help of physical boundary layers consisting of inter-metallic galvanized zinc layers, to see additional insights which have not been obtained in any research considered previously.

Through an integrated approach combining finite element modeling and a thorough review of experimental and numerical data from literature, the study revealed several important insights. Firstly, our research demonstrated that these brittle inter-metallic layers are prone to micro-cracking even under standard preload conditions. The von Mises yield criterion suggests that a material will only begin to fail when the maximum distortion energy is equal to or greater than the distortional energy limit required to yield the material. This is represented as the von Mises stress value in finite-element based numerical analysis. Based on the von Mises stress values seen from the comparison between galvanized and ungalvanized M36 threaded fasteners in the first section, which equalizes to the fracture stress of the inter-metallic layer as seen in the results, we foresee the formation of microcracks in these brittle layers. These microcracks, also visible in the scanning electron microscope images discussed, serve as stress concentrators, especially at the interface between the coating and the steel substrate where most of these crack tips were noticed. When subjected to cyclic loads typical of

wind turbine operation, these flaws significantly increase the risk of fatigue crack initiation and subsequent propagation. Also, the effect of these stress-concentrating cracks needed to be quantified, which we see in the subsequent section of fracture mechanical analysis. Alongside this, we also identified that the δ inter-metallic layer behaves differently to others based on their plastic strain development behavior and damage analysis reported in the results, and this difference led to a peculiar way of crack formation inside the galvanized zinc layer and not just on the surface, which is not seen in an ungalvanized thread fastener where cracks typically begin from the surface, as confirmed also by fractography reported in SEM images by TNO. Overall the presence of micro-cracks at nominal preload levels is concerning looking at it from a fatigue or fracture mechanics perspective, with its effect on the steel substrate requiring further analysis done subsequently in this research.

The second conclusion corresponds to the understanding of difference in local stress states in larger diameter threaded fasteners with a change in thread geometry. Numerical simulations conducted as part of this research provided a good understanding of how these effects scale with fastener size. This is done so as to quantify the geometric size effect in notched components such as the threaded fasteners, to confirm if various quantified parameters can point towards a detrimental impact on the lifetime of these fasteners. This is especially important due to the variation in thread pitch and nominal diameter which leads to variation in thread geometry and notch sharpness, which are key for local stress concentration. With regards to this, we see a greater stress concentration by 2 percent with larger stress peaks in all our stress results. The small increase cannot be ruled out since it is accompanied by a shift in peak closer to the thread root boundary by 1 percent on the normalized scale, signifying the increased susceptibility to accelerated crack propagation due to this higher stress, as well as the reduced support effect and lack of redistribution of stress in larger fasteners reduced by approximately 3 percent in larger diameter threaded fasteners. These insights, when seen together with reduced stress distribution in the interior of the fasteners as well as plastic deformation of thread root region points towards few interesting insights: firstly, the design of these fasteners' geometry must be done to ensure consistent behavior among various sizes; secondly, a higher and more localized stress concentration found in larger diameter fasteners is concerning when it comes to crack propagation into the steel substrate. As mentioned earlier, the effect of brittle cracking of galvanized zinc layer is magnified by the presence of a highly localized, highly stressed region seen in larger diameter fasteners' thread roots. Therefore a fracture mechanics approach is considered to effectively evaluate the extent of detrimental impact in such galvanized, threaded fasteners.

The study's fracture mechanics analysis, using the J-integral as a measure of crack-driving force, further highlighted that larger fasteners have a greater energy release rate at potential crack sites, which could accelerate crack growth once initiated. The consideration of an already cracked galvanization layer is consistent with our initial results as well as fractography analysis of galvanized specimens. Also, the comparison of J-integral values instead of stress intensity factor (K) values is done to ensure more accuracy in results since the analysis of elastic-plastic material properties under monotonous loading is important at the local, highly stressed thread root region we have considered. The J-integral values show a 50 percent increase signifying a clear detrimental effect due to the presence of crack tip at the interface between the steel substrate and zinc layer. Being a measure of the crack driving force, this increasing value is a result of the effects discussed in the comparison of local stress effects: the increased peak stress values, the reduced support effect and the reduced redistribution of stresses.

The research also validated the use of two-dimensional axisymmetric finite element models for detailed local analysis when including the physical modeling of galvanized zinc layers which could represent the comparison between larger diameter fasteners and the fracture mechanics approach, showing that these models can capture the critical stress and strain fields at the thread root while offering significant computational efficiency. To this end, the three-dimensional approach cannot be fully disregarded, since it can provide detailed insights as well as comprehensive results including the modeling of threaded fastener geometry aspect which cannot be represented in simple 2D models,

keeping in mind the computational capacity and time required to run these finite-element analyses.

In summary, the thesis underscores a fundamental trade-off in the use of hot-dip galvanization for large-diameter fasteners: while it is essential for long-term corrosion resistance, it can compromise mechanical integrity by introducing brittle phases and microcracks that act as initiation sites for fatigue failure. This has also been highlighted in S-N curves considered by codes which consider the detrimental effect of hot-dip galvanization. The adverse effects become more pronounced as fastener size increases, due to both geometric and aforementioned material factors. The effect of a reduction in endurance limit with an increasing diameter has been experimentally established for hot-dip galvanized thread fasteners [14], the mechanics of which is further reinforced by the conclusions formed in our research of an increasing crack driving force, larger local stress concentration and larger highly-stressed region in the immediate vicinity of the thread root seen in larger diameter fasteners. These findings have direct implications for the design, manufacturing, and maintenance of offshore wind turbine connections. Provided that these findings are also validated by experimental results, we must account for the size-dependent risks associated with galvanization, and that further research is needed into alternative coating technologies, improved thread geometries, and advanced inspection methods to ensure both durability and safety in the next generation of offshore wind installations. Ultimately, this work advances the understanding of the interplay between protective coatings and mechanical performance in large-scale structural fasteners, providing a scientific basis for more robust and reliable offshore wind turbine designs as the industry continues to evolve. On the numerical analysis front, we understand from this study the importance of including the physical boundary layers, the effect of which might not be evident in comparative analysis of local stress and strain but shows a major difference when it comes to the fracture mechanical approach. Therefore, future studies incorporating these boundary layers will be important to capture the real-life effects on these large, preloaded threaded fasteners.

8.2 Limitations

Throughout this research, we have seen results which signify the behavior of galvanized, preloaded threaded fasteners as concluded earlier. With these consideration comes certain limitation which have been introduced to simplify our scope while keeping the core outcome of the research valid. This is done so as to ensure that we obtain results which we can compare to form valuable insights and to ensure that these valid outputs could be utilized further to expand the study.

We shall first look at certain limitations on the geometry. The tolerance between engaged threads has been mentioned in chapter 4 in the model set up. ISO 965-1:2013 [30] suggests that engaged threads should preferably be made to form H/g, H/h or G/h fits, to guarantee sufficient overlaps. The difference in local stress distribution due to these different tolerance classes is not looked into in our study. Also in this study, the effect of imperfections that arise due to manufacturing is not considered, and it is understood that it can have an effect on the local stress state in engagement. This is partially covered by research such as [40]. Therefore, the perfect geometry of threads might be a limitation here, but it must be understood that imperfect geometry for different sizes of fasteners will not allow for valid comparison between the behavior of these components.

In line with this, we must understand the actual behavior of ring flange segments is not being considered in our scope of study. Ring flanges in an offshore environment is subject to external loading, which are transferred to the threaded fastener joining them as axial forces and bending to the eccentricity of the support structure's wall. The focus of our study being to analyze the effect on galvanization due to uniaxial preloading, we do not consider any external loading action. It is important to understand that quantifying the effects due to galvanization layers under uniaxial preloading is only considered in the scope to study the effect of cracking in these layers before being subject

to external loading. This effect can be regarded as future scope to understand the extended effect of external loading on these fasteners as it might have aggravated and detrimental impacts. Regardless, a fully representative model consisting of washers and segments have been considered, making the application of external loads to the developed model framework simple, provided the data on external loading and their frequency is available.

The considerations for the galvanized zinc coating has been based on observations from SEM images and codal provisions suggesting only minimum and maximum limits to thickness. The chances of a thicker galvanized zinc coating for larger diameter fasteners is a possibility in theory owing to the larger thermal mass in fasteners of increasing diameters. Experimental research also mentions the effect of silicon content on the structure and thickness of zinc coating applicable on the steel specimen, with thickness increasing with increasing Si content [52]. Yet, the fasteners analyzed using scanning electron microscope imagery by TNO shows that threaded fasteners of all sizes have on average the same coating thickness. This could be due to the increased manufacturing quality practices followed by the manufacturer, but it remains to be seen the extent to which it can vary. We therefore proceeded with the data available. Finally, the SEM images also suggest a large number of cracks formed in the galvanized zinc layers, which can cumulatively have a larger effect on the stiffness of the galvanized zinc layers and the stress concentrations at the tip of each of these cracks. The local stress state due to contact between engaged threads might be slightly different, especially at the engaged flanks of the threads, and the calculation of crack tip energies would vary. For the sake of comparison and to form conclusions with the idealized geometry, the crack is considered at one location for all fasteners.

Finally, we have seen the computational limitation while comparing the two-dimensional and three-dimensional stress plots. This is a major limitation which has been discussed in chapter 5. Even when there is a general agreement between the trends of values, reported in this study as well as from the literature review, the scatter in 3D plot is attributed to the limitation of the mesh size we can provide and the inability to have a hexahedral mesh for the complicated helical pitch geometry of the thread, which was considered so as to stay within the limits of time and computation capacity. Nevertheless, our focus on physically modeling the galvanized zinc boundary layers makes the two-dimensional approach a good one, giving us the ability to understand in detail the local stress values and fracture mechanics parameters. An ideal approach would be to incorporate these modeling considerations in a three-dimensional model consisting of the right mesh properties and incorporating all geometrical parameters affecting the local stress concentration.

8.3 Recommendations

In light of the conclusions drawn and the limitations encountered in this study, several avenues for future research are recommended to deepen and broaden the understanding of hot-dip galvanized large-diameter threaded fasteners, especially in offshore wind turbine applications. First and foremost, there is a pressing need for extensive experimental validation to complement the numerical findings presented here. While advanced finite element modeling has provided valuable insights, full-scale laboratory testing of galvanized fasteners under realistic service conditions—including variable preloading and the complex external loads typical of offshore environments — will be essential for confirming and refining these results. The focus of these experimental studies should be to verify and evaluate the cracking behavior of galvanized zinc layers and the propagation of cracks. Therefore, highly extensive experimental setups which can capture crack formation in real-time at predefined locations could be useful. Experiments such as the three-point bending test can induce controlled stress at specific locations which can be observed in real-time with the help of optical or scanning electron microscopy, as well as innovative fractographic approaches like the laser scanning confocal microscope which can be used to reconstruct 3D surfaces. It could also be experimental tests such as preloading or bending of a section of these fasteners subjected to a digital image correlation, which

is an optical technique used to track and analyze deformation by comparing images taken at a fixed frequency. This could be used to calculate the strain values and relate them to the cracking or fracture properties of these metallic layers. Such experiments should also account for variations in thread geometry, manufacturing tolerances, and the presence of real-world imperfections that may influence mechanical performance and fatigue life. Integrating these into both experimental and computational studies will provide a more comprehensive understanding of the mechanisms leading to crack initiation and propagation within the galvanized layers. Expanding the scope to include the behavior of entire joint assemblies, rather than isolated fasteners, will further enhance the relevance of the findings to actual offshore wind turbine structures, but understanding this microscopic behavior when conducting tests on a sizable scale would only be possible with a multi-scale approach, currently applicable in numerical analysis.

Given the trade-offs between corrosion protection and mechanical integrity in hot-dip galvanization, it is also advisable for future work to explore alternative or hybrid coating technologies. Comparative studies based on the trade-off between thickness of coating providing ample stiffness against early life cracking and brittle or reduced absolute strength of these layers compared to steel substrate could be conducted under both laboratory and field conditions, proving valuable in identifying optimal protective strategies for offshore applications. There are various galvanization procedures utilized by the industry today, which promote formation of inter-metallic layers of varying thickness and properties, which is discussed by research such as [21]. Therefore the performance of these galvanization techniques under operational conditions of preloaded fasteners can be studied. A deeper investigation into the microstructural characteristics of zinc coatings, particularly the formation and growth of brittle inter-metallic phases and microcracks, will be beneficial and support the parameters to be considered in numerical modeling to give more comprehensive results. Systematic studies on the effects of coating thickness variations and manufacturing processes will also contribute.

On the computational front, the challenges faced with three-dimensional finite element modeling—such as mesh refinement in complex thread geometries—highlight the need for further advancements in numerical techniques and greater computational capacity. Employing adaptive meshing, multi-scale modeling, or machine learning-assisted simulations may offer higher accuracy and efficiency, enabling more detailed investigations across a broader range of fastener sizes and loading conditions. An ideal scenario would be a full three-dimensional model analysis incorporating the thickness of galvanization layers with their mechanical and geometric properties such as hardness values which can alter the behavior under stress, as well as incorporating all the geometric properties of the threaded fastener which the actual production considers. To this end, the recommendation for the inclusion or exclusion of physical galvanization layers in finite-element models is subjective: throughout this research, we understood that the comparison of local stress-state depends more on the geometric size effect, while evaluating the fracture parameters depends on both the geometry and material properties of both the substrate and galvanized zinc layers. Therefore, development of constitutive models incorporating the behavior of galvanized zinc layers will be sufficient for the former, similar to the engineering models approach by Oechsner[41] and Eichstadt[14]. For the latter requirement, it is definitely beneficial to consider modeling these layers in the finite element model.

Finally, long-term field studies are strongly recommended to monitor the in-service performance of galvanized fasteners in operational offshore wind turbines. Such monitoring will provide valuable data on corrosion progression, mechanical degradation, and failure modes over time, bridging the gap between controlled laboratory research and real-world application. Insights gained from these studies should inform updates to industry standards and design codes, ensuring that evolving knowledge is translated into safer and more reliable offshore wind energy infrastructure. By pursuing these directions, future research can significantly enhance the understanding and management of the complex interactions between corrosion protection and mechanical reliability in large-diameter fasteners, ultimately supporting the continued growth and sustainability of offshore wind energy projects.

Bibliography

- [1] ABAQUS, Inc. *ABAQUS Version 6.6 Documentation*. Build ID: 2006_03_01-08.54.35 22833. 2006. URL: <https://classes.engineering.wustl.edu/2009/spring/mase5513/abaqus/docs/v6.6/books/popups/info.html> (visited on 07/05/2025).
- [2] Andrea Arguillarena et al. ‘Life-cycle assessment as a tool to evaluate the environmental impact of hot-dip galvanisation’. In: *Journal of Cleaner Production* 290 (Mar. 2021). ISSN: 09596526. DOI: [10.1016/j.jclepro.2020.125676](https://doi.org/10.1016/j.jclepro.2020.125676).
- [3] Walter von Baekmann, Wilhelm Schwenk and Werner Prinz. *Handbook of Cathodic Corrosion Protection: Theory and Practice of Electrochemical Protection Processes*. 3rd ed. Elsevier Science, 1997. ISBN: 9780884150565.
- [4] Hagar El Bamby et al. ‘The influence of high preloading forces on the behaviour of the bolt in ring flange connection’. In: *Nordic Steel 2024* (2024).
- [5] A Amine Benzerga and Jean-Baptiste Leblond. ‘Ductile fracture by void growth to coalescence’. In: *Advances in Applied Mechanics*. Advances in applied mechanics. Elsevier, 2010, pp. 169–305.
- [6] Jarryd Braithwaite et al. ‘Sensitivity analysis of friction and creep deformation effects on preload relaxation in offshore wind turbine bolted connections’. en. In: *Appl. Ocean Res.* 101.102225 (Aug. 2020), p. 102225.
- [7] I A Burchitz. *Adaptive through-thickness integration strategy for shell elements Publication number: P07.1.016 Netherlands Institute for Metals Research*. Tech. rep. 2007.
- [8] Lu Cheng et al. ‘FE-assisted investigation for mechanical behaviour of connections in offshore wind turbine towers’. In: *Engineering Structures* 285 (June 2023), p. 116039. ISSN: 01410296. DOI: [10.1016/j.engstruct.2023.116039](https://doi.org/10.1016/j.engstruct.2023.116039). URL: <https://linkinghub.elsevier.com/retrieve/pii/S0141029623004534>.
- [9] L. Collini et al. ‘Slip strength of COR-TEN and Zn-coated steel preloaded bolted joints’. In: *Results in Engineering* 22 (June 2024). ISSN: 25901230. DOI: [10.1016/j.rineng.2024.102009](https://doi.org/10.1016/j.rineng.2024.102009).
- [10] Deutscher Ausschuss für Stahlbau (DAST). *DAST-Richtlinie 021: Schraubenverbindungen aus feuerverzinkten Garnituren M39 bis M72 entsprechend DIN EN 14399-4, DIN EN 14399-6*. Düsseldorf: Stahlbau Verlags- und Service GmbH, 2013. ISBN: 978-3-941687-16-5.
- [11] DNV. *Energy Transition Outlook 2024 Executive Summary: A Global and Regional Forecast to 2050*. Executive summary of DNV’s annual energy transition forecast. Høvik, Norway: DNV, 2024. URL: https://ppl-ai-file-upload.s3.amazonaws.com/web/direct-files/attachments/40622646/b5ce9fad-462d-4db5-b2c5-3963a1aec254/DNV_ETO_2024_Exec_Summary_highres.pdf.
- [12] Joseph P Domblesky and Feng Feng. ‘A parametric study of process parameters in external thread rolling’. In: *Journal of Materials Processing Technology (121)* (2002).

- [13] M. A. Eder, P. U. Haselbach and O. V. Mishin. ‘Effects of Coatings on the High-Cycle Fatigue Life of Threaded Steel Samples’. In: *Journal of Materials Engineering and Performance* 27 (6 June 2018), pp. 3184–3198. ISSN: 1059-9495. DOI: [10.1007/s11665-018-3399-2](https://doi.org/10.1007/s11665-018-3399-2). URL: <http://link.springer.com/10.1007/s11665-018-3399-2>.
- [14] Rasmus Eichstadt. *Fatigue Assessment of Large-Size Bolting Assemblies for Wind Turbine Support Structures-Ermüdungsbewertung sehr großer Schraubenverbindungen für Tragstrukturen von Windenergieanlagen*. Tech. rep. 2019.
- [15] European Committee for Standardization. *High-strength structural bolting assemblies for pre-loading – Part 4: System HV – Hexagon bolt and nut assemblies*. Dutch adoption of EN 14399-4:2015. Delft, Netherlands, 2015.
- [16] Emmanuel E Gdoutos. *Fracture mechanics*. en. 3rd ed. Solid mechanics and its applications. Cham, Switzerland: Springer Nature, Mar. 2020.
- [17] Ralf Glienke et al. ‘Further development of detail categories for bolt-assemblies subjected to normal stress in steel constructions’. In: *ce/papers* 6 (3-4 Sept. 2023), pp. 1256–1262. ISSN: 2509-7075. DOI: [10.1002/cepa.2596](https://doi.org/10.1002/cepa.2596).
- [18] Hao Gong, Jianhua Liu and Xiaoyu Ding. ‘Study on the mechanism of preload decrease of bolted joints subjected to transversal vibration loading’. en. In: *Proc. Inst. Mech. Eng. Pt. B: J. Eng. Manuf.* 233.12 (Oct. 2019), pp. 2320–2329.
- [19] E. L. Grimsmo et al. ‘Failure modes of bolt and nut assemblies under tensile loading’. In: *Journal of Constructional Steel Research* 126 (Nov. 2016), pp. 15–25. ISSN: 0143974X. DOI: [10.1016/j.jcsr.2016.06.023](https://doi.org/10.1016/j.jcsr.2016.06.023).
- [20] Philipp Jörg Hammer. *Numerical Simulation of Crack Propagation during the Deformation of Galvanized PHS Sheets*. Tech. rep. Chair of Mechanics - Montan Universitat, Leoben, 2020.
- [21] Jinshan He et al. ‘Fracture properties of zinc coating layers in a galvanized steel and an electrolytically galvanized steel’. In: *Materials Science and Engineering: A* 732 (Aug. 2018), pp. 320–325. ISSN: 09215093. DOI: [10.1016/j.msea.2018.05.084](https://doi.org/10.1016/j.msea.2018.05.084).
- [22] David V. Hutton. *Fundamentals of Finite Element Analysis*. Boston: McGraw-Hill, 2004. ISBN: 9780072395365.
- [23] Huyett. *Stages and Types of Steel Corrosion*. Accessed: 2025-07-28. 2024. URL: <https://www.huyett.com/blog/steel-corrosion>.
- [24] International Organization for Standardization. *Fasteners – Hot dip galvanized coatings*. Adopted from EN ISO 10684:2004, identical to ISO 10684:2004. Delft, Netherlands, July 2004.
- [25] International Organization for Standardization. *ISO general purpose metric screw threads – Tolerances – Part 2: Limits of sizes for general purpose external and internal screw threads – Medium quality*. Dutch adoption of ISO 965-2:2024. Delft, Netherlands, 2024.
- [26] International Organization for Standardization. *ISO general purpose metric screw threads – Tolerances – Part 5: Limits of sizes for internal screw threads to mate with hot-dip galvanized external screw threads*. Dutch adoption of ISO 965-5:1999. Delft, Netherlands, 1999.
- [27] International Organization for Standardization. *ISO general purpose screw threads – Basic profile – Part 1: Metric screw threads*. Dutch adoption of ISO 68-1:2023. Delft, Netherlands, 2023.
- [28] International Organization for Standardization. *Mechanical properties of fasteners made of carbon steel and alloy steel – Part 1: Bolts, screws and studs with specified property classes – Coarse thread and fine pitch thread*. Dutch adoption of EN ISO 898-1:2013, identical to ISO 898-1:2013. Delft, Netherlands, 2013.

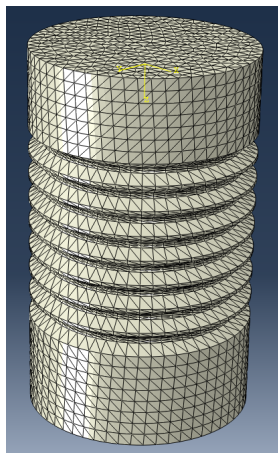
- [29] International Organization for Standardization. *Plain washers – Normal series – Product grade A*. Dutch adoption of ISO 7089:2000. Delft, Netherlands, 2000.
- [30] *ISO general purpose metric screw threads — Tolerances — Part 1: Principles and basic data*. International Standard. ICS 21.040.10. Geneva, Switzerland: International Organization for Standardization, 15 Sept. 2013.
- [31] R. Lanzafame, T. van Woudenberg and S. Verhagen. *Modelling, Uncertainty and Data for Engineers (MUDE) Textbook*. CC BY 4.0. 2024. URL: <https://mude.citg.tudelft.nl/book> (visited on 13/06/2025).
- [32] Gui Li and Xiaoyu Long. ‘Mechanical behavior and damage of zinc coating for hot dip galvanized steel sheet DP600’. In: *Coatings* 10 (3 Mar. 2020). ISSN: 20796412. DOI: [10.3390/coatings10030202](https://doi.org/10.3390/coatings10030202).
- [33] Diogo Tubertini Maciel et al. ‘Characteristics of machined and formed external threads in titanium alloy’. In: *International Journal of Advanced Manufacturing Technology* 79 (5-8 July 2015), pp. 779–792. ISSN: 14333015. DOI: [10.1007/s00170-015-6858-z](https://doi.org/10.1007/s00170-015-6858-z).
- [34] Andrea L Mack et al. *FINITE ELEMENT MODEL MESH REFINEMENT EFFECTS ON QUALIFICATION OF NUCLEAR GRADE GRAPHITE COMPONENTS*. Tech. rep. Idaho National Laboratory, Idaho Falls, Idaho, 2023. URL: <http://www.inl.gov>.
- [35] C A Madsen et al. ‘Analytical and numerical investigation of bolted steel ring flange connection for offshore wind monopile foundations’. In: *IOP Conf. Ser. Mater. Sci. Eng.* 276 (Dec. 2017), p. 012034.
- [36] Frithjof Marten and Peter Schaumann. ‘Fatigue Resistance of High Strength Bolts with Large Diameters’. In: *Proceedings of [Conference Name, if known]*. Accessed: 2025-06-21. Hannover, Germany, 2008. URL: https://www.stahlbau.uni-hannover.de/fileadmin/stahlbau/publications/2009-03-12_Marten.pdf.
- [37] Clifford Matthews. ‘Fasteners and couplings – better design’. In: *Case Studies in Engineering Design*. Elsevier, 1998, pp. 86–100.
- [38] Ali Mehmanparast, Saeid Lotfian and Sukumara Pillai Vipin. ‘A review of challenges and opportunities associated with bolted flange connections in the offshore wind industry’. In: *Metals* 10.6 (2020), p. 732. DOI: [10.3390/met10060732](https://doi.org/10.3390/met10060732).
- [39] Shin-Ichi Nishida, Chikayuki Urashima and Hidetoshi Tamasaki. ‘A new method for fatigue life improvement of screws’. In: *European Structural Integrity Society*. ESIS publication. Elsevier, 1997, pp. 215–225.
- [40] Nao Aki Noda et al. ‘Effect of pitch difference between the bolt-nut connections upon the anti-loosening performance and fatigue life’. In: *Materials and Design* 96 (Apr. 2016), pp. 476–489. ISSN: 18734197. DOI: [10.1016/j.matdes.2016.01.128](https://doi.org/10.1016/j.matdes.2016.01.128).
- [41] M. Oechsner and Peter Schaumann. *Experimental and computational evaluation of the fatigue strength of large-sized bolts in steel construction taking into account edge layer influences*. 2016. ISBN: 978-3-96780-014-2. URL: www.stahlforschung.de.
- [42] Norihiko L. Okamoto et al. ‘Compression deformability of and Fe-Zn intermetallics to mitigate detachment of brittle intermetallic coating of galvanized steels’. In: *Scripta Materialia* 69 (4 Aug. 2013), pp. 307–310. ISSN: 13596462. DOI: [10.1016/j.scriptamat.2013.05.003](https://doi.org/10.1016/j.scriptamat.2013.05.003).
- [43] Norihiko L. Okamoto et al. ‘Fracture toughness of the Fe-Zn intermetallic compounds measured by bend testing of chevron-notched single-crystal microbeams’. In: *ISIJ International* 58 (9 Sept. 2018), pp. 1569–1577. ISSN: 09151559. DOI: [10.2355/isijinternational.ISIJINT-2018-068](https://doi.org/10.2355/isijinternational.ISIJINT-2018-068).

- [44] Ivan Okorn et al. 'Examining the effects on a fatigue life of preloaded bolts in flange joints: An overview'. en. In: *Metals (Basel)* 14.8 (July 2024), p. 883.
- [45] Orsted. *Orsted's first Dutch offshore wind farm fully commissioned*. 2020. URL: <https://orsted.com/en/media/news/2020/11/448070886682487> (visited on 27/11/2020).
- [46] Qinxue Pan et al. *Research Review of Principles and Methods for Ultrasonic Measurement of Axial Stress in Bolts*. Dec. 2020. DOI: [10.1186/s10033-020-0431-x](https://doi.org/10.1186/s10033-020-0431-x).
- [47] Hyungkwon Park et al. 'Effect of galvannealing temperature on coating microstructure evolution correlated to flaking degradation on galvannealed interstitial-free steel'. en. In: *Surf. Coat. Technol.* 404.126446 (Dec. 2020), p. 126446.
- [48] Peter Schaumann and Rasmus Eichstädt. 'Experimental and Analytical Fatigue Assessment of High-Strength Bolts for Wind Turbine Structures'. In: *Festschrift Jörg Lange*. Heft 120. This paper was published in a special issue (Festschrift) dedicated to Prof. Dr.-Ing. Jörg Lange on the occasion of his 60th birthday. Darmstadt, Germany: Technische Universität Darmstadt, Institut für Stahlbau und Werkstoffmechanik, July 2018. URL: https://www.researchgate.net/publication/335703565_Experimental_and_Analytical_Fatigue_Assessment_of_High-Strength_Bolts_for_Wind_Turbine_Structures.
- [49] M. Seidel and P. Schaumann. 'Measuring Fatigue Loads of Bolts in Ring Flange Connections'. In: (2001). Available at: University of Hannover, Institute for Steel Construction, Appelstr. 9A, D-30167 Hannover.
- [50] Iman Shakeri et al. 'Effect of manufacturing defects on fatigue life of high strength steel bolts for wind turbines'. In: *Engineering Failure Analysis* 141 (Nov. 2022), p. 106630. ISSN: 13506307. DOI: [10.1016/j.engfailanal.2022.106630](https://doi.org/10.1016/j.engfailanal.2022.106630). URL: <https://linkinghub.elsevier.com/retrieve/pii/S1350630722006033>.
- [51] Şule Yıldız Şirin. 'The effect of hot dip galvanizing process on the fatigue properties of hot rolled and quenched-tempered AISI 4340 steel'. In: *Pamukkale Univ. J. Eng. Sci.* 24.4 (2018), pp. 626–634.
- [52] Milan Šmak et al. 'The influence of hot-dip galvanizing on the mechanical properties of high-strength steels'. en. In: *Materials (Basel)* 14.18 (Sept. 2021), p. 5219.
- [53] TNO. *Bolt and Beautiful: Publieke samenvatting / Public summary*. HER+21-02867818. Project supported by the Dutch Ministry of Economic Affairs and Climate Policy, Topsector Energie. Grant amount: €2,822,854. The Hague, Netherlands: Nederlandse Organisatie voor toegepast-natuurwetenschappelijk onderzoek (TNO), 2022. URL: <https://ppl-ai-file-upload.s3.amazonaws.com/web/direct-files/attachments/40622646/9aff0c80-030d-41c3-a354-c89fe5eeae56/project-bolt-and-beautiful-37060.pdf>.
- [54] Fei Yang et al. 'Fracture simulation of a demountable steel-concrete bolted connector in push-out tests'. In: *Engineering Structures* 239 (July 2021). ISSN: 18737323. DOI: [10.1016/j.engstruct.2021.112305](https://doi.org/10.1016/j.engstruct.2021.112305).
- [55] X.G. Zhang. 'Galvanic Corrosion of Zinc and Its Alloys'. In: *Journal of The Electrochemical Society* 143 (1996), p. 1472. DOI: [10.3390/met10060732](https://doi.org/10.3390/met10060732).

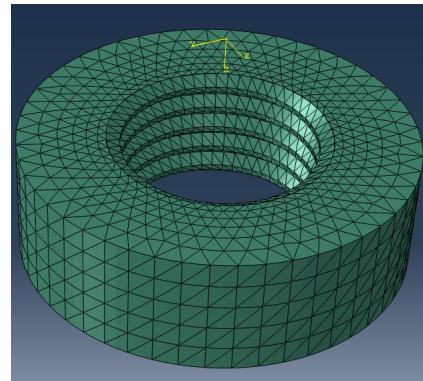
Appendix A

3D axisymmetric model

Along with the comparison between axisymmetric 2D and full 3D models, we have also seen results from a similarly axisymmetric 3D model. This is because the full three-dimensional model requires time and effort for an effective and optimum partition of layers, so as to get a consistent mesh, while at the same time keeping in mind computation times required for running the analysis on parts with more than 100,000-200,000 elements. With the three dimensional axisymmetric model, the partitioning was easier and we were able to achieve optimum number of elements to get a first look into the results of the analysis.



(a) Meshes axisymmetric nut - M36



(b) Meshed axisymmetric stud - M36

Figure A.1: Meshed part of the 3D axisymmetric model

ABAQUS/Explicit analysis is used to attain the results from the 3D analysis. The material models remain same as discussed in the two-dimensional model. In terms of the definition of contact, the explicit solver has the option of mechanical constraint formulation whereby the penalty contact method is chosen. The sliding formulation considered is the finite sliding formulation, which is different from that considered for the two-dimensional model since the assembly of components in the 3-D model might not have the same nodes on the slave surface interact with the same local area of the master surface throughout the analysis, mainly because of the coarser mesh considered for the global analysis. As for the contact interaction property, parameters have not changed from the two-dimensional model.

A major drawback in the three-dimensional analysis, in both the axisymmetric as well as full thread models, is the inability to optimally model the inter-metallic layers. As discussed earlier, the idea of having the sub-model in analyzing local stress and strain concentration using a finer mesh would be implemented keeping in mind the fine boundary layer of the inter-metallic layer. As a start, we

have modeled these inter-metallic layers as separate parts and assembled them to the thread and nut substrate, as shown in figures A.2 and A.3.

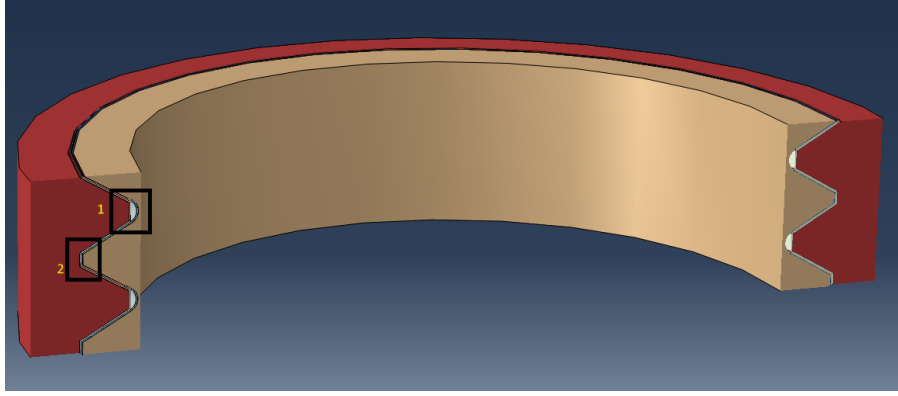
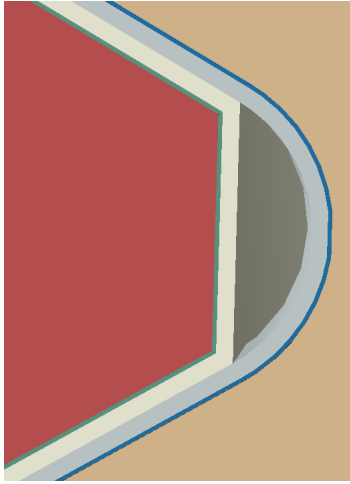
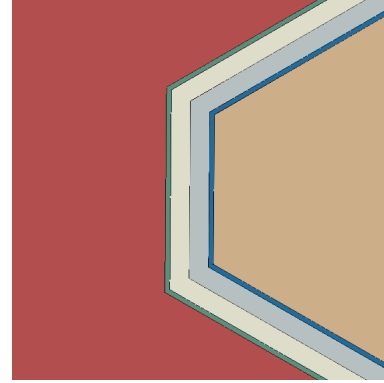


Figure A.2: Three-dimensional axisymmetric submodel representing inter-metallic layers in assembly. Box 1 and 2 are further explained in the next figure



(a) Box 1 - at the external thread root



(b) Box 2 - at external thread crest

Figure A.3: Magnified locations of interest. The layers are as follows (left to right): Nut steel substrate, δ phase on nut, ζ phase on nut, ζ phase on stud, δ phase on stud, stud steel substrate

As discussed in section 4.1, the thickness of δ phase is $15\mu\text{m}$. This thickness compared to the general dimensions of the flank and roots of the two engaged threads is very small. As seen in figure A.4, the general dimensions of the delta layer boundaries depict an aspect ratio of 25 between the thickness of the layer and the next smallest dimension of the layer. This makes seeding and meshing of these layers very hard, in the sense that a large number of elements are required for a successful mesh. Provided that the local stress and strain results are consistent in both the 2D and 3D axisymmetric analyses, and the fact that our major focus in this study is understanding the effect of galvanization layers on this local state, it needs to be discussed if the three-dimensional approach involving larger computation time and effort is a real necessity.

A.1 Results

As a first check, we shall look at the general stressed state of the engaged threads. From figure A.5, it is clear that the first two engaged threads show higher stress concentrations than the subsequent engaged threads, the magnitude gradually decreasing. The principal stresses have been discussed here to have a comparison with the local stress values obtained in the two-dimensional axisymmetric model

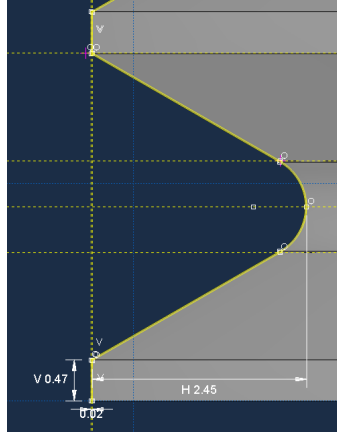


Figure A.4: Sketch of the δ phase from ABAQUS

as well as with literature [14]. Same goes with the local plastic strains, as the first and second engaged thread roots have developed considerably plastic strain, which is also the reason for the higher local stress concentration compared to other threads. This is a well-documented phenomenon, with the plastification playing a beneficial role in redistributing the load evenly among engaged threads, reducing the risk of localized failure. Both numerical and experimental studies support that controlled plastification is a critical mechanism for safe and robust load transfer in threaded fastener assemblies [19]. The values are in close agreement with the results obtained from the two-dimensional axisymmetric model for ungalvanized fasteners.

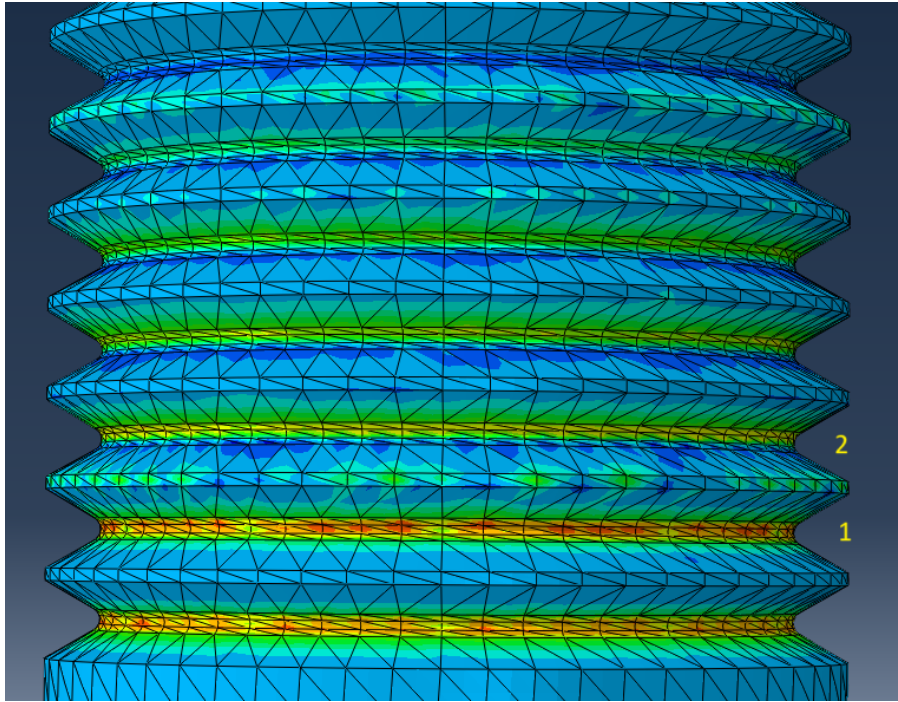


Figure A.5: Principal stress map at the engaged thread roots. The numbers signify the first and second engaged thread root.

A.2 Discussions

From the results obtained on the 3D axisymmetric models, the behavior at the engaged thread has been well replicated, as validated by previous numerical and experimental studies. We shall compare the results obtained from axisymmetric 2D and 3D models to see if any one reports changes compared to the other. Both results of models with and without galvanized zinc layers will be discussed below. We see from the results that stress along critical section matches the trend from 2D model, but details

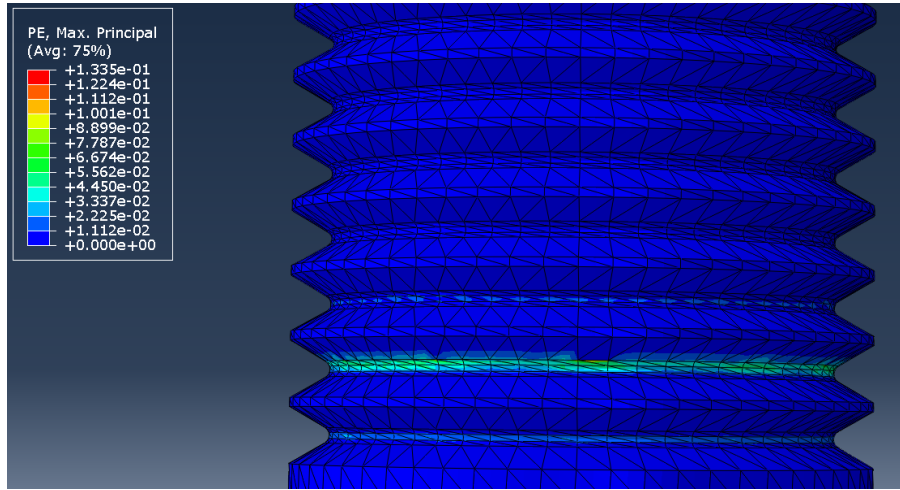
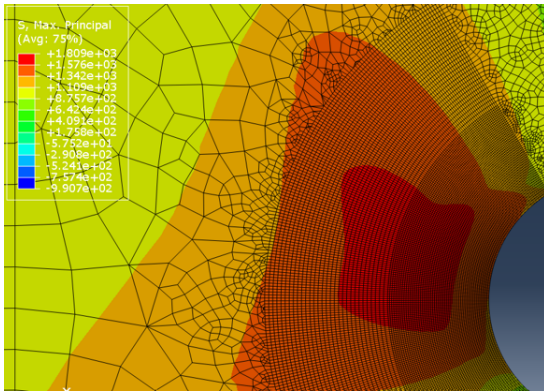
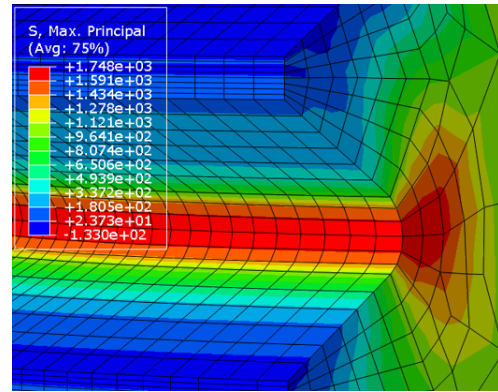


Figure A.6: Principal strain map at the engaged thread roots

are much less. Since global mesh size does not allow inter-metallic layer, they are considered in the local submodel of the first engaged thread, which is discussed further below. The principal stress peak is consistent as we go into the critical section, but the stress at thread root is not captured in sufficient detail in the 3D due to larger mesh size.

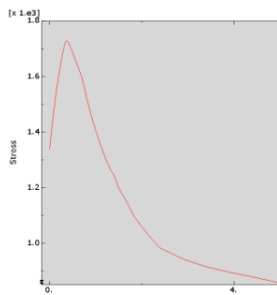


(a) Principal stress distribution from 2D model

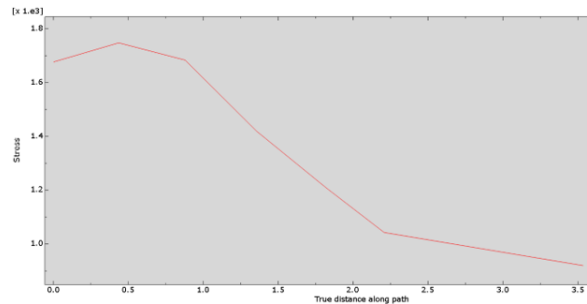


(b) Principal stress distribution from 3D model

Figure A.7: Max principal stress distribution at first engaged thread root for 2D and 3D axisymmetric model - Ungalvanized



(a) Principal stress plot from 2D model

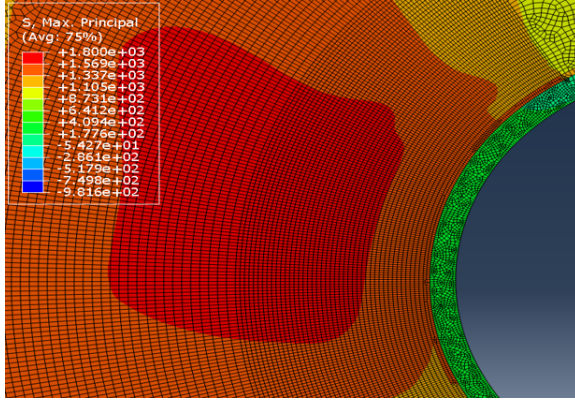


(b) Principal stress plot from 3D model

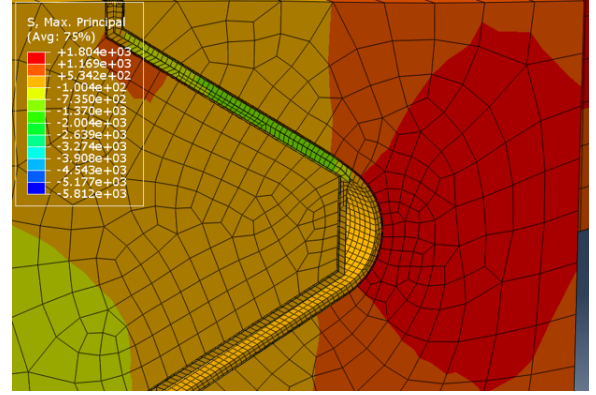
Figure A.8: Max principal stress plots for 2D and 3D axisymmetric model - Ungalvanized

Similar observations can be made from the sub-model including the galvanized zinc layers. The local stress-strain results are similar when it comes to the comparison, but it is much more detailed when it comes to the axisymmetric 2D model. A larger mesh density allows a deeper and more detailed analysis of stress development with increasing preload. Apart from this, the damage initiation location can be pin-pointed with much more detailed mesh. With the two-dimensional axisymmetric model

we can obtain more accurate results at the thread root boundary. This accuracy helps us utilize 2D models for fracture mechanics analysis. Therefore a good balance of results accuracy and detailed output makes 2D axisymmetric modeling a great option for the comparative analysis of larger size fasteners as all these models capture the same mechanics of stress development.

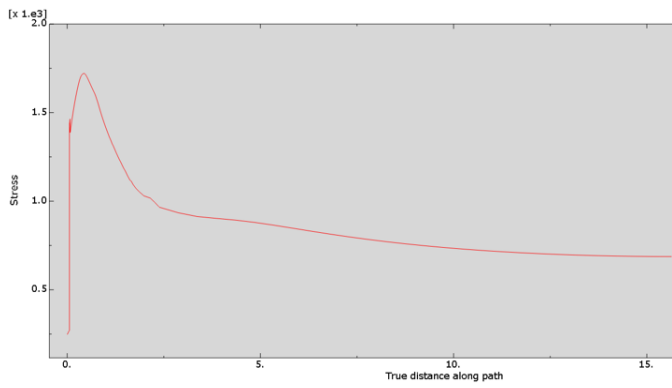


(a) Principal stress distribution from 2D model

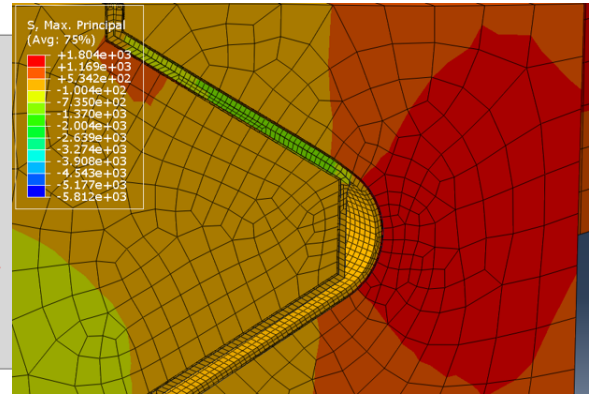


(b) Principal stress distribution from 3D model

Figure A.9: Max principal stress distribution at first critical thread root for 2D and 3D axisymmetric model - Galvanized

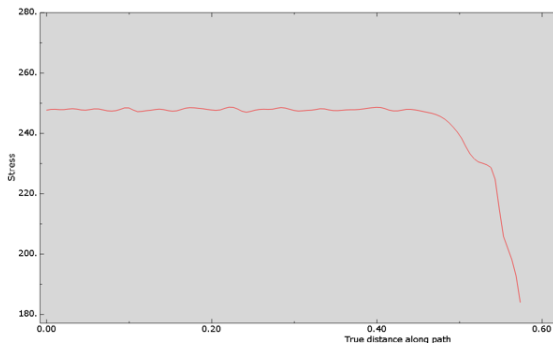


(a) Principal stress plot from 2D model

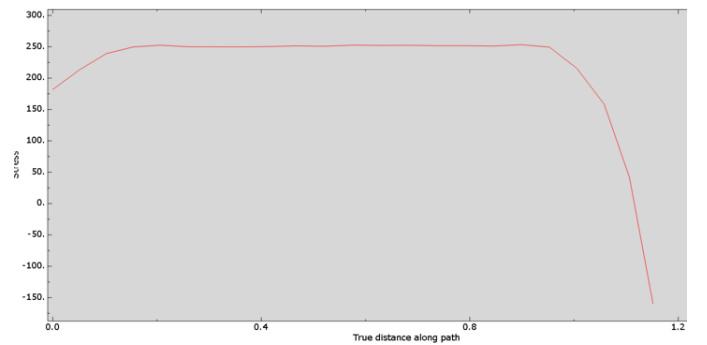


(b) Principal stress plot from 3D model

Figure A.10: Max principal stress plot for 2D and 3D axisymmetric model - Galvanized



(a) Strain plot from 2D model



(b) Strain plot from 3D model

Figure A.11: Strain plot for ungalvanized 2D and 3D axisymmetric model along the thread root radius

Appendix B

Model parameters and inputs

This will serve as a reference to inputs in ABAQUS/CAE in both 2D and full 3D models

Young's Modulus (N/mm ²)	Poisson's Ratio (-)
110000	0.33

Table B.1: Elastic properties of δ layer

Young's Modulus (N/mm ²)	Poisson's Ratio
82400	0.33

Table B.2: Elastic properties of ζ layer

Young's Modulus (N/mm ²)	Poisson's Ratio
205109	0.33

Table B.3: Elastic properties of steel substrate

Yield stress (N/mm ²)	Poisson's Ratio (-)
1100	0
1120	0.001
1200	0.002
1220	0.003

Table B.4: Plastic properties of δ layer

Yield stress (N/mm ²)	Poisson's Ratio (-)
120	0
133.33	0.002
146.67	0.004
160.01	0.006
173.35	0.008
186.69	0.01
200.03	0.012
213.37	0.014

Table B.5: Plastic properties of ζ layer

Yield stress (N/mm ²)	Poisson's Ratio (-)
1045	0
1064	0.0002
1057	0.005
1076	0.012
1095	0.018
1114	0.024
1133	0.030
1152	0.037
1171	0.048

Table B.6: Plastic properties of steel substrate

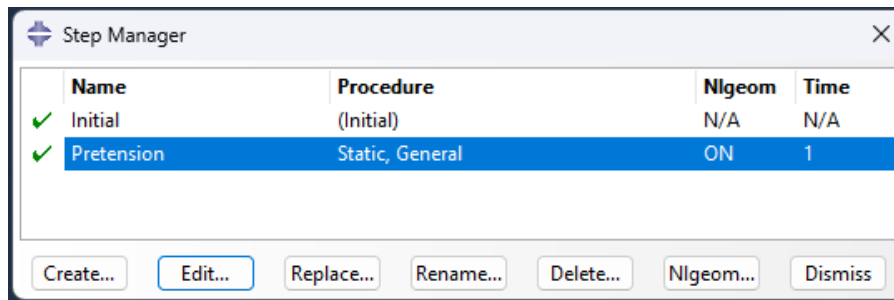
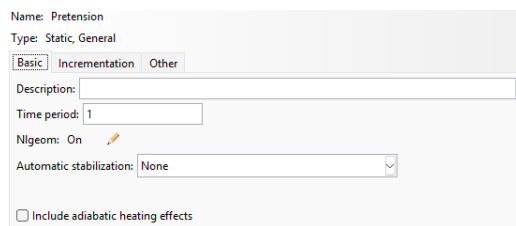
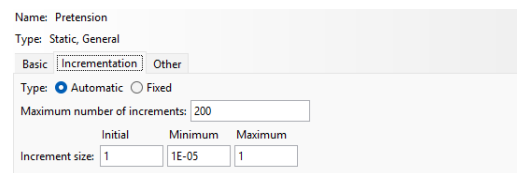


Figure B.1: Step definition manager



(a) Time period and NLGEOM of Pretension step



(b) Incrementation definition

Figure B.2: Step definition details

Edit Field Output Request [X]

Name: F-Output-1
Step: Pretension
Procedure: Static, General

Domain: Whole model ☐ Exterior only
Frequency: Every n increments n: 1
Timing: Output at exact times
Element output position: Integration points

Output Variables
☐ Select from list below ☒ Preselected defaults ☐ All ☐ Edit variables

CDISP,CF,CSTRESS,LE,PE,PEEQ,PEMAG,RF,S,U,

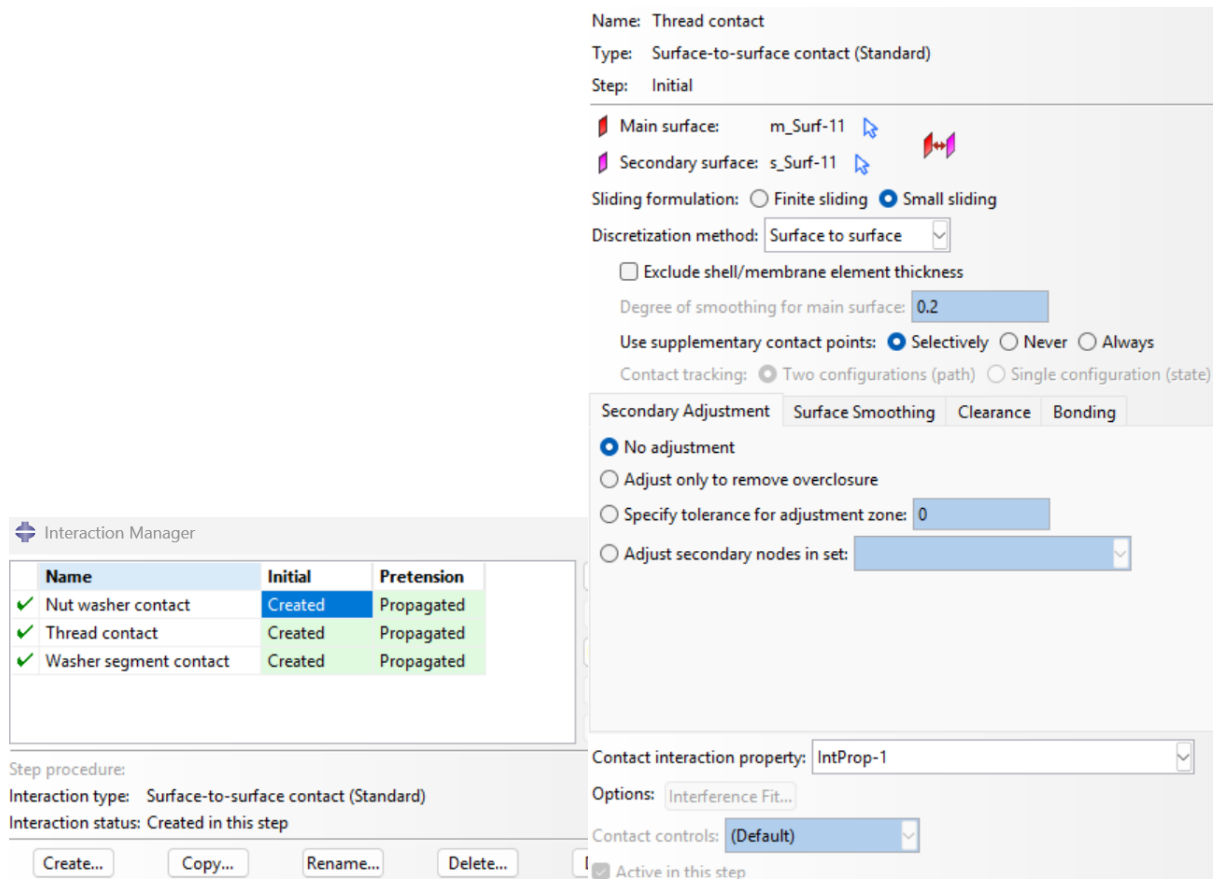
- ▶ ☒ Stresses
- ▶ ☒ Strains
- ▶ ☒ Displacement/Velocity/Acceleration
- ▶ ☒ Forces/Reactions
- ▶ ☒ Contact
- ▶ ☐ Energy
- ▶ ☐ Failure/Fracture
- ▶ ☐ Thermal

Note: Some error indicators are not available when Domain is Whole Model or Interaction.

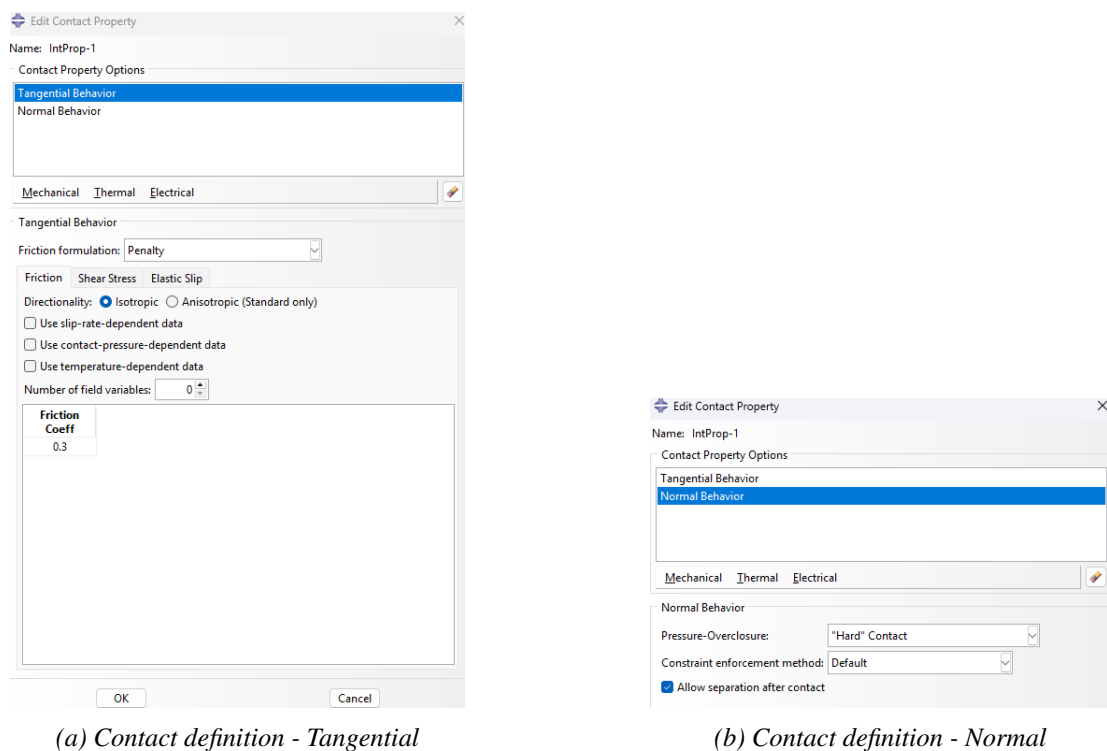
☐ Output for rebar
Output at shell, beam, and layered section points:
☒ Use defaults ☐ Specify:
☒ Include local coordinate directions when available

OK Cancel

Figure B.3: Field output selection




(a) Interaction manager (b) Contact interaction for thread contact
Figure B.4: Contact interaction definition



(a) Contact definition - Tangential (b) Contact definition - Normal


Figure B.5: Contact property definition



 Edit Load ×

Name: Load-1

Type: Pressure

Step: Pretension (Static, General)

Region: Surf-22 

Distribution:  

Magnitude:



Amplitude:  

Figure B.6: Load input manager

(Page left intentionally blank)